COMPOSITE FILMS FOR MODIFYING EVANESCENT WAVE CHARACTERISTICS IN LONG-PERIOD GRATING BIOSENSORS

by

Jennifer E. Martin

Thesis submitted to the Faculty of Virginia Polytechnic Institute and State University in partial fulfillment of the requirements for the degree of

MASTER OF SCIENCE

In

Chemical Engineering

APPROVED:

_____
William H. Velander, Ph.D., Chair

_____ _____
Richey M. Davis, Ph.D. Kimberly E. Forsten, Ph.D.

February 9, 2001
Blacksburg, VA

KEYWORDS: Biosensor, Long-Period Gratings (LPG), Evanescent Wave, Titanium Dioxide (TiO_2), Affinity Ligand Film

COMPOSITE FILMS FOR MODIFYING EVANESCENT WAVE CHARACTERISTICS IN LONG-PERIOD GRATING BIOSENSORS

by

Jennifer E. Martin

William H. Velander, Ph.D., Chairman

ABSTRACT

Biosensors are detection devices that couple biological recognition elements to physiochemical transducers to generate quantifiable signals. Immunosensors are biosensors that use antibodies as the recognition element. The highly specific nature of antibody-antigen binding is exploited to create immunosensors that are sensitive to analytes in complex mixtures and demonstrate a rapid response. Fiber optical immunosensors based on long-period gratings have limited sensitivity at the refractive index of ordinary aqueous solutions (~1.33). A composite film was designed to raise the local refractive index of the sensor, thus increasing sensitivity. Titanium dioxide deposition raised the refractive index of the sensor to ~1.42. Bovine serum albumin was immobilized onto a dextran hydrogel and attached to the LPG element via reductive amination. The thickness of the hydrogel was estimated to be 500 nm using Environmental Scanning Electron Microscopy. The affinity film was probed by an evanescent wave to detect changes in refractive index due to the binding of anti-BSA IgG. Under these conditions, the sensor yielded a signal ratio of approximately 10^{-4} refractive index units per nm signal. Reproducible binding was shown over multiple exposures, with no cross reactivity for non-specific antibodies and other proteins. Anti-BSA IgG (20 μg/mL) in whole serum was recycled through the fiber holder with an accompanying peak wavelength shift that averaged 2 nm on an Optical Spectrum Analyzer with a noise level of 0.1 nm. The BSA affinity film was regenerated 50 times and showed a baseline shift of –1.3 nm.

ACKNOWLEDGEMENTS

Funding for this research was provided by Luna Innovations, Blacksburg, Virginia.

I would like to thank my advisor, Dr. William H. Velander, for his guidance, enthusiasm and motivation. Since I left Virginia Tech before completing this thesis, Dr. Velander's remarkable display of patience provided the motivation to continue working on this document while working full-time. I also owe special thanks to Roger Van Tassell for his assistance, ideas, infinite patience, and friendship. I learned so much by watching you, and talking with you helped me to remain centered. Thanks for treating me with respect and caring not only about my scientific development, but about me as a person. Additionally, I would like to acknowledge Kevin Van Cott and Mark Jones for all of their help with this research.

Thanks go out to my friends at Virginia Tech who made my two years in Blacksburg memorable. Dave, I don't have the time to recall all the fun we had, but please know that I treasure your friendship and thank you so much for always being there. Ellie also thanks you for taking such good care of her and always being willing to play. I would also like to thank Jeff. There is no way I could have made it through grad school without you. Thanks for the shoulder to lean on when things weren't going as planned. Thanks also goes out to Matt O. You were a great study partner, but more than that, I enjoyed all the fun times playing poker and embarrassing myself at darts. I sincerely thank you and Tanya for opening up your home to me and cooking all those wonderful meals. Last but not least, I would like to say thank you to Christine, Matt J., and Brian, it's people like you who made grad school a complete experience. And to Jen, I am truly blest to have you as a friend.

Finally, I would like to express my deepest gratitude to my family. Never once did they give up on me, even when I had given up on myself. To my husband, Steve, thank you so much for your unwavering support and love. Without you, this could not have been possible. Your patience and understanding can never be repaid. To my parents, Barbara and Harold Mosser, and my brother, Matt, your love and encouragement have been the most influential forces in my life. Thank you so much for the constant faith you have shown me. It was your never-ending support and encouragement that gave me the strength to finally finish this thesis. Words can't express the love and respect I have for you. I only hope that in time I can repay you for everything you have given me.

This thesis is dedicated in honor of my grandparents, Mary and Edwin Michael and Mary and Chester Mosser. Their love, support and strength of character will always be an inspiration for me.

TABLE OF CONTENTS

LIST OF ABBREVIATIONS

anti-BSA	Anti-Bovine Serum Albumin
BSA	Bovine Serum Albumin
ºC	Degrees Celcius (also termed Centigrade)
d	Diameter
DDW	Distilled, Deionized Water
ESEM	Environmental Scanning Electron Microscope
H_20	Water
IgG	Immunoglobulin G
kDa	KiloDalton
KPO_4	Potassium Phosphate
L	Periodicity of a Long-Period Grating
LPG	Long-Period Grating
M	Molar (moles/liter)
min	Minute
mL	Milliliter (10^{-3} liter)
mm	Millimeter (10^{-3} meter)
MW	Molecular Weight
nm	Nanometer (10^{-9} meter)
OSA	Optical Spectrum Analyzer
rhPC	Recombinant Human Protein C
RI	Refractive Index
TiO_2	Titanium Dioxide
μm	Micrometer (10^{-6} meter)

LIST OF TABLES

LIST OF FIGURES

Chapter 1

INTRODUCTION

Biosensors exploit the highly specific molecular recognition system of biological organisms to report precise and sensitive measurements for an array of biomolecules. A biosensor is a device that couples a biological sensing element to a transducer to generate a signal in response to a specific analyte. The measurable signal is accomplished by selective transduction of a specific biological reaction.

Biosensors are classified according to the biomaterial component of the device. Biomolecules such as enzymes, antibodies, receptors and nucleic acids, as well as whole cells, organelles, and tissues have been used as the sensory element. Furthermore, biosensors are divided into biocatalytic and bioaffinity categories. Biocatalytic sensors include enzyme, microorganism, and tissue elements that are involved with the catalytic activity of a specific biological reaction. Bioaffinity sensors rely on molecular recognition by antibodies, receptors or binding proteins.

The requirements for a successful biosensor are high selectivity and sensitivity. The selectivity is a function of the biological sensing element and its ability to interact with the analyte. High sensitivity is achieved when there is sufficient interaction between the recognition element and the analyte to be efficiently detected by the transducer.

The high degree of specificity of biosensors is best typified by the antibody-antigen interaction. The binding between these molecules is highly specific, even in the presence of interferents. Biosensors, including immunosensors, have

several advantages over conventional biological assays. Many biosensors can directly detect analyte molecules, thus avoiding the addition of various reagents, which requires operator skill, therefore adding cost and increasing the duration of the assay. The ability to directly monitor specific analytes leads to rapid response times and overall shortened assay times.

When indirect detection is necessary, it is possible to integrate some of the necessary reagents within the sensing system so as to minimize sensor reagent usage. Most biosensors are not portable, due to the bulk of the combined sensor, sample fluidics system and data management hardware. Decreasing the amount of sample handling and data management would contribute to smaller margins of error, and hence more reliable results. Additionally, it is desirable to multiplex and monitor arrays of analytes and replicate samples. Finally, the possibility of continuous measurements is advantageous in many settings.

The versatility of biosensors is best described by the ever-expanding arenas of use. Applications for infectious disease diagnosis are being explored, and biosensors for in-home patient use, such as glucose monitors, are widely used. Clinical drug monitoring can be done continuously, as well as quality control in industrial processes such as fermentation. The portability of biosensors is needed for many applications of field testing in environmental monitoring or for the detection of biological agents used in biowarfare.

The purpose of this research was to investigate the feasibility of developing an immunosensor based on a modified long-period grating sensing element which could have enhanced sensitivity. Long-period gratings (LPGs) are written onto optical fibers and detect target binding within an affinity film by the accompanying

change in refractive index. The affinity-ligand film of the sensor is probed by an evanescent wave which detects changes in refractive index based upon mass binding. However, low sensitivity occurs in the low refractive index (approximately 1.33) of ordinary aqueous conditions.

A composite film was developed that modified the evanescent wave characteristics of the long-period grating biosensor. Titanium dioxide adsorbed onto the LPG surface enhanced the refractive index change upon target binding. This lead to an increase in biosensor sensitivity for biological targets in aqueous solutions.

The problem of biosensing can be divided into several parts. One issue is the physics of the sensor platform. The mass transfer of the target to the sensor film surface also needs to be optimized. Additionally, the adsorption kinetics of the target within the sensor adsorbent film is an issue. Lastly, the key issues of specificity and sensitivity to the adsorbed target ultimately define how well a biosensor performs.

This thesis consists of several parts of work. First, a model affinity film was assembled to detect the binding of anti-bovine serum albumin (BSA) IgG to BSA. Binding studies were performed to evaluate the sensor's ability to repetitively detect anti-BSA IgG capture by BSA. The specificity and sensitivity of the affinity film and target binding were verified by orthagonal methods such as enzyme-linked immunosorbent assay (ELISA). The film thickness and coverage was visualized by microscopy, and the amount of target bound was quantified by ELISA.

Non-specific binding of the sensor was also examined. The biosensor was tested against mixtures containing proteins similar to the anti-BSA IgG target to deduce its specificity. Detection of target in complex mixtures, such as serum, was investigated.

A comparison between a desktop Optical Spectrum Analyzer (OSA) and a scanning Fabry-Perot spectral filter was done to examine the noise levels of each instrument. The sensitivity of the sensor is affected in part by the noise level of the electronic demodulation system.

Finally, mass transport through the film was briefly addressed. Target was introduced under conditions of 0 mL/min (0 cm/min), 5 mL/min (125 cm/min), and 50 mL/min (1250 cm/min) through the fiber holder to investigate any major affects on target capture. The binding kinetics were not explored in this thesis but kinetic analysis was possible based upon the initial work done here.

Chapter 2

LITERATURE REVIEW

2.1 Immunosensors

Immunosensors are biosensors that use antibodies as the recognition element. Interest in immunosensors has evolved from the multi-million dollar industry of immunodiagnostics. Conventional immunoassays require skill and time to get reliable analytical results. Immunosensors are a way to provide scientists and clinicians with precise measurements of a variety of analytes in complex mixtures over a range of concentrations. Advantages over other immunoassays include the convenience of not having to accurately pipette various reagents in a multitude of steps, the possibility of designing a portable unit, the ability to measure more than one analyte simultaneously, and a decrease in the time between sample collection and obtaining results.

2.1.1 Antibodies

Immunosensors rely on the highly selective nature of molecular recognition systems to measure the amount of antibody, antigen or hapten present in a sample. Antibodies are immunoglobulins which are produced by the body in response to antigens. An antigen is any molecular species that is recognized by the body as foreign and triggers an immune response. Immunoglobulins fall into five classes, IgG, IgA, IgM, IgD, and IgE. These classes are structurally related glycoproteins that differ

in size, charge, amino acid composition, and carbohydrate content. Antibodies are often chosen as the biological recognition element because they have a high degree of specificity that allows them to recognize the appropriate analyte in the presence of interferents. Antibodies can recognize a range of targets from haptens (low molecular weight molecules) to particulate matter such as bacteria. Only a specific portion of the antigen, called the antigenic determinant or epitope, elicits an immune response. The epitope also serves as the binding site for the corresponding antibody.

In theory, antibodies can be made for an unlimited number of antigenic determinants. Upon antigen challenge, a variety of antibodies are generated that, although they respond to the same antigen, bind to different sites on the antigen and have different affinities for that antigen. They belong to different subclasses and have differences in epitope specificity. These heterogeneous antibodies which respond to the same antigen are termed polyclonal. Monoclonal antibody technology allows for the production of large quantities of homogenous antibodies. These antibodies respond to the same epitope of an antigen. Thus, monoclonal antibodies have the same affinity and specificity for a given antigen. In general, monoclonal antibodies have a higher specificity but lower affinity than polyclonal antibodies. However, the high heterogeneous nature of polyclonal antibodies is a major drawback.

2.1.1.1 Antibody-Antigen Binding Forces

The forces present during any bimolecular reaction are responsible for stabilizing the interaction between antibody and antigen. The forces of hydrogen bonding, electrostatic interactions, Van der Waals interactions, and hydrophobic interactions constitute the element of affinity (Rabbany *et al.*, 1994).

Electrostatic interactions can be either attractive or repulsive forces between charged molecules or dipole-dipole interactions between highly polar molecules. In proteins, the polar amine and carbonyl groups of the polypeptide backbone lead to permanent dipoles. Polar and charged residues of the side chains also contribute to the dipoles. Hydrogen bonds are considered a subset of electrostatic interactions. They occur between a highly electronegative proton donor and an unbound pair of electrons on a highly electronegative proton acceptor. The amine groups constitute a proton donor, and the carbonyl groups function as a proton acceptor. These hydrogen bonds and electrostatic interactions contribute to binding strength, and in aqueous solutions they are the predominant contributors to intermolecular stabilization (Buckingham, 1993).

Van der Waals forces occur between weaker dipoles than electrostatic interactions. Electric fields of nearby molecules induce the temporary dipoles responsible for these forces. Although these interactions are relatively weak, the cumulative force from several interactions can contribute up to 50% of the total binding strength (Roitt, 1984).

Hydrophobic interactions are repulsive forces that occur between nonpolar molecules and water. Driven by entropy, nonpolar regions act to exclude water and thus attain lower, more favorable energy levels. If these nonpolar regions exist at a reaction site, achievement of thermodynamic stability leads to intermolecular stabilization and increased binding strength (Rabbany *et al.*, 1994).

The binding site of an antibody characteristically contains a hydrophobic pocket lined with charged groups and hydrogen bond donors and acceptors. The dipoles present interact with the dipoles of the antigen and pull

together to assume an orientation suitable for binding. While these electrostatic interactions and hydrogen bonding are the primary contributors to intermolecular stabilization, the other forces provide supplementary attraction (Rabbany *et al.*, 1994). Contradictory to these binding forces are repulsive forces due to steric hindrance. Steric forces are repulsions between interpenetrating electron clouds of nonbonded atoms, and are minimized as the complement between reactants increases (Steward, 1977).

2.1.1.2 Kinetics of Antibody-Antigen Binding

The fundamental thermodynamic principle governing antibody-antigen interactions in solution is expressed by:

$$Ab + Ag \underset{k_d}{\overset{k_a}{\Leftrightarrow}} AbAg \tag{2.1}$$

where Ab represents free antibody, Ag represents free antigen, AbAg is the antibody-antigen complex, and k_a and k_d are the association and dissociation rate constants, respectively. The equilibrium constant, or the affinity, is given by:

$$K = \frac{k_a}{k_d} = \frac{[AbAg]}{[Ab][Ag]} \tag{2.2}$$

In solution, both association and dissociation are relatively rapid. The association rate is affected by the diffusion of reactants and the probability that a collision will result in a binding event. Dissociation is determined by the strength of the antibody-antigen bond, and the thermal energy available for the activation energy needed to break the bond. The equilibrium constant for monoclonal antibodies is typically 10^5 to 10^9 $Molar^{-1}$ (Rabbany *et al.*, 1994).

For use in immunosensors, antibodies (or antigens) are typically immobilized onto a solid surface. Immobilization can alter the properties of the antibody (or antigen), thus affecting binding kinetics. Of interest is the effect on the dissociation rate constant. In solution k_d values are typically 10^2 to 10^{-5} $Molar^{-1}sec^{-1}$, for immobilized reactants, k_d ranges from 10^{-4} to 10^{-5} $Molar^{-1}sec^{-1}$. Since K in solution is primarily governed by dissociation rate, binding by immobilized antibodies is "functionally irreversible" compared to a practical assay duration (Rabbany *et al.*, 1994).

2.1.2 Detection Reagents and Labels

Detection of a measurable signal from an antibody-antigen binding event is traditionally accomplished with labels. As in immunoassays, labels can be used for signal amplification. Labels can be fluorescent dyes or enzymes that produce fluorophores or chromophores upon substrate addition. Linear, multiplicative and cascade strategies are useful types of signal amplification.

With linear strategies the number of labels is linearly proportional to the number of binding events. Thus, the generated signal is directly related to the amount of target bound. Multiplicative amplification uses enzyme labels that act as catalysts to continuously produce fluorophores or chromophores upon substrate availability. The signal is proportional to both the antigen concentration and time. The main disadvantage of this system is that background noise also increases with time due to nonspecific cleavage of the substrate (Thompson and Ligler, 1991). Cascade amplification is similar to multiplicative except the label is a catalyst that creates more catalyst, which in turn produces the signal. The signal has a logarithmic relationship with antigen concentration, i.e., it is proportional to antigen concentration and the time

squared. The primary disadvantage is the complexity of maintaining excess second enzyme and substrate in addition to coordinating the working range of the assay with the working range of the instrument (Thompson and Ligler, 1991).

2.1.2.1 Chemiluminescent

Chemiluminescent immunosensors have been created utilizing enzyme labels that generate photons. A competitive assay is performed between labeled and unlabeled target, which compete for the binding positions on the immobilized ligand. The light emitted from the bound enzyme label is transmitted to a photomultiplier. One such immunosensor was designed on the basis of subtle differences in antibody bioaffinity for the corresponding antigen (Aizawa, 1994). Porcine insulin was bound on the surface of an optical fiber and complexed with peroxidase-labeled anti-bovine insulin IgG. The fiber was immersed in a solution of free bovine insulin. The porcine-anti-bovine complex dissociated and the anti-bovine IgG formed a stable complex with the free bovine insulin. Peroxidase catalyses the luminescent reaction of luminol to generate photons. By measuring the change in amount of peroxidase remaining on the fiber, the amount of insulin in solution could be determined.

2.1.2.2 Electrochemiluminescent

Electrochemically active substances have also been used as labels in immunosensing devices. Ikariyama *et al*. (1985) reported that a labeled antigen exhibits electrochemical reactivity and generates luminescence, but when it is immunochemically complexed, the labeled antigen is found to lose its electrochemiluminescence property. Optical fibers can be sputtered with platinum, which maintains optical transparency, and work as electrodes. Photons generated at

the surface of the electrode are collected and sent to a photomultiplier. An optical fiber electrode with IgG as the antigen has been made using luminol as the label (Aizawa, 1994). Luminol is oxidized by anodic excitation to generate radicals, followed by photon emission. In the presence of hydrogen peroxide, luminol-labeled IgG generates electrochemical luminescence, however, immunocomplexation with anti-IgG decreases the luminescence produced. The change in luminescence is used to quantify the target. The lower limit of detection is reported to be in the range of 10^{-12} g/mL of antibody (Aizawa, 1994).

2.1.3 Polymer Films

For binding to occur, there must exist an optimum environment that provides appropriate hydrophilic or hydrophobic characteristics. While the aforementioned forces are responsible for creating an affinity between antibody and antigen, an inappropriate binding environment would preclude any such intermolecular interactions. Since biosensor targets can include hydrophilic or hydrophobic proteins or amphiphilic molecules, polymer films need to be engineered to provide a balance of these domains.

Hydrophilic films such as those made from dextran or cellulose derivatives are used when both the ligand and target are hydrophilic. A customized film can be made by crosslinking dextran macromonomers (MW 500 kDa, 26 nm hydrodynamic radius) into a hydrogel of known thickness. Films can easily be made that range from 100 to 500 nm in hydrodynamic diameter. Solubilized dextran can react with bisoxirane and crosslink into macropolymers. Reaction schemes for fiber silylation and attachment of activated macropolymers are well-known (Hermanson *et al.*, 1992). Hydrogel attachment can be done through reaction of the residual epoxy

groups on the dextran macropolymer to the activated fibers. In this thesis, the dextran was activated with aldehyde groups and then attached to the silylated TiO_2 fiber. Either amino- or thio-silylation, accomplished by 3-aminopropyltriethoxysilane or 3-mercaptopropyltriethoxysilane, respectively, can activate fibers.

Capture of hydrophobic proteins or amphiphilic molecules is not efficient in a hydrophilic film. Activating acrylamide hydrogels with glutaraldehyde polymers can create a hydrophobic environment. The fibers are silylated with vinyl groups to which the acrylamide hydrogel is attached (Hermanson *et al.*, 1992). Amphiphilic domains can also be introduced by creating a copolymer of varied hydrophilic/ hydrophobic acrylamide ratios. For hydrophobic or amphiphilic ligands and targets, a balance in the hyrophobicity of the affinity film will lead to better mass transfer and more efficient binding. Figure 2.1 shows how a hydrogel can be tailored to create the optimum environment to stabilize binding to an immobilized ligand.

2.1.4 Ligand Immobilization

The most elementary method of ligand immobilization is nonspecific adsorption. Although this may result in a favorable ligand density, problems exist including disassociation and variable activity. Disassociation of the ligand may occur under conditions of high salt concentrations, in the presence of serum, or under high flow conditions (Rabbany *et al.*, 1994). The activity of the ligand may also be compromised due to the uncontrollable manner by which the ligand adsorbs to the hydrogel surface. Binding sites may be unavailable or obstructed by a disorderly deposition pattern. Covalent attachment, on the other hand, is stable and functionally reproducible.

Attachment of affinity ligands to the hydrogel matrix is also accomplished through well-known methods (Hermanson *et al.*, 1992). Covalent linkages between ligands and the hydrogel can be created by reacting aldehydes or ketones with primary or secondary amino groups to form Schiff bases. The Schiff base can be stabilized by a reducing agent such as sodium borohydride or sodium cyanoborohydride. Aldehyde groups can be created on polysaccharide matrices by mild oxidation of glucose units with sodium meta-periodate. Periodate oxidation cleaves the carbon-carbon bond between adjacent hydroxylic groups and produces two formyl functionalities. Reductive amination then couples the periodate-activated matrix to the ligand via amine linkages. By varying the density of aldehyde groups introduced on the polymer film, the ligand density can be controlled.

2.1.5 Mass Transfer

Transport of the target through the matrix and the kinetics of binding govern ligand-target interactions. Before binding can proceed, several transport issues must be accomplished. The bulk flow rate will affect the macroscopic transport through the system to the sensor surface (Glaser, 1993). Secondly, diffusion through the nonstirred boundary layer depends on bulk flow rate, geometry of the flow cell, and the diffusion coefficient of the target in solution (Glaser, 1993). Transport issues also include diffusion through the array of binding sites within the immobilized matrix. This is dependent on the size and charge of the target, thickness and density of the hydrogel matrix, and the diffusion coefficient of the target in the polymer solution (Schuck, 1996).

The Thiele modulus is a dimensionless quantity that describes the ratio of a surface reaction rate to the rate of diffusion through a matrix:

$$\Phi^2 = \frac{R^2 kC}{D_{eff}} \tag{2.3}$$

where R is the radius of the matrix, k is the reaction rate constant, C is the ligand concentration, and D_{eff} is the effective diffusivity of the protein in the matrix. The diffusion of proteins through low density hydrogels is governed by the characteristic distance of diffusion (R^2) and D_{eff}. In low density hydrogels, D_{eff} for proteins is assumed to be equivalent to that in pure aqueous solutions (Subramanian *et al.*, 1994).

The overall transport rate is determined by diffusion within the gel and transport from the bulk solution to the gel. Many theories have been presented to describe the transport of analytes through hydrogel films (Schuck, 1997; Karlsson and Fält, 1997; Morton and Myszka, 1998). De Gennes (1979) found that if probes are smaller than the mesh size of the polymer solution, and if there are no long-range interactions between the polymer and the probe, then the presence of a polymer matrix will not affect the diffusion of the probe. Unless the analyte is much larger than IgG molecules and the ionic strength is low enough that electrostatic interactions can not be screened, diffusion of analyte through a dextran matrix will be reduced by a factor less than 5 (Witz, 1999). Stenberg *et al.* (1991) also found that the surface plasmon resonance (SPR) response to a range of sizes from chymotrypsinogen (M_r 25,700) to IgG (M_r 150,000) was the same.

Even though mass transport through the gel may not be rate limiting under ideal conditions, several variables can affect analyte transport. Diffusion can be affected by the concentration of ligands within the gel. Very high local densities of immobilized ligands on the outer layer of the gel can disrupt the transport of analytes through the gel by steric hindrance. Additionally, if the bulk concentration of free mobile reactant is not maintained, the immobilized binding sites compete for a limited

supply of analyte and the kinetics are said to be transport-limited. Glaser (1993) reports that under conditions of mass transport limitation the thickness of the hydrogel does have an influence on an SPR signal. This occurs because the SPR signal is dependent on the distance a bound analyte is from the surface, and the outer fringe of the gel becomes saturated earlier than the ligands near the surface.

Interactions between antibody and antigen in solution have been well understood. The binding of an antibody in solution to antigen immobilized on a surface can be described by a two-step process (Sadana and Madugula, 1993). The binding rate (Γ_1) of a single arm of an antibody to an antigen attached to the surface is given by:

$$\frac{d\Gamma_1}{dt} = k_f[Ag][Ab]\Gamma_0 \tag{2.4}$$

where Γ_0 is the total concentration of the antigen sites on the surface, k_f is the combination of k_1 and k_2, the forward reaction rates for one arm of an antibody binding to one antigen and for both arms of an antibody binding to two antigens, respectively. Taking lateral interactions between antibody-antigen complexes on the surface in account:

$$\frac{d\Gamma_1}{dt} = \frac{k_f^2}{k_2}[Ag][Ab]^2\Gamma_0 \tag{2.5}$$

The dual-step binding expression exhibits a first-order dependence on both the antibody concentration close to the surface, [Ab], and on the antigen on the surface available for binding, [Ag]. This is not surprising since one antibody molecule has two arms involved in the dual-step binding process. When extended to lateral interactions, the second-order dependence on antibody concentration in solution near the surface is expected since two Ag-Ab complexes are involved. Lateral interactions

between macromolecules are thought to stabilize the adsorbed protein and antigen-antibody complexes on the surface, leading to an increase rate of binding and an increase in the antibody concentration near the surface (Sadana and Madugula, 1993).

2.1.6 Classical Sensor Platforms

Immunosensors are classified according to the measuring principle utilized. Electrochemical (including potentiometric and amperometric), optical, piezoelectric acoustic, and thermometric sensing elements have been used as platforms for immunosensors. The majority of immunosensors are characterized as either electrochemical or optical. Furthermore, all types can be categorized as either direct or indirect immunosensors.

Direct sensors are designed so that formation of the antibody-antigen complex induces physical changes in the signal. Electrodes, membranes, piezoelectric material, or optically active material surfaces are sensitive enough to construct direct immunosensors. The target analyte is present in solution and reacts with the complementary antibody or antigen bound on the sensing matrix. Formation of the immunocomplex alters the physical properties of the surface, such as electrode potential, membrane potential, the intrinsic piezofrequency, or the optical properties allowing for target measurement (Aizawa, 1994). However, the potential problem of nonspecific adsorption of molecules on to the surface exists.

Indirect sensors rely on labels conjugated to either the antibody or antigen to visualize the binding event. High sensitivity can be induced by incorporation of enzymes, catalysts, fluorophores, electrochemically active molecules, and liposomes as labels (Aizawa, 1994). An immunocomplex may be formed in a variety of ways, but

the final step must include incorporation of a label, which is then determined by potentiometric, amperometric, or optical measurements.

The principles of the classical sensing platforms, including electrochemical, piezoelectric acoustic, and thermometric will be discussed. Also included in this section are optical immunosensors which are not based on evanescent wave phenomenon. Reflectometric and ellipsometric immunosensors fall into this category. Examples of immunosensors will be given for each category and advantages/disadvantages discussed.

2.1.6.1 Electrochemical

The two basic electrochemical sensors are potentiometric and amperometric. Potentiometric sensors measure the change in potential at an ion selective electrode due to an ionic product of a reaction. The electrode surface of the working electrode is modified for selectivity and the potential difference is taken between that electrode and a reference electrode when no current is flowing between them. The electrodes are either submerged into a sample or separated from the sample by a membrane and placed into a defined electrolyte solution. The most common potentiometric devices are pH electrodes and other ion-selective electrodes. The electrode potential (E) measured is described by the Nernst equation and is dependent on the activity of a defined ion (α_i). If equilibrium between the solution and electrode is obtained, the electrode potential is given by:

$$E = E^o + \frac{RT}{zF}\ln\alpha_i \qquad (2.6)$$

where E^o is the standard potential, R is the gas constant, F is the Faraday constant, z is the number of electrons transferred between each molecule of the analyte and the

electrode, and T is the temperature. The measured potential difference is taken with respect to the reference electrode and is dependent on all potential differences that appear at the various phase boundaries, including that of the reference electrode and differences between electrolytes (Liu and Yu, 1997). The main disadvantage of this system as an immunosensor is that changes in potential due to antibody-antigen binding are very small (1-5 mV) and, consequently, the reliability and sensitivity are limited by background effects (Marco and Barceló, 1996). In contrast to amperometry, the upper linear range of potentiometry is restricted and the detection limit is usually on the order of micromoles (Person *et al.*, 2000).

Amperometric devices are based on measuring the current produced by the oxidation or reduction of an electroactive compound at an electrode while constant potential is applied to this electrode with respect to a second electrode. A typical example is the glucose biosensor, which makes use of the electrochemical detection of the species produced (hydrogen peroxide) or consumed (oxygen) by the enzyme glucose oxidase, which is immobilized on an electrode surface. Electrochemically active substances such as horseradish peroxidase (HRP), an oxidoreductase, or alkaline phosphatase (AP), a hydrolytic enzyme, can be used as labels in amperometric immunosensors. Faraday's law describes the measured current (I) as a direct measurement of the electrochemical reaction rate (oxidation or reduction rate of the analyte at the electrode):

$$I = zF \times \frac{dn}{dt} \tag{2.7}$$

where dn/dt is the oxidation or reduction rate (in mol s^{-1}), z is the number of electrons transferred between each molecule of the analyte and electrode, and F is the Faraday constant. The rate of reaction depends on the rate of electron transfer at the surface of

the electrode, and on the rate of mass transport of the analyte to the surface. The former can be accelerated by increasing the potential difference between the electrodes and the latter is influenced by bulk concentration of the analyte, the area of the electrode, and diffusion and convection conditions (Liu and Yu, 1997). The sensitivity of these devices can be extremely high due to chemical amplification through enzyme cycling.

2.1.6.1.1 Potentiometric Immunosensors

Three types of potentiometric immunosensors have been proposed. The first is the transmembrane potential immunosensor, the second is the electrode potential immunosensor, and thirdly, the field effect transistor immunosensor.

The transmembrane potential immunosensor measures the potential across an antibody (or antigen) membrane that specifically binds a corresponding antigen (or antibody) in solution. As changes in transmembrane potential occur during immunocomplex formation, the sensor measures this change on the membrane surface and determines the concentration of target. Transmembrane potential consists of diffusion potential and interfacial potential (Aizawa and Suzuki, 1977b; Kobatake *et al.*, 1965). Membrane charge density makes up the interfacial potential. The charge density changes with the binding of the corresponding antigen onto the antibody surface. Results from potentiometric immunosensors for syphilis and blood typing have been reported by Aizawa *et al.* (Aizawa, 1994; Aizawa *et al.*, 1977a; Aizawa *et al.*, 1980a). In blood typing, for example, the transmembrane potential across an immunoresponsive membrane prepared by immobilizing blood group substances is measured by a pair of reference electrodes. A membrane immobilized with blood group A substances and fixed to a transmembrane potential measurement device

would show a potential change when challenged with blood group B substances, due to immunocomplexation. However, no transmembrane change in potential would be detected when challenged with like substances.

The second type of potentiometric immunosensor is based on the determination of the electrode potential. An electrode surface is modified with either antibody or antigen, and upon immunocomplexation with the complementary target there is a change in surface charge that consequently affects the electrode potential. The concentration of analyte in solution is related to this change. Such a sensor has been made that responds to human chorionic gonadotropin (hCG) in solution by coating the electrode surface with anti-hCG (Aizawa, 1994).

The third type of potentiometric immunosensor is the ion-selective field effect transistor (ISFET) immunosensor. The ISFET is based on the field effect transistor (FET) used in electronics to detect voltage variations with minimal current drain. In the ISFET, a local potential is generated by surface ions from a solution. Then, as in a conventional FET, this potential modulates the current flow across a silicon semiconductor. ISFETs function as a solid-state counterpart to ion-selective electrodes. Heparin has been detected in the range of 0.3 to 2.0 units/mL by coating the sensor with a protamine (an affinity ligand) immobilized membrane (Pearson *et al.*, 2000). The immunoFET devices have suffered from practical problems associated with membrane performance (North, 1985). Additionally, FET drift, lack of selectivity and difficulty in making a stable, miniaturized reference electrode has made commercial development of these sensors difficult (Pearson *et al.*, 2000).

These potentiometric immunosensors represent simplicity of operation, however, they demonstrate insufficient sensitivity. Most biological molecules have a

low charge density compared with background interferences such as ions, and thus give low signal-to-noise ratios. They also show a marked dependence of signal response on sample conditions such as pH and ionic strength (North, 1985).

2.1.6.1.2 Amperometric Immunosensors

There are three types of amperometric devices: enzyme labels with an oxygen electrode; electrochemically active labels; and enzyme labels with electrochemically active products.

Enzymes such as catalase, glucose oxidase, and peroxidase are detected with high sensitivity. These enzymes are associated with a change in oxygen concentration that can be monitored with an oxygen electrode (Aizawa *et al.*, 1976; Aizawa *et al.*, 1979). An example of such a device is one in which α-fetoprotein (AFP), one of the marker substances in cancer diagnosis, is detected by an amperometric immunosensor, which utilizes catalase as the labeling enzyme (Aizawa *et al.*, 1980b). The AFP antibody is immobilized on a polymer membrane and attached to an oxygen electrode. The sensor is placed in contact with a test solution to which a known amount of catalase-labeled AFP is added. The labeled AFP and test solution AFP competitively bind to the immobilized antibody. After rinsing and a background measurement of dissolved oxygen is obtained, hydrogen peroxide is injected and the sensor quantifies the amount of oxygen produced. Steady state can be reached within 30 seconds, and the lower limit of detection was shown to be $5x10^{-11}$ g/ml (Aizawa *et al.*, 1980b).

The second type of amperometric immunosensor utilizes redox substances that can be used as labels for electrochemical immunoassays. Ferrocene, one such label, has been used as an electron acceptor for glucose oxidase (Gleria *et al.*,

1986). Antibody is immobilized to an electrode, then exposed to ferrocene-labeled antigen. Immunocomplexation inhibits ferrocene's ability to act as a mediator in the glucose oxidase catalyzed reaction and the catalytic current decreases. Addition of non-labeled antigen competes for binding sites and displacement of the ferrocene-labeled antibody reverses the decrease in current. The catalytic current generated depends on the concentration of analyte. Lidocaine in plasma was detected over the concentration range of 5-50 nM (Aizawa, 1994).

Thirdly, there are enzyme labels with electrochemically active products. Alkaline phosphatase is commonly used as a label in enzyme-linked immunosorbent assays (ELISAs). It catalyzes the hydrolysis of phenyl phosphate, which is electroinactive, to phenol and phosphate. The liberate phenol is detected electrochemically by oxidation on a glassy carbon paste working electrode at 870 mV versus Ag/AgCl following separation by either liquid chromatography or flow-injection analysis. The separation step eliminates interference from electroactive constituents that may be present in the sample and possible fouling of the electrode by adsorption of protein films (Aizawa, 1994). If the product is electroactive at a potential below 200 mV, the separation step may be omitted. These electrochemical sensors may be coupled with ELISAs based on the amperometric determination of alkaline phosphatase products. Immunocomplexation takes place in a microtiter plate well, but instead of an optical plate reader, an electrochemical sensor is connected to the well and the active product detected (Aizawa, 1994).

Amperometric immunosensors have shown promise in the detection of antibody/antigen binding. As long as enzymes are available that produce a product,

which can be detected by a suitable redox electrode, an amperometric biosensor can be made for any analyte (Paddle, 1996).

2.1.6.2 Piezoelectric Acoustic

A piezomaterial, such as a polished quartz crystal, resonates at a specific frequency by electric excitation. Metal transducers (e.g. gold) on the surface of the crystal send acoustic waves into the material at ultrasonic frequencies. The crystal orientation, thickness of the piezoelectric material, and geometry of the metal transducer determine the type of acoustic wave generated and the resonance frequency (Paddle, 1996). A change in weight on the crystal can be determined by measuring the shift in resonating frequency, wave velocity, or amplitude. The frequency shift of the piezoelectric crystal is proportional to mass change:

$$\Delta F = \frac{C_Q f^2 \Delta m}{A} \tag{2.8}$$

where ΔF is the change in fundamental frequency, C_Q is the sensitivity (which for quartz = 2.26×10^{-6} cm^2 g^{-1}), f is the resonant frequency of the crystal, A is the area of the crystal, and Δm is the mass change deposited (Sauerbrey, 1959).

Piezocrystals can also respond to physical property changes such as interfacial mass density, elasticity, viscosity, and layer thickness at the interface between the crystal and some fluid (Aizawa, 1994). Changes in acoustic wave propagation are then correlated to the amount of analyte captured on the crystal surface.

Both direct and indirect immunosensors have been developed for antibody recognition. Thompson *et al*. (1987) used a bulk wave sensor to observe antibody in a liquid phase. The sensor surface was coated with goat anti-human immunoglobulin

(IgG) either by attachment to a polyacrylamide gel with glutaraldehyde or by silylation onto the surface, then exposed to human IgG in solution. Ebersole and Ward (1988) used a sandwich assay format for piezoelectric immunosensors for adenosine 5′-phosphate and human chorionic gonadotropin. An antibody-coated crystal was exposed to sample antigen, then to a secondary antibody conjugated with horseradish peroxidase (HRP). When the HRP substrate was added, a precipitate formed via an enzyme-catalyzed reaction. The precipitate was deposited on the crystal surface leading to a change in resonating frequency. The advantage of the indirect method over the direct is that for a given amount of analyte bound, the mass of precipitate is much greater than that of the original bound analyte, hence sensor response is amplified.

Variations of the acoustic wave sensor include the use of bulk acoustic waves, surface acoustic waves, and acoustic plate waves (Aizawa, 1994). Acoustic plate waves may be the choice for biological applications, since they offer high sensitivity and can be used in biological environments (Andle *et al.*, 1993). The acoustic gas sensors have an increased sensitivity over the acoustic chemical sensors because the acoustic wave energy in the gas sensor is more easily distributed adjacent to the sensing surface (Aizawa, 1994). For liquid phases, the Lowe plate, which consists of a base layer and an overlayer, is an alternative waveguide that gives can respond to small changes in interfacial mass (Gizeli *et al.*, 1992). However, the Lowe plate does suffer from acoustic loss and instability.

All piezoelectric immunosensors tend to exhibit significant levels of non-specific binding to the piezoelectric crystal, which makes accurate analyte quantification difficult (Byfield and Abuknesha, 1994). Additionally, only high

molecular weight analytes can be measured directly; low molecular weight analytes have to be linked to a high molecular weight structure in order to generate enough of a change in mass to register (Pearson *et al.*, 2000). Their advantage lies in their small size and low manufacturing cost, and they may play an important role in the YES/NO detection of gaseous chemicals used in applications such as security monitoring (Guilbault and Luong, 1988).

2.1.6.3 Thermometric

Most biochemical reactions involving enzyme catalysis are exothermic. Enthalpy changes associated with enzyme catalysis can result in a detectable thermal signal. The heat produced is proportional to the molar enthalpy and also is dependent on the heat capacity of the system by:

$$Q = -n_p(\Delta H) \tag{2.9}$$

$$Q = C_p(\Delta T) \tag{2.10}$$

where Q is total heat, n_p is moles of product, ΔH is molar enthalpy change, and C_p is heat capacity of the system. The change in temperature is proportional to the enthalpy change and inversely proportional to the heat capacity of the reaction:

$$\Delta T = -\frac{\Delta H \times n_p}{C_p} \tag{2.11}$$

A thermometric measurement is based on the sum of all enthalpy changes in the system. By co-immobilizing oxidases with catalase, the sensitivity can be doubled while nullifying the effects of hydrogen peroxide and reducing oxygen consumption (Xie *et al.*, 1999). Sensitivity can also be increased by using substrate or coenzyme recycling systems to amplify the enthalpy change (Danielsson, 1991).

The enzyme thermistor (ET) is the most common type of thermal biosensor. Enzymes are immobilized on a thermally insulated column and as the substrate flows through the column the temperature increases. This increase in temperature is monitored by a thermistor mounted at the top of the column and is related to analyte concentration. Thermistors are resistors with a high negative temperature coefficient of resistance; they are the most sensitive of the common transducers.

The ET has been applied to a variety of analytical activities. Clinical analysis of blood and urine in the micro- and millimolar range has been demonstrated. Enzyme thermistors have been modified for enzyme activity analysis (Danielsson and Larsson, 1990) and on-line monitoring of metabolites produced in fermentation processes (Hundeck *et al.*, 1997). Environmental monitoring has used ETs to measure toxicity of heavy metal ions by determining inhibition of enzyme activity (Xie *et al.*, 1999), and toxin influence on microorganisms by observing metabolism changes (Lammers and Scheper, 1999).

Application to immunoanalysis has resulted in the procedure called TELISA (thermometric enzyme-linked immunosorbent assay). Immobilized antibodies are placed in a column and set into an ET, sample is injected, allowed to bind, and then unbound molecules removed. Antibodies conjugated with enzymes are added and a sandwich formed. After addition of substrate, the change in heat is measured and correlated to analyte concentration. One of the first immunosensors developed was for albumin and followed the TELISA format (Mattiasson *et al.*, 1977).

Thermal biosensors, enzyme thermistors in particular, have several advantages. Long-term stability is good since there is no chemical contact between

transducer and sample, inertness to disturbances in the optical or ionic sample characteristics, and the possibility of use in continuous flow operations. For immunosensing applications, the TELISA has to compete with fluorescent assays, which are more sensitive and faster due to a lack of dependence on conjugate antibodies.

2.1.6.4 Reflectometric and Ellipsometric

Reflectometric immunosensors are based on the theory that if a substance is absorbed on a surface between two media, and its refractive index is different, then it will affect the reflectance characteristics of the surface. Using an antibody coated indium surface, the binding of the antigen can be monitored by the change in refractive index. The magnitude of the change is then used to quantify the analyte.

Ellipsometry uses changes in phase and amplitude of reflected light to detect biological molecules. One example is that of a silicon oxide wafer coated with human fibronectin (Paddle, 1996). Upon incubation with anti-human fibronectin the binding event triggered optical changes in the reflected light.

The configuration used in reflectometry and ellipsometry is called external reflection whereby light has to pass in and out of the liquid. Disturbances from air bubbles and particles alter the device sensitivity and hence severely restrict the design of the flow cell for *in situ* analysis (Jönsson and Malmqvist, 1992).

2.2 Evanescent Wave Optical Sensing Devices

The field of optical immunosensors has experienced rapid growth in the past few years. This is partly due to the ever-improving optoelectronics designed for telecommunications, and advances in material science, which have led to better

fabrication materials and improved methods of signal generation and reading (Aizawa, 1994). The transducers used for optical sensors can be either planar waveguides, surface plasmon resonance devices, or fiber optics. Optical immunosensors function by detecting antigen-antibody binding through changes in optical characteristics such as absorption, rotation, refractive index, bio/chemiluminescence, and fluorescence. Optical immunosensors can be described as either direct or indirect, just like the other sensing platforms. The direct systems rely solely on antigen-antibody binding to modulate the signal being measured, while indirect sensors depend on the use of labels to visualize the binding event. The advantage of the direct type is that the assay is essentially "reagentless" in that no additional substances are needed for detection. The disadvantages are that sensitivity may be limited by non-specific binding, and the analyte size may limit the use of standard assay formats (Paddle, 1996). The indirect format has the advantage of improved sensitivity and selectivity due to the label, as well as a reduced amount of non-specific binding. Normal assay formats can still be used with indirect sensors since the labels will serve to amplify the optical sensor response even to small molecules bound to the transducer. The main disadvantage of the indirect sensors is the additional need for labeled reagents.

Immunosensors that use evanescent waves detect target binding by measuring parameters such as absorbance, fluorescence, or refractive index. Surface plasmon resonance (SPR) is a phenomenon arising from the presence of evanescent waves. These devices detect target binding by changes in refractive index. This thesis centers on the recent development of sensors based on fiber optical long-period gratings (LPG). The gratings are written onto the core of optical fiber and also detect target binding events by refractive index changes within the evanescent field. The

problem with LPG sensors is that at the refractive index of normal aqueous solutions (approximately 1.33), the sensor has low sensitivity. By engineering composite affinity films that increase the refractive index of the sensor an increase in sensitivity can be attained.

2.2.1 Evanescent Wave

Optical biosensors based on the evanescent wave (EW) use the technique of attenuated total reflection (ATR) spectroscopy and surface plasmon resonance (SPR) to measure real-time interaction between biomolecules. The basis of ATR is the reflection of light inside the core of a waveguide when the angle of incidence is less than the critical angle. Waveguides can be slab guides, planar integrated optics or optical fibers. Light waves are propagated along fibers by the law of total internal reflection (TIR). This law states that incident light striking nearly parallel to the interface between two media of differing refractive indices, entering through the media of higher refractive index will be reflected or refracted according to Snell's Law:

$$n_1 \sin \Theta_1 = n_2 \sin \Theta_2 \tag{2.12}$$

where n_1 is the higher refractive index (core), Θ_1 is the incident ray angle through the core, n_2 is the lower refractive index (cladding), and Θ_2 is the angle of either internal reflection back into the core or refraction into the cladding. TIR occurs when the angle of incidence is greater than the critical angle. The critical angle is defined as:

$$\Theta_c = \sin^{-1} \frac{n_2}{n_1} \tag{2.13}$$

Even though the light is totally internally reflected, the intensity does not abruptly fall to zero at the interface. The intensity exponentially decays with distance,

starting at the interface and extending into the medium of lower refractive index. The evanescent wave is the electromagnetic field created in the second medium. It is characterized by the penetration depth defined as the distance from the interface at which it decays to 1/e of its value at the interface (Squillante, 1998). The wavelength of light, ratio of the refractive indices, and angle of the light at the interface determine the penetration depth (Thompson and Ligler, 1991). The penetration depth (d_p) is related to these factors by:

$$d_p = \frac{\lambda}{2\pi\left(n_1^2 \sin^2 \Theta_1 - n_2^2\right)^{1/2}} \tag{2.14}$$

where Θ_1 is the incident ray angle with the normal to the n_1/n_2 (core/cladding) interface, and λ is the wavelength of light (Place *et al.*, 1985). Penetration depths are typically 50 to 1000 nm for visible light ($d_p<\lambda$), thus the EW is able to interact with many monolayers at the surface of the probe (Lave *et al.*, 1991).

If the cladding is stripped and a substrate (such as a ligand) immobilized on the core, the EW travels through this layer into the sample medium. Reactions occurring very close to the interface perturb the evanescent field and the change in signal can be related to the amount of binding between the target and immobilized ligand at the interface. The measured parameter may be absorbance, fluorescence, or refractive index.

2.2.1.1 Absorbance

To measure absorbances, the evanescent wave transduction is dependent on the target being an UV-visible chromophore. The light passed along the fiber corresponds with a highly absorbed wavelength. However, because a relatively small percentage of the total light beam interacts in the form of an evanescent wave with the

antibody-antigen complex, a low signal-to-noise ratio is obtained (Byfield and Abuknesha, 1994).

2.2.1.2 Fluorescence

Fluorescent measurements can also be used to monitor the binding events occurring on the surface of optical immunosensors. When light traveling through the optical waveguide excites fluorophores within the evanescent field, the fluorescent signal is propagated back up the fiber and detected by a fluorimeter. By exploiting the detection of fluorescence-emitting labels, specific antibody/antigen immunocomplexation can be monitored. Hirshfeld and Block (1984) demonstrated that evanescent wave sensing excites fluorophores primarily bound to the fiber as opposed to those in the bulk solution. Fluorescent radiation propagates back through the fiber in high order modes. As the fluorescent light enters the cladded portion of the fiber it is susceptible to loss because the higher refractive index of the cladding does not support higher order modes (Ligler *et al.*, 1993). To improve excitation and recovery of the fluorescent signal, Thompson and Villarruel (1991) patented tapered optical fibers. When uncladded fiber is immersed in water, which has a lower refractive index than the cladding, the fiber's modal capacity is increased (Anderson *et al.*, 1996). To efficiently couple the returning fluorescence into propagating modes, the modal capacity of the probe portion must match the cladded portion. Tapering the probe region acts as a mode converter and improves fluorescent signal propagation. These developments when combined with affinity ligand immobilization have led to the development of powerful optical biosensors.

In recent years, success has come to fluorescent biosensors. Immunosensors for a variety of targets have been experimented with, everything from

lipopolysaccharides to Yersinia pestis F1 antigen to Clostridium botulinum Toxin A. A fluorescent-based fiber optic biosensor for the detection of ricin, a potently toxic protein, has been reported to measure levels in the picogram per milliliter range (Narang *et al.*, 1997). To immobilize the anti-ricin IgG on the fiber, two schemes were used: 1) direct immobilization onto the silanized surface using a crosslinker; and 2) avidin coated fibers incubated in biotinylated anti-ricin IgG. Before immobilization of the ligand, the fiber was tapered twice; first, rapidly for modal matching, and second, the distal end was slowly tapered to improve the optical efficiency of collection of fluorescent light (Narang *et al.*, 1997). After the two methods of anti-ricin attachment, the fiber was incubated in varying concentrations of ricin, and then exposed to Cy5-labeled anti-ricin antibody. It was demonstrated that avidin-biotin immobilization prior to the sandwich assay gave a signal response 100-fold greater than for direct immobilization. The linear dynamic range of detection for ricin in buffer using the avidin-biotin chemistry was 100 pg/ml to 250 ng/ml (Narang *et al.*, 1997). The same assay performed in river water gave the limit of detection as 1 ng/ml (Narang *et al.*, 1997). This result is comparable to the results of Poli *et al*. (1994) whom achieved a detection limit of 100 pg/ml in phosphate buffered saline, human serum, and human urine by a colorimetric and chemiluminescence ELISA. With the relatively quick assay time (around 20 minutes), selective and sensitive detection, and simplicity of operation, fluorescent biosensors such as this one show future promise for a variety of applications.

Another fluorescent-based immunosensor under development is the fluorescent capillary fill device (FCFD). It consists of two planar glass plates held apart a distance of 100 μm. A fixed volume of sample enters the gap by capillary

action, thus delivering a highly reproducible volume for each assay. The baseplate functions as an optical waveguide upon which the capture antibody is immobilized. Fluorescently labeled analyte is trapped in a water-soluble matrix on the top plate. Upon filling with sample, the labeled analyte is released and competes with the unlabeled sample analyte for the antibody binding sites. After a fixed incubation period, all fluorophores within the evanescent field are excited directly. Light leaving the optical edge of the baseplate is collected via an aperture and sent to a photodetector. The aperture functions to reject the solution signal arising from unbound fluorophores. Sensitivities of 3 ng/ml and 0.5 ng/ml have been obtained for human chorionic gonadotrophin in serum and estrone-3-glucuronide in urine, respectively (Robinson, 1991).

Several practical problems exist, however. Gap filling with whole blood samples is poor because of the viscosity of blood compared with water, therefore, incubation time increases due to slow dissolution of the labeled analyte matrix. Measurement in blood is also difficult due to the presence of fluorescent and highly colored molecules, such as hemoglobin (Byfield and Abuknesha, 1994). Despite these shortcomings, the FCFD immunosensor meets many of the clinical market needs. The fixed gap consistently meters the appropriate sample volume, and therefore the assay reaction rate is not limited by the kinetics of diffusion but by the kinetics of antibody/antigen binding. Equilibrium can be reached within five minutes of sample addition (Robinson, 1991). It has been shown to operate in a range of samples, such as serum, plasma, or urine. Additionally, all the reagents needed for the assay are contained within the device, making it appear reagentless.

2.2.1.3 Refractive Index

Optical immunosensors may also be used to monitor refractive index changes within the evanescent field. Biomolecular interaction within the evanescent field increases the surface concentration, which affects the refractive index, and shifts the resonance angle to greater values. The magnitude of the angular shift depends on the mean refractive index change in the probed area (Jönsson and Malmqvist, 1992). The shift can be used to quantify the amount of analyte bound in the evanescent field. Two optical sensors currently on the market that are based on this measurement are surface plasmon resonance and interferometers.

2.2.1.3.1 Surface Plasmon Resonance

Surface plasmon resonance (SPR) is the phenomenon that occurs as the result of total internal reflection of light at a thin metal film-liquid interface. If the light is monochromatic and plain polarized and the interface film is very thin ($<\lambda$), the evanescent wave will interact with free oscillating electrons (plasmons) in the metal film (Paddle, 1996). Energy from the incident light is lost to the metal, resulting in a decrease of reflected light intensity. This reflectance minimum appears in the reflected light at an acutely defined incident angle (resonance angle), which is dependent on the refractive index of the medium close to the metal film surface. Changes in refractive index within the evanescent field result in a shift of resonance angle, defined as an SPR response. When biomolecules are adsorbed or interact with already immobilized molecules within a probed volume, defined by the size of the illuminated area and the evanescent wave depth, an increase in surface concentration occurs and the resonance angle shifts to greater values (Jönsson and Malmqvist, 1992). When used to detect biomolecules, two types of transducers are typically used in SPR. These transducers

are either prisms coated with a thin film of metal, usually gold or silver (~55 nm thick), typically known as the Kretschmann configuration, or metallised diffraction gratings where the metal thickness can be much greater (up to 150 nm thick) (Robinson, 1991).

Initially, the ligands used in SPR-based immunosensors were immobilized directly onto the metal surface by passive adsorption (Cullen and Lowe, 1990). With this approach comes the problem of non-specific binding to the metal surface when the device is presented with complex biological samples such as whole serum. The non-specific binding of proteins, ions or small organic molecules leads to a decrease in the signal-to-noise ratio for an antibody-antigen binding event. Another common problem is the denaturation of the antibody when it is adsorbed onto the metal surface resulting in a decrease in binding efficiency toward the antigen. Additionally, the instability of non-covalent adsorption at the metal surface with respect to leakage of antibody was a problem. Pharmacia (Uppsala, Sweden) has developed a biosensing system based on the SPR phenomenon (BIAcore™) that addresses these concerns. By linking a hydrogel matrix based on carboxy-methylated dextran to the metal surface, the BIAcore™ promotes biological binding by creating a hydrophilic environment, which reduces non-specific binding. The dextran layer also serves as a protector to keep other components from reaching the solution-surface interface. Most importantly, the dextran optimizes the antibody-antigen interaction by providing a flexible, chemically modifiable support of large effective surface area for immobilization of antibodies or antigens (Byfield and Abuknesha, 1994). This allows for much greater control and versatility of immobilization chemistry and also creates a high degree of accessibility for the target molecules by reducing steric hindrance. Under mild denaturing

conditions the sensor is reusable, although care must be taken as not to denature the covalently bound ligand.

The SPR response primarily reflects the concentration of biomolecules in the sensor surface matrix. The BIAcore™ system has detected low concentrations of clinically important substances in whole serum. For example, β2-microglobulin was determined within a detection limit of 1.7-83 nM in eight minutes, and the drug theophylline was detected in mM levels in five minutes in whole serum (Byfield and Abuknesha, 1994).

Another method of increasing the SPR response is to use a matrix that would amplify the change in refractive index properties of the sensor surface-solution interface. Mass labels such as latex nanoparticles have been linked to analytes. The beads amplify the change in refractive index when antibodies bind to the immobilized antigen layer on the sensor surface. This leads to a larger shift in resonance angle. If the specific interactions between the latex-labeled antibodies and the sensor surface are minimal, the signal-to-noise ratio will improve and the sensitivity will increase (Byfield and Abuknesha, 1994).

Although SPR technology demonstrates high sensitivity for a variety of applications, its lack of portability hinders use in field situations. The component alignment necessary to accurately determine resonance angle shifts precludes development of a small, rugged system.

2.2.1.3.2 Interferometers

Similar to SPR, optical interferometers measure refractive index changes due to biomolecular binding on a waveguide surface. When a binding event occurs, water within the evanescent region is displaced by the analyte and the phase of

propagating light is changed. The interferometer's signal is a differential measurement of the phase propagation between two light paths, one acting as reference to the other (Schneider *et al.*, 1997). Both light paths are exposed to the sample, but one path is coated with a specific recognition element. After exposure to the analyte, the light paths are combined to give an interference signal that is referenced to nonspecific binding.

Devices based on optical interferometric techniques are said to give an order of magnitude improvement in detection limits over other types of evanescent wave optical sensors, due to the increased interaction pathlength (Schneider *et al.*, 1997). This translates to an estimated detection capability of 1 pg/mm^2 for bound analyte (Lechuga *et al.*, 1995). The Hartman interferometer is a proprietary integrated optic sensor designed for a variety of biomedical applications (Hartman, 1997). The Hartman configuration couples light from a diode laser into the waveguide film as a single broad beam by means of input gratings fabricated into the optical chip. The light passes through parallel sensing regions on the chip, some of which are coated with specific ligands and some with nonspecific ligands. Integrated optic elements combine the light to create an interference signal. This arrangement allows for multiple analyte monitoring in a single assay, with built-in reference channels for measurement of nonspecific binding.

To demonstrate detection of protein antigens, a direct assay for human chorionic gonadotropin was performed. A detection limit of ~2 µg/L was achieved when a phase response equal to 10% change in signal intensity was used as the detection limit (Schneider *et al.*, 1997). Advances in signal processing can reduce the detection limit at least ten fold, however, nonspecific binding effects will likely

restrain the overall improvement that can be achieved (Schneider *et al.*, 1997). It may also be possible to improve the limit of detection by a sandwich assay using nanoparticle coated secondary antibodies. Gold or latex nanoparticles have the potential to provide a thousand fold amplification in detection and hence serve to improve the sensitivity of the device (Schneider *et al.*, 1997).

2.2.2 Long-Period Gratings

The foundation of the sensing system used in this research is optical fiber gratings. Explicitly, long-period gratings (LPG) are used as fiber optic sensors. Gratings have existed since photosensitivity in optical fibers was discovered by Hill *et al*. in 1978 (Hill *et al.*, 1978). They are well characterized and are used in a variety of high-performance communication and sensing devices. Gratings are fabricated by spatially modulating the refractive index of germanium-doped fibers by a periodic ultraviolet pattern. Gratings selectively reflect or couple light at a particular wavelength. The most common optical grating is the Bragg grating, a short-period grating, where the periodicity is typically less than one micron. Long-period gratings have periodicities of hundreds of microns. Figure 2.2 shows a schematic of the long-period grating. Light is launched into the guided core mode and upon interaction with the grating is converted to different cladding modes. The grating periodicity, Λ, must satisfy the phase matching condition as defined by:

$$\Delta\beta = \beta_{01} - \beta_{cl}^{n} = \frac{2\pi}{\Lambda} \tag{2.15}$$

where β_{01} and β^{n}_{cl} are the propagation constants of the forward fundamental mode and the forward cladding mode of order n, respectively. Using the definition:

$$\beta = \frac{2\pi n}{\lambda} \tag{2.16}$$

where n is the effective mode index, the wavelength reflected by the grating is given by:

$$\lambda_R = 2n\Lambda \tag{2.17}$$

Light in the fundamental guided mode is perturbed by the grating and when the phase matching condition is satisfied (Equation 2.15), power is coupled from one guided mode to another (Hill *et al.*, 1990). The cladding modes are rapidly attenuated due to bends in the fiber and absorption by the polymer jacket surrounding the fiber. This attenuation results in a loss band in the transmission spectrum at distinct wavelengths. The locations of the spectral loss bands are due to differences in effective indices of the guided mode and the corresponding cladding modes (Bhatia, 1996). The coupling wavelength, λ, for a specific resonance band is given by:

$$\lambda = \left(n_g - n_{cl}\right)\Lambda \tag{2.18}$$

where Λ is the grating period, and n_g and n_{cl} are the effective indices of the guided and cladding modes, respectively. Variations in Λ, n_g or n_{cl} will shift the position of the resonance band.

The effective indices of the cladding modes are strong functions of the index of refraction, n, of the medium surrounding the cladding (Bhatia, 1996). Changes in refractive index surrounding the cladding affect propagation in the cladding modes. This is because the coupling wavelength, λ, is dependent on n_{cl} through the phase-matching condition:

$$\lambda = \left(\delta_{n_{eff}}\right)\Lambda \tag{2.19}$$

where Λ is the grating periodicity and δ_{neff} is the differential effective index between the guided and a cladding mode. Any change in n will effectively vary the value of λ. Hence, LPG fibers can be used to sense changes in the refractive index of the medium surrounding the cladding. The shift in resonance band is usually detected with an optical spectrum analyzer and related to the magnitude of refractive index change.

The guided mode is assumed to be well confined to the fiber core, and not influenced by changes in the refractive index of the surrounding medium, due to the large diameter of the cladding (Bhatia, 1996). Therefore, wavelength shifts are related to change in medium index, n, by:

$$\frac{d\lambda}{dc} = \frac{d\lambda}{dn_{cl}} \frac{dn_{cl}}{dc} \tag{2.20}$$

where dn_{cl}/dc is the refractive index increment for the target. A change in the effective index of each cladding mode due to medium index change is dependent on the order of that particular cladding mode (Tran *et al.*, 1996). Hence, shifts in the resonance bands of a grating will be different.

The wavelength shift of the resonance bands increase non-linearly with increasing refractive index of the surrounding medium. The normal operating range of these LPG fibers is 1.0 to 1.444. When the refractive index of the surrounding medium becomes 1.444, the resonance bands disappear since the effective indices of the cladding modes equal that of the surrounding medium. Wavelength shift is an increasing function of the order of the cladding mode for operation in the normal region. Hence, if all modes operate in the normal region, the resonance bands at higher wavelengths will undergo larger shifts with change in surrounding refractive index (Bhatia, 1996). It has been shown that an LPG fiber with Λ=300μm had resonance bands located at 1525.1 nm, 1323.5 nm, 1225.1 nm, and 1165.4 nm for

n=1.0. The overall shifts for these bands from n=1.0 to 1.444 were measured to be -66.9 nm, -19.7 nm, -9.0 nm, and -3.4 nm, respectively. Thus, the values of the minimum detectable refractive index changes are 4.49×10^{-4}, 1.77×10^{-4}, and 1.86×10^{-5} in the range of 1.33-1.398, 1.398-1.426, and 1.426-1.444, respectively (Bhatia, 1996).

Additionally, etching the cladding diameter with hydrofluoric acid serves to enhance the wavelength shift. Spectral shifts for index change from n=1.0 to 1.448 were measured to be -10.69 nm, -19.31 nm, and -40.52 nm for cladding diameters 125 μm, 109.7 μm, and 99.5 μm, respectively, without loss of fiber strength (Bhatia, 1996). Consequently, LPGs can be tailored to operate with the refractive index sensitivity needed for a particular application by altering the grating sensitivity through period changes, etching of the cladding, use of different fibers and varying writing conditions (Bhatia, 1996).

The temperature-sensitivity of LPG arises from the thermal-induced changes in the differential effective index and in the periodicity (Bhatia, 1996). Fibers can be designed that counterbalance the material and waveguide contributions for specific cladding modes resulting in temperature insensitivity. A grating written on a fiber with a special refractive index profile showed a shift of –0.25 nm for a 100 °C variation (Bhatia,, 1996). Temperature-insensitive gratings can be written in standard fibers by using specific periods that operate in the anomalous region. Gratings with Λ=40 μm (which is smaller than the typical values used to obtain bands in the normal region) showed a temperature dependence of -0.18 nm for a 100 °C change (Bhatia, 1996).

Demodulation is accomplished by commercially available software programs that monitor shifts in the resonance bands and display real-time sensorgrams

of the wavelength shift with time. Typically, benchtop optical spectrum analyzers (OSA) are used to evaluate band shift. Light from an LED is launched into the fiber with a long-period grating under perturbation. The spectral shifts are monitored by the OSA and displayed on a desktop computer. Additionally, a scanning Fabry-Perot spectral filter can be used for demodulation of the signal. Again, light is launched to the fiber from an LED and the output displayed on a desktop computer. This Fabry-Perot filter is much smaller in size than the OSA and provides for a portable sensor system.

2.2.3 Affinity Coatings Suitable for LPG Biosensors

Composite affinity films can be engineered to increase the sensitivity of an LPG sensor. By adsorbing a refractive index modifier (e.g. titanium dioxide) onto the LPG surface, the local refractive index can be raised, leading to a higher sensitivity than an unmodified LPG sensor.

2.2.3.1 Titanium Dioxide Deposition

The response of LPGs to refractive index changes increases non-linearly with refractive index increases in the evanescent field. The minimum refractive index change that can be detected at RI=1.44 ($\sim 10^{-5}$) is an order of magnitude smaller than at 1.33 ($\sim 10^{-4}$). For this reason, it is desirable to operate the LPG at the upper end of the refractive index range. This can be achieved two ways: by altering the refractive index of the sample solution; or by modifying the refractive index of the LPG itself. Increasing the sample solution refractive index can be done with glycerol, however, the viscosity of the solution is inherently increased. This can affect the affinity ligand

efficiency for binding a target. Mass transfer from the bulk solution to the hydrogel layer will also be decreased.

The LPG can be modified with a composite film of titanium dioxide to increase the refractive index. Titanium dioxide is commercially available and has been extensively used in the paint industry because of its ability to efficiently scatter visible light. Titanium dioxide can be deposited onto the fiber from an aqueous solution until the desired surface coverage is achieved. Once adsorbed onto the fiber, the TiO_2 layer can be condensed to yield a stable film. The particles can be silylated and an activated hydrogel attached. Figure 2.3 shows the construction of a high sensitivity affinity ligand film with LPG surface modification by titanium dioxide. As reported in this thesis, the titanium dioxide particles are silylated and activated dextran attached, followed by ligand immobilization. Figure 2.4 shows the signal shift to higher wavelengths upon increasing the local refractive index of the sensor. Fibers coated with dextran only have an average refractive index of approximately 1.33. A titanium dioxide composite film raises the local refractive index to approximately 1.42, consequently shifting the wavelength of the resonance band as much as 70 nm. By modifying the LPG refractive index in this manner, the sensor can achieve optimum sensitivity without altering the sample.

2.2.3.2 Binding Predictions

The following equation (Jönsson and Malmqvist, 1992) relates the film thickness and refractive index change, detected by SPR, to surface concentration of target protein:

$$\Gamma = \frac{d\Delta n}{dn/dc} \tag{2.21}$$

where Γ is the surface concentration (ng mm^{-2}), d is the mean thickness of the protein-dextran layer (nm), Δn is the change in refractive index, and dn/dc is the refractive index increment of the protein (mL g^{-1}). Experimental results have shown that the refractive index increment for proteins is constant up to high concentrations (De Feijter *et al.*, 1978). The dn/dc for proteins is estimated to be 0.18 mL g^{-1} (Stenberg *et al.*, 1991). The surface concentration of the protein ($\Gamma_{protein}$) is calculated from a given protein concentration ($C_{protein}$) by:

$$\Gamma_{protein} = C_{protein} \times d \tag{2.22}$$

where d is the layer thickness (Stenberg *et al.*, 1991). Combining the previous two equations gives the concentration of protein in the hydrogel layer:

$$\Delta n = \left(\frac{dn}{dc} \right)_{protein} \times C_{protein} \tag{2.23}$$

A sensitivity of $\Delta n \approx 10^{-4}$ would correspond to $C_{protein} \approx 6 \times 10^{-4}$ g/mL.

The surface concentration of adsorbed target protein can be calculated for a range of hydrogel film thickness once $C_{protein}$ in the gel is known. Normalizing $C_{protein}$ to surface coverage gives an estimate of sensitivity based on total mass captured. The optical fiber used for the LPG biosensors has a diameter of 120 μm, and the grating is approximately 10 mm in length. Table 2.1 shows the calculated surface concentration of target protein for two polymer films, assuming a sensitivity of $\Delta n \approx 10^{-4}$.

Table 2.1 Surface coverage of target protein based on the concentration of mass captured. Calculations are based on a fiber diameter of 120 µm and a grating length of 10 mm, resulting in an adsorptive surface area of 4 mm^2.

Film Thickness (nm)	Mass of Adsorbed Target (pg)	Surface Coverage of Target (pg/mm^2)
100	210	56
500	1000	280

SPR measurements for a 100 nm-thick dextran hydrogel layer report that the minimum detectable surface concentration of protein was estimated to be 50 pg/mm^2 on an active surface area of 1 mm^2 (Stenberg *et al.*, 1991). Thus, the normalization of adsorbed target concentration to surface coverage is equivalent between an SPR device and an LPG sensor for a given polymer film thickness.

With an estimate of adsorbed target protein concentration the concentration of required affinity ligand can be calculated:

$$C_{ligand} = \frac{C_{protein}}{\varepsilon MW_{protein}} \tag{2.24}$$

where ε is the efficiency of protein capture by the ligand. Depending on the functionality after ligand immobilization, capture efficiency may be between 20% and 60% (Subramanian *et al.*, 1994). A conservative estimate of required affinity loading (ε = 0.2) gives $0.2 - 3 \times 10^{-7}$ moles/mL of ligand for the range of MW_{target} 10 to 155 kDa. With a binding efficiency of ε = 0.6, the affinity ligand loading range is $0.6 - 9 \times 10^{-8}$ moles/mL.

Based on ligand concentration, the amount of bound target can be calculated. With a predicted sensitivity, the change in refractive index for the

hydrogel-target layer and wavelength speak shift can also be determined. It has been estimated that LPG sensitivity to change in refractive index is $\lambda\ 10^{-4}$. Using this prediction, the amount of target bound can be estimated for a variety of ligand concentrations, various target-ligand binding stoichiometries, and binding efficiencies. Table 2.2 shows binding predictions for the model system of anti-BSA IgG binding to BSA. The calculations are based on the assumption that the affinity coating occupies the full evanescent field and that the evanescent field is of uniform strength. Additional binding predictions for anti-BSA IgG/BSA, lipopolysaccharide/polymyxin B, and anti-β-galactosidase/β-galactosidase can be found in the Appendix.

Table 2.2 Estimates of anti-BSA IgG (MW = 155 kDa) binding to LPG BSA (MW = 68 kDa) biosensor in a 100 nm thick hydrogel with an LPG surface area of 4 mm^2, assuming a capture efficiency of 20% and a sensor sensitivity of approximately 10^{-4}.

Ligand Conc. (mg/mL)	Ligand Present (g)	Ligand Present (moles)	Target/ Ligand Stoic.	Target Bound (moles)	Target Bound (g)	Target Film Conc. (mg/mL)	ΔRI	Shift Observed (nm)
1	4E-10	6E-15	1	1E-15	2E-10	5E-04	8E-05	0.8
10	4E-09	6E-14	1	1E-14	2E-09	5E-03	8E-04	8
20	8E-09	1E-13	1	2E-14	3E-09	9E-03	2E-03	16
1	4E-10	6E-15	2	2E-15	3E-10	9E-04	2E-04	2
10	4E-09	6E-14	2	2E-14	3E-09	9E-03	2E-03	16
20	8E-09	1E-13	2	4E-14	7E-09	2E-02	3E-03	33

A low resolution spectrometer having a noise threshold of 0.5 nm would be capable of detecting 200 pg of bound anti-BSA, as presented in Table 2.2. The

same calculations can be made for a high resolution spectrometer with a sensitivity of approximately 10^{-6}.

Table 2.3 Estimates of anti-BSA IgG (MW = 155 kDa) binding to LPG BSA (MW = 68 kDa) biosensor in a 100 nm thick hydrogel with an LPG surface area of 4 mm^2, assuming a capture efficiency of 20% and a sensor sensitivity of approximately 10^{-6}.

Ligand Conc. (mg/mL)	Ligand Present (g)	Ligand Present (moles)	Target-Ligand Stoic.	Target Bound (moles)	Target Bound (g)	Target Film Conc. (mg/mL)	ΔRI	Shift Observed (nm)
0.01	4E-12	6E-17	1	1E-17	2E-12	5E-06	8E-07	0.8
0.10	4E-11	6E-16	1	1E-16	2E-11	5E-05	8E-06	8
0.20	8E-11	1E-15	1	2E-16	3E-11	9E-05	2E-05	16
0.01	4E-12	6E-17	2	2E-17	3E-12	9E-06	2E-06	2
0.10	4E-11	6E-16	2	2E-16	3E-11	9E-05	2E-05	16
0.20	8E-11	1E-15	2	4E-16	7E-11	2E-04	3E-05	33

A high resolution spectrometer having a noise threshold of 0.03 nm would be quite capable of detecting all wavelength shifts in Table 2.3. With a high sensitivity device, as little as 2 pg of bound material would elicit a large wavelength shift. While the data presented in Tables 2.2 and 2.3 show the same wavelength shifts, it must be realized that a low sensitivity sensor system would barely register a shift corresponding to binding 200 pg of target. A sensor system with high sensitivity can detect 2 pg of bound material with a signal about 60 times greater than the noise threshold.

An increase in sensor sensitivity can be achieved by either improving the LPG sensor element, demodulation procedure or spectrometer, or by optimizing the

affinity adsorption of target. The former is accomplished through advances in electric engineering, while the latter is improved by developing high sensitivity films.

The affinity film can be tailored to take advantage of the entire evanescent field to increase the mass of bound target. A balance must be found so that the thickness of the hydrogel does not interfere with sample transport to the ligands. Additionally, the ligand density must be optimized to avoid hindering mass transport due to steric hindrance imposed by a high density of ligands on the outer fringe of the gel. Choosing affinity ligands with low dissociation constants, and engineering the hydrogel to control the hydrophilicity/hydrophobicity and immobilization orientation will increase the binding between target and ligand.

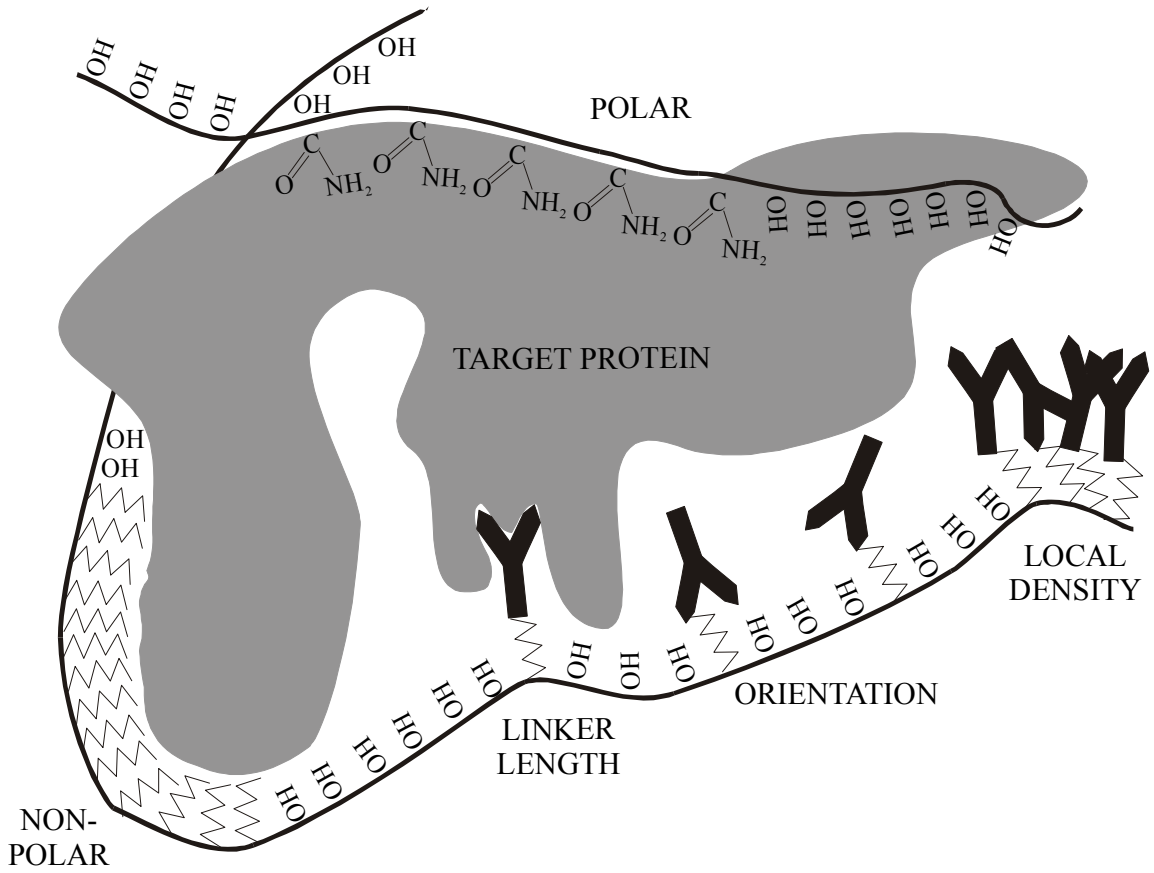

Figure 2.1 Interaction between target protein and polar/non-polar regions created within the affinity ligand hydrogel.

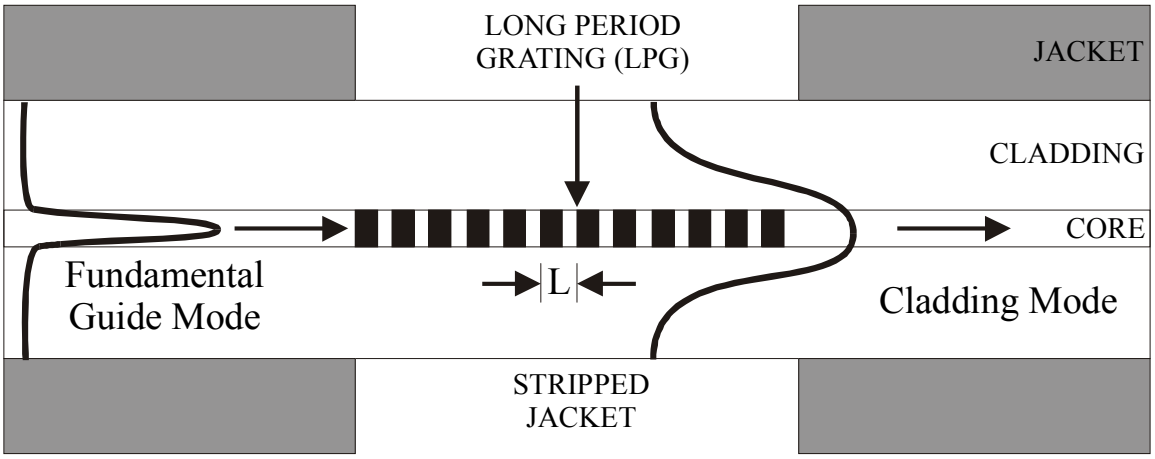

Figure 2.2 Operational principle of long-period gratings showing the coupling of light from the forward fundamental guided mode to the cladding modes. Periodicity of the grating is L.

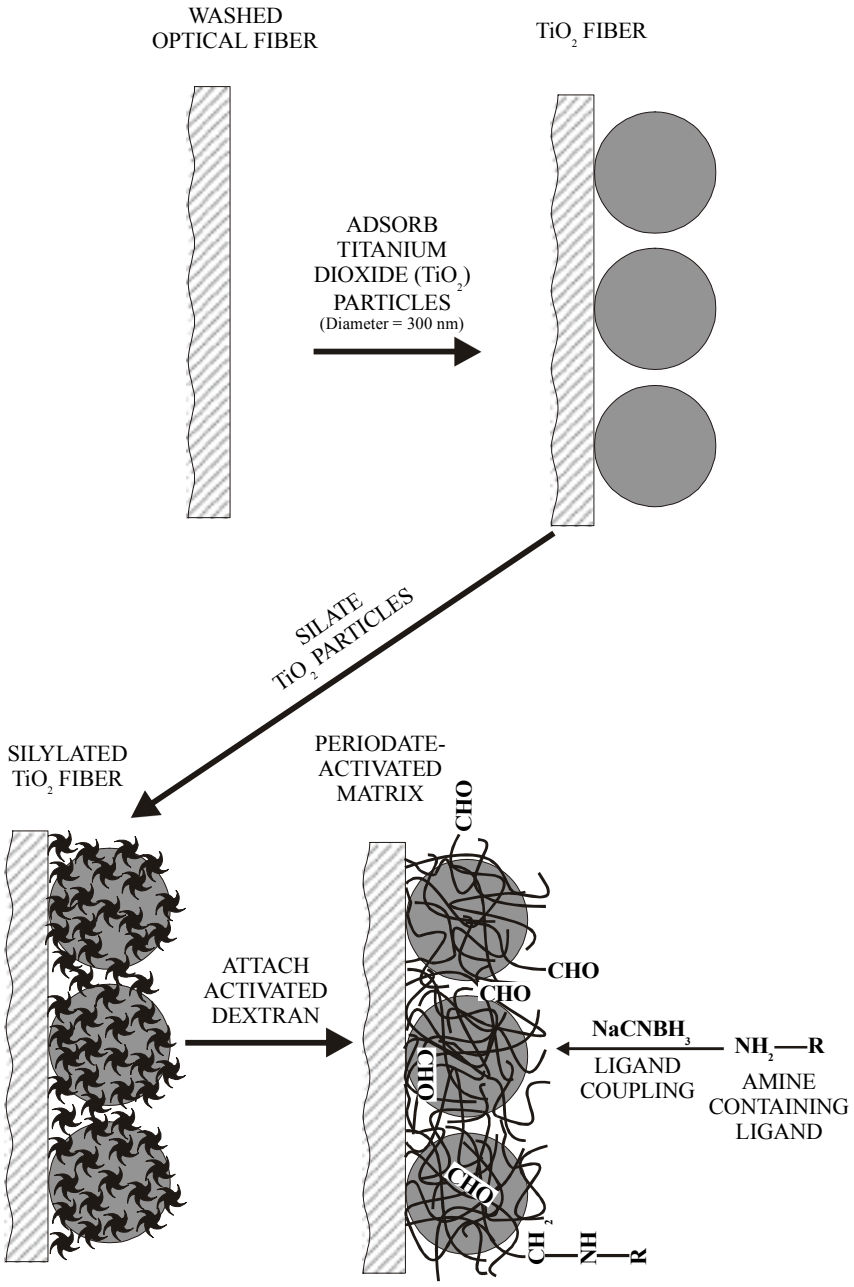

Figure 2.3 Construction of a high sensitivity affinity ligand film with LPG surface modification by titanium dioxide, attachment of aldehyde-activated dextran to the silylated TiO_2 layer, and ligand coupling by reductive amination.

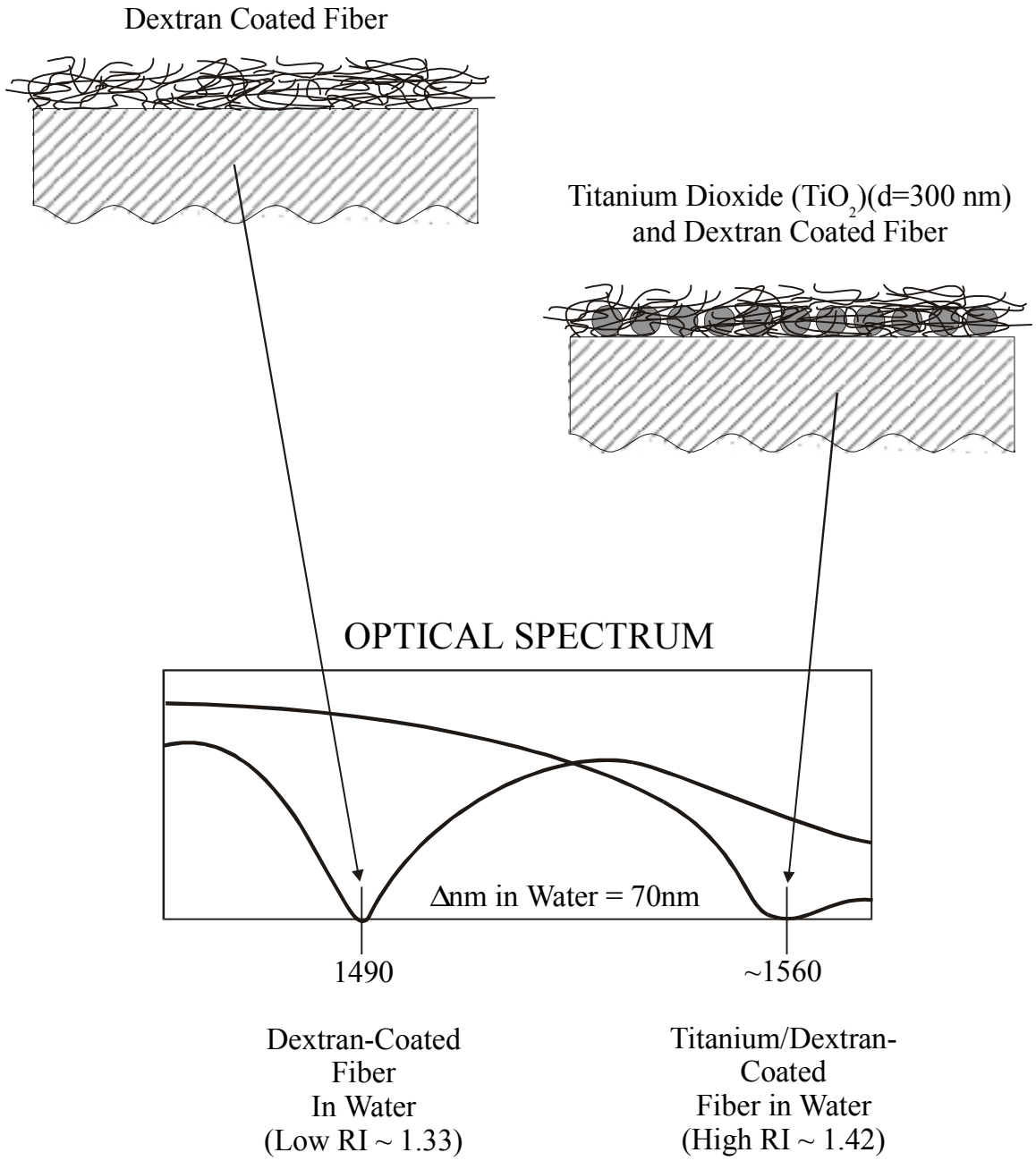

Figure 2.4 Resonance band shift due to an increase in local refractive index induced by a titanium dioxide composite film as compared to only a dextran film.

Chapter 3

MATERIALS AND METHODS

3.1 Materials

The Long Period Grating (LPG) optical fiber, light source, Optical Spectrum Analyzer (OSA), and Fabry-Perot spectrometer (Queensgate Instruments, Bracknell, UK) were supplied by Fiber & Sensor Technologies (Blacksburg, VA). Titanium dioxide was DuPont Ti-Pure® (Wilmington, DE) and Nanophase NanoTek® (Romeoville, IL). DuPont Ti-Pure® is rutile titanium dioxide with an Al_2O_3 surface treatment, and an average particle size of 300 nm. Nanophase NanoTek® titanium dioxide is ≥ 80% anatase, has no chemical surface treatment, and an average particle size of 28 nm. Methanol, acetone, and ethanol were HPLC grade purchased from Fisher Scientific (Pittsburgh, PA). Glycerol was also purchased from Fisher. All tubing used for pumping or as fiber holder parts was Masterflex viton tubing, size 14 (Cole Parmer, Vernon Hills, IL). All pumping was done with a Masterflex peristaltic pump. Dextran T500 was purchased from Pharmacia Biotech (Uppsala, Sweden). Type I distilled deionized water was produced by a Nanopure Barnstead system (Dubuque, IA). Dialysis was done using Pierce Snake Skin dialysis tubing (Rockford, IL). Cellulose CF-11 was provided by Dr. Kevin Van Cott (Virginia Tech, Blacksburg, VA). Aminopropyl silane, sodium periodate, sodium azide, sodium cyanoborohydride, ethanolamine, potassium phosphate (monobasic and dibasic), sodium thiocyanate, glycine, triethylamine, sodium carbonate, tris-hydrochloride,

sodium chloride, and Tween 20 were purchased from Sigma (St. Louis, MO). Bovine serum albumin, rabbit anti-bovine serum albumin (whole serum), goat serum, rabbit anti-cholera toxin (whole molecule), and goat anti-rabbit immunoglobulin horseradish peroxidase were also purchased from Sigma. Acetic acid and sulfuric acid came from Fisher Scientific. Porcine casein was provided by Dr. Arthur Degener (Virginia Tech, Blacksburg, VA). Immulon II microtiter plates were purchased from Fisher Scientific. O-Phenylenediamine-2HCl tablets were purchased from Abbott Laboratories (Chicago, IL). ELISA plates were read with a Bio-Tek Microplate reader Model EL 308 (Bio-Tek Instruments, Inc., Winooski, VT). The syringe filters were Anotop10 inorganic membrane filters with a diameter of 10 mm from Whatman (Fisher, Pittsburgh, PA). A DynaPro-801 Dynamic Light Scattering Instrument purchased from Protein Solutions Incorporated (Charlottesville, VA) was used for size measurements. Data analysis of DLS measurements was done using Auto Pro software. Environmental scanning electron microscopy images were taken on an ElectroScan E-3 ESEM by Mr. Brian Sines (Virginia Tech, Blacksburg, VA). Refractive indices were measured on an Abbe refractometer Model 60/ED (Bellingham & Stanley LTD., Atlanta, GA). Viscosity measurements were made with a Brookfield Digital Viscometer Model DV-II (Brookfield Engineering Laboratories, Inc., Middleboro, MA).

3.2 Biosensor Production

3.2.1 Titanium Dioxide Coating of Fibers

To increase the index of refraction of the fiber, DuPont Ti-Pure® titanium dioxide (TiO_2) was adsorbed onto the grating area. The LPG region was

cleaned by wiping five times each with a Kimwipe wetted with methanol followed by acetone. The fiber was carefully situated in the holder and the end fittings tightened. A recycle loop was set up between the fiber holder and a magnetically stirred beaker. To monitor the peak wavelength, one end of the fiber was connected to the light source and the other to the OSA, making sure that the LPG region within the holder remained straight and taut. First, the fiber's baseline peak was found in distilled, deionized water (DDW). A two percent (w/v) TiO_2 solution was made by adding 1.0 g of TiO_2 to 50 mL of DDW and stirring vigorously for one to two minutes until all aggregates were dispersed. The TiO_2 solution was recirculated through the fiber holder at 5 mL/min until a peak shift of 40 to 60 nm was achieved. If necessary, additional TiO_2 was added in 0.5 g amounts to drive the titanium adsorption onto the fiber. When the fiber's peak reached the appropriate shift, the recirculation tubing was unhooked and the feed end was placed in a clean beaker of fresh DDW. The DDW was pumped through the holder at 5 mL /min for two to three minutes until the excess TiO_2 was washed out of the holder and the peak wavelength stabilized. Unless stated otherwise, it can be assumed that all solutions were pumped through the fiber holder at 5 mL/min. Then a clean beaker of dry methanol was pumped through the holder for two to three minutes until the wavelength re-stabilized. The holder was drained and 2 mL of a 2% aminopropyl silane (APS) (v/v) in methanol solution pipetted into the holder. The holder ends were closed and the fiber incubated for one minute in the APS solution. The holder was then drained and rinsed with 2 mL of methanol, drained again, and dried overnight at room temperature with the holder ports open. After drying, DDW was pumped through the holder and the peak recorded, this gave the overall shift due to TiO_2 adsorption on the fiber surface.

3.2.2 Dextran-Aldehyde Activation and Attachment

To provide a flexible area for ligand attachment, a hydrogel layer was put over the TiO_2 film. A 10% dextran solution was made by dissolving 10 g of Dextran T500 in 100 mL of DDW and put on a rotator overnight at room temperature. To the dissolved dextran, 6.42 g of sodium periodate ($NaIO_4$) was added and the mixture rotated at room temperature for one hour. To quench the reaction, 4.5 mL of glycerol was added and again rotated for one hour. Next, the dextran-aldehyde solution was dialyzed against 2.5 L of DDW in 6,000-8,000 molecular weight cut-off (MWCO) tubing. The DDW was changed after an hour of magnetically stirred dialysis for a total of five cycles. The size of the dextran polymer was measured on a Dyna-Pro 801 Molecular Sizer. A 1:50 dilution in DDW was made and then filtered through a 0.2 µm syringe filter. After size analysis, sodium azide was added to give 0.02% and the dextran-aldehyde solution stored at 4 °C.

Hydrogel attachment onto the TiO_2-coated LPG was accomplished by incubating the fiber in a mixture of 0.5 M sodium cyanoborohydride ($NaBH_3CN$):dextran-aldehyde (1:10) for two hours at room temperature. Following a DDW wash, the fiber was ready for ligand attachment.

3.2.3 Ligand Immobilization

For the purpose of this research, bovine serum albumin (BSA) and anti-BSA IgG were chosen as the ligand and target, respectively. Bovine serum albumin was immobilized on the LPG surface with cyanoborohyride chemistry. Sodium cyanoborohydride (0.5 M $NaBH_3CN$) was mixed 1:10 with 10 mg/mL of BSA and injected into the fiber holder. The fiber was incubated in the ligand for 18 hours at room temperature. Following a DDW wash, any residual active groups were blocked

with 1 M ethanolamine, pH 9.0 for 30 minutes at room temperature. After a final DDW wash, the fiber was stored in 0.1 M potassium phosphate buffer (KPO_4), pH 7.2 at room temperature.

3.2.4 Hydrogel Crosslinking with Cellulose

On some fibers, 1% cellulose was used as a cross-linker to add stability to the TiO_2/polymer/antibody film. First, the holder was drained of all liquid, then 1 mL of 1% cellulose in dimethyl acetamide/lithium chloride (DMAC/$LiCl_2$) was injected and incubated for approximately 20 seconds. Next, the cellulose was withdrawn from the holder by a pipette and then three injections of 1 mL each of ethanol:DDW (80:20) were slowly passed through the holder. Finally, the fiber was washed with DDW and stored in phosphate buffer.

3.2.5 The Fiber Holder

The device used to securely hold the fiber and protect the sensing area is shown in Figure 3.1. The LPG region was placed within a one-inch long piece of Tygon tubing (identified as "8" in Figure 3.1) and the ends fitted with short pieces of Masterflex size 14 tubing. These end pieces held the fiber in place and prevented any fluid leakage from the chamber. T-connectors were placed on either side of the LPG chamber to serve as solvent ports; both attached to pieces of Masterflex size 14 tubing, one being pumped from the solvent reservoir and the other leading to the waste container. All other connectors and end pieces were made of chemical resistant nylon and could easily be loosened so that the fiber could be pulled from the holder and either wiped clean or discarded.

3.2.6 OSA and the Light Source

Figure 3.2 is a schematic diagram of the Optical Spectrum Analyzer (OSA) and the connections between the light source and the fiber. One end of the optical fiber was connected to a light source while the other end connected to the OSA. The fiber holder was clamped to a ring stand in a vertical position. Solvents were pumped from a reservoir to the fiber holder by a peristaltic pump, entering the holder by the bottom port. The top port of the holder led to a waster container or was recycled back to the solvent reservoir if necessary. Manual sample injection was done by disconnecting the bottom port to the solvent reservoir and directly pipetting the sample into the LPG chamber. When incubating the sample in the chamber during target detection experiments, the top and bottom ports were connected together to prevent fluid from leaving the chamber.

3.3 Experimental Procedures

3.3.1 Initial Recycling

After deposition of TiO_2, hydrogel attachment, and ligand immobilization, each fiber underwent stability testing. Stability of the TiO_2/dextran/ligand film was tested by ten continuous cycles of 2 M sodium thiocyanate (NaSCN) and 0.1 M glycine/2% acetic acid (HAC), pH 2.5 with a phosphate buffer rinse after each step. Each solution, including the rinse step, was pumped for 2 to 3 minutes at 5 mL/min. In some cases, an additional recycle step of 0.1 M triethylamine (TEA), pH 11.5 was also included, and is noted when appropriate.

3.3.2 Target Detection

Prior to target exposure, a baseline wavelength reading was taken in either phosphate buffer and/or glycerol-phosphate buffer. After the reference measurement, the LPG portion of the fiber was exposed to a 1:100 dilution of rabbit anti-BSA IgG (whole serum), which is approximately 20 μg/mL, for 5 minutes. If target exposure was to occur under static conditions, 1 mL of the anti-BSA IgG solution was pipetted into the fiber holder and the ports closed. If the exposure was to occur under flow conditions a recycle loop was set up from a polypropylene test tube containing 4 mL of the antibody solution to the holder and back to the sample tube. The target solution was then drained from the holder and the fiber washed in either phosphate buffer or glycerol-phosphate buffer. Peak shift was determined by the change in wavelength before and after antibody exposure. Regeneration of the immobilized ligand followed the procedure outlined below in section 3.3.4. The cycle of target exposure followed by ligand regeneration was repeated as desired, making sure that at the conclusion of the experiment the fiber was stored in phosphate buffer.

3.3.3 Negative Controls

Two negative controls were tested, goat serum and rabbit anti-cholera toxin (whole molecule). Phosphate buffer and glycerol-phosphate buffer were pumped through the holder for 3 to 5 minutes each until a stable baseline was achieved. Four milliliters of a 1:100 dilution of goat serum in phosphate buffer were recycled through the holder. The peak wavelength was recorded and the holder drained. The final baseline reading was taken after washing the fiber with phosphate buffer and glycerol-phosphate buffer. One regeneration cycle of 2 M NaSCN, phosphate buffer, and 0.1 M glycine/2% HAC (2 minutes each) was done. A new baseline in phosphate buffer

and glycerol-phosphate buffer was obtained. Four milliliters of a 1:100 dilution of rabbit anti-cholera toxin (whole molecule) in phosphate buffer was recycled through the holder. Again, the final baseline reading was taken after washing with phosphate buffer and glycerol-phosphate buffer. A final regeneration step of 2 M NaSCN, phoshphate, and 0.1 M glycine/2% HAC was done. The fiber was brought back into phosphate buffer and stored.

3.3.4 Regeneration

Regeneration of the fiber ligand after exposure to samples consisted of stripping the antibody from the attached antigen by exposure to isothiocyanate and low pH. Unless otherwise stated, the following procedure was used. It can be assumed that each solution was pumped through the fiber holder at 5 mL/min for 2 to 3 minutes. Following the post-exposure phosphate buffer reading, the LPG region was washed with 2 M NaSCN. Before changing to a low a pH solution, the holder was thoroughly rinsed with phosphate buffer. After sufficient rinsing, the LPG was washed again with 0.1 M glycine/2% HAC. Again, the holder was thoroughly rinsed with phosphate buffer to remove any traces of the regenerate solution. Occasionally, additional solutions were added to the process; 4 M sodium chloride (NaCl) and 0.1 M TEA, pH 11.5 were used periodically to test their effect on regeneration efficiency. If either of these regenerates were used, it is noted when discussing the results.

3.3.5 Recovery of Bound Anti-BSA from Fiber

Following the target detection scheme outlined in section 3.3.2, the fiber was exposed to 1:100 dilution of rabbit anti-BSA (approximately 20 μg/mL) for 5 minutes under recycle conditions. Bound antibody was eluted by pipetting enough 2

M NaSCN to fill the holder and letting it sit for 2 minutes. The solution was withdrawn from the holder and put into a microcentrifuge tube that had been coated with 1% porcine casein in phosphate buffer. This process was repeated ten times, after which each aliquot was brought up to 0.5 mL with 2 M NaSCN. The ten tubes were then combined and dialyzed in 10,000 MWCO dialysis tubing against 500 mL DDW. The water was changed four times and the remaining dialyzed solution fractionated back into the ten original casein coated tubes, which had been rinsed with DDW. The tubes were frozen at -90°C and lyophilized overnight to dryness. The ten tubes were rehydrated with phosphate buffer to give a total of 1.5 mL of "affinity purified" anti-BSA.

3.3.6 Estimation of Anti-BSA from Fiber Elutions

An enzyme-linked immunosorbent assay (ELISA) was used to measure the amount of anti-BSA eluted from the target binding runs. Immulon II microtiter plates were coated overnight with 100 μL/well of 1 ng/mL bovine serum albumin in 50mM sodium carbonate ($NaHCO_3$), pH 9.6 at 4°C. Wells were then washed three times with 12.5 mM Tris- HCl, 50 mM NaCl, 0.05% Tween 20, pH 7.2 (TBST), and blocked with 12.5 mM Tris-HCl, 50 mM NaCl, 1% casein (TBS-casein) for 30 min at room temperature. Six serial ten-fold dilutions of 2 mg/mL rabbit anti-BSA (whole serum) in phosphate buffer and elution samples from Section 3.3.5 were added in triplicate (100 μL/well) and incubated at 37°C for 60 minutes. Wells were washed seven times with TBST and the anti-BSA detected by the addition of 1:1000 goat anti-rabbit immunoglobulin (IgG) horseradish peroxidase (HRP) conjugate incubated at 37°C for 30 minutes. Wells were again washed seven times with TBST and the bound chromophore detected with o-Phenylenediamine (OPD) substrate. The reaction was

stopped with 100 µL/well of 3 M sulfuric acid (H_2SO_4) and absorbance measured at 490 nm using an EL308 Bio-Tek Microplate reader.

3.3.7 Exposure of "Affinity Purified" Anti-BSA to Fiber

The "affinity purified" antibody eluted from the fiber was re-exposed to the fiber. After ELISA quantification, the "affinity purified" anti-BSA was brought up to 4 mL in phosphate buffer and recycled through the holder at 5 mL/min. It was noticed that after 10 minutes of recycling, the peak shift was very small, therefore, the "affinity purified" anti-BSA was circulated for an additional 20 minutes. The initial and final baseline peaks were found in phosphate buffer and the fiber regenerated with 2 M NaSCN and 0.1 M glycine/2% HAC, as described in section 3.3.4.

3.3.8 Dynamic Light Scattering (DLS) Measurements

Light scattering measurements of the dextran-aldehyde hydrogel matrix were done on a DynaPro-801 Dynamic Light Scattering Instrument. The DLS was washed with 2 mL of DDW through a 0.2 µm syringe filter until a photon count rate of 5000 was obtained. Dextran-aldehyde samples were diluted 1:50 in DDW and 500 µL injected through a 0.2 µm syringe filter. AutoPro software was used to derive the hydrodynamic radius from the translational diffusion coefficient of the molecules in the sample cell from the scattered light intensity data of the DLS.

3.3.9 Environmental Scanning Electron Microscope (ESEM)

Fiber images were collected with an ElectroScan E-3 ESEM. A one centimeter section of fiber from the region of interest was mounted on the sample stage with double-sided transparent tape. The chamber closed and pictures taken at various magnification as the chamber pressure was increased from 5 torr to 10 torr. To

burn a spot in the fiber film, magnification was increased to 10,000 for 2 minutes. To view the burnt area, magnification was decreased and chamber water pressure dropped to 5 torr. A slow increase in water pressure to 10 torr allowed the dextran film to hydrate, thus revealing the burnt area. Estimation of hydrogel layer thickness was made by comparing the thickness to the size of embedded TiO_2 particles of known diameter.

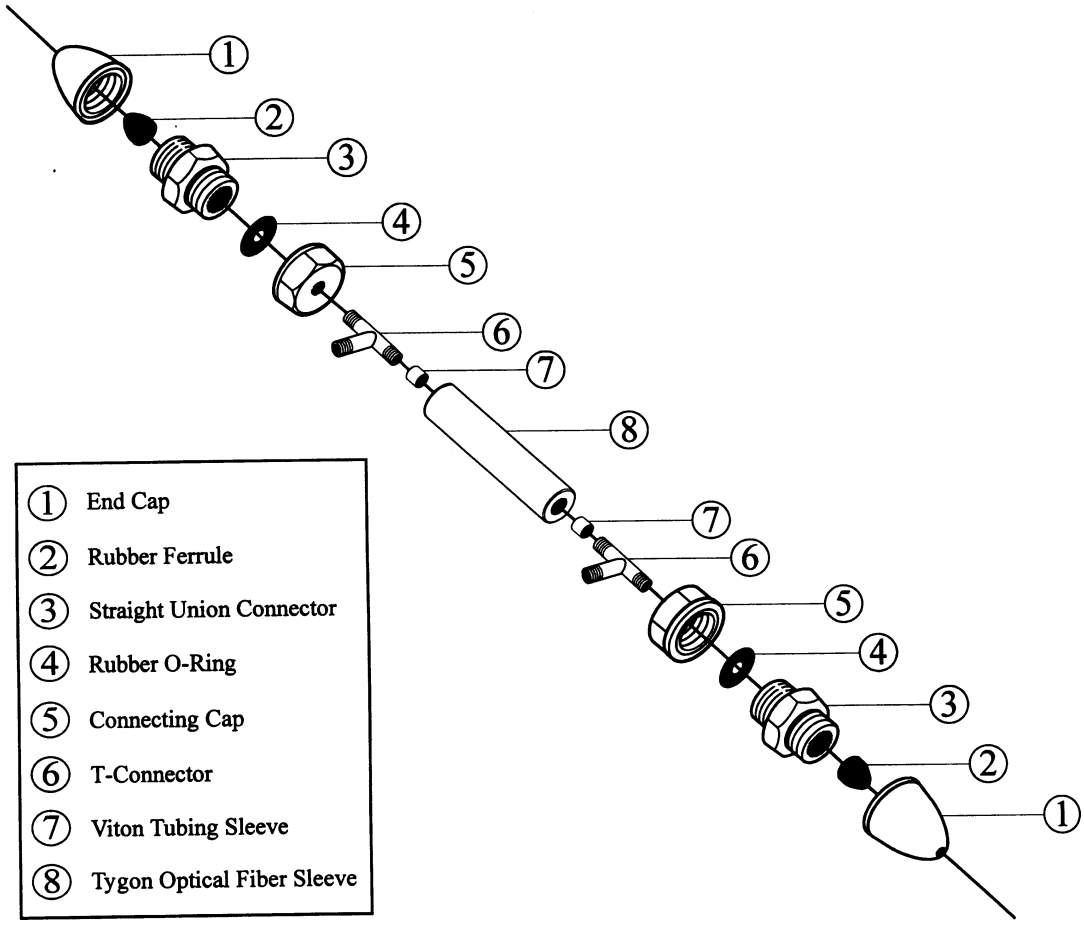

Figure 3.1 Detailed diagram of an LPG sensor element holder.

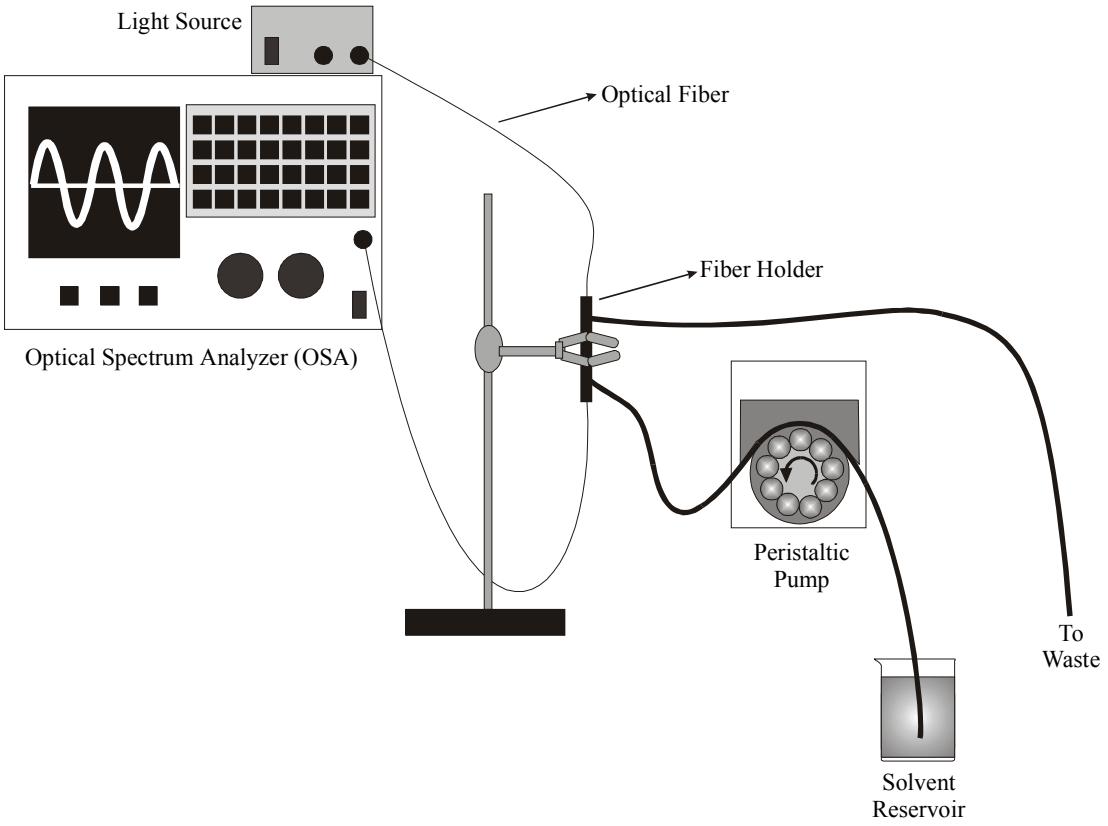

Figure 3.2 Schematic diagram of the experimental setup including the OSA, LPG sensor element, and pumping system.

Chapter 4

RESULTS AND DISCUSSION

4.1 Refractive Index Measurements

4.1.1 Refractive Index of Glycerol Solutions

In order to establish sensitivity curves for the LPG fibers, refractive index measurements of glycerol solutions first needed to be taken. The refractive index of these solutions is linearly dependent on the percent by volume of glycerol and can be calculated by the following equation:

$$n = \left(y_{glycerol} \times 1.475\right) + \left(y_{water} \times 1.333\right) \tag{4.1}$$

The calculated refractive indices were checked by comparing them to measured indices from a refractometer (Abbe refractometer Model 60/ED). The close correlation between the calculated and measured refractive indices is shown in Table 4.1

Table 4.1 Refractive indices of glycerol-water solutions, calculated from Equation 4.1 and measured with a refractometer.

% Glycerol	Calculated RI	Measured RI	% Difference
0	1.333	1.331	-0.15
30	1.376	1.376	0.00
50	1.404	1.405	0.07
60	1.418	1.419	0.07
70	1.432	1.433	0.07
72.5	1.436	1.437	0.07
75	1.440	1.442	0.14
77.5	1.443	1.444	0.07
80	1.447	1.445	-0.14

Once the refractive indices of the glycerol solutions were established, the response of the LPG fibers to changes in index of refraction was tested. Fiber response to changes in refractive index was determined by exposing the fibers to a range of glycerol solutions and monitoring the wavelength change of the fibers' peak on the Optical Spectrum Analyzer (OSA). The sensitivity curves of three fibers, whose initial peak wavelengths vary over a 100 nm range, and whose curves are characteristic of fibers that start around that same wavelength, are shown in Figure 4.1. The results show that fibers whose initial peak occurs at a lower wavelength exhibit a greater change in peak wavelength at lower refractive indices than do fibers whose initial peak is at a higher wavelength. Based on these results, fibers with lower initial wavelengths would be preferred because they would have a greater sensitivity for target detection. To bring the fiber into the sensitive part of the curve, the steep region, the refractive index at the LPG sensing area ideally needed to be around 1.44. It was undesirable to use 75% glycerol solutions to detect target binding, therefore the

refractive index of the fibers needed to be modified by other means. Detection in 75% glycerol was undesirable for two reasons. First, an environment concentrated with glycerol will be very viscous, and may inhibit complex formation between target and ligand. Secondly, a stable baseline on the OSA was not achieved with 75% glycerol. Figure 4.2 shows the unstable baseline of 75% glycerol. Over a ten minute time frame, the baseline in 75% glycerol varied between 1554.9 nm and 1555.9 nm. Any small change in temperature or concentration gradient throughout the glycerol solution alters the refractive index and was reflected by a change in peak wavelength. To avoid using high percent glycerol solutions, titanium dioxide was chosen as a refractive index modifier.

For the purpose of this research, sensitivity is defined as the ability of the fiber to exhibit large peak wavelength shifts upon small refractive index changes. The sensitivity can be expressed by the equation:

$$S = \frac{\Delta RI}{\Delta nm} \tag{4.2}$$

A refractive index of 1.44 within the LPG area corresponds to a sensitivity of 1×10^{-4}. Table 4.2 shows the increasing sensitivity that accompanies an increasing refractive index within the sensing region of three fibers.

Table 4.2 Typical experimental RI sensitivities for three blank LPG sensor elements calculated from Equation 4.2, peak wavelength shifts measured with an OSA.

RI of glycerol Solutions	RI/nm for Fiber 331-7	RI/nm for Fiber 331-6	RI/nm for Fiber 313-2
1.376	2.4E-03	2.6E-03	3.3E-03
1.404	1.1E-03	1.3E-03	1.6E-03
1.418	6.6E-04	7.3E-04	8.9E-04
1.432	3.8E-04	4.3E-04	5.2E-04
1.436	3.0E-04	3.1E-04	2.8E-04
1.440	1.8E-04	1.8E-04	2.0E-04
1.443	1.2E-04	1.2E-04	1.4E-04

4.1.2 Refractive Index of Titanium Dioxide Solutions

Titanium dioxide has a high refractive index (2.73 for rutile TiO_2 and 2.55 for anatase) and is too opaque to be used with a conventional refractometer. The refractive index of various TiO_2 solutions was calculated by the effective medium approximation (Nagpal and Davis, 1995) and is shown in Table 4.3.

Table 4.3 Refractive indices of TiO_2 (d=28 nm) solutions calculated by the effective medium approximation. Estimated RI values made by correlating the wavelength detected with an OSA for three fibers in each of seven TiO_2 solutions to the corresponding refractive index from each fiber's response curve (Figure 4.1). Percent differences between the estimated and calculated RI values are also shown.

		331-7		331-6		313-2	
% TiO_2	Calc. RI	Est. RI	% Diff.	Est. RI	% Diff.	Est. RI	% Diff.
5	1.373	1.375	0.15	1.375	0.15	1.369	-0.29
8	1.397	1.399	0.14	1.394	-0.22	1.392	-0.36
10	1.414	1.416	0.14	1.412	-0.14	1.411	-0.21
11	1.422	1.423	0.07	1.420	-0.14	1.419	-0.21
12	1.431	1.431	0.00	1.429	-0.14	1.427	-0.28
12.5	1.435	1.435	0.00	1.434	-0.07	1.433	-0.14
13	1.439	1.441	0.14	1.439	0.00	1.440	0.07

Response curves for fibers in various TiO_2 solutions are shown in Figure 4.3. The curves were determined like the previous glycerol curves shown in Figure 4.1, by monitoring the peak wavelength of various fibers as a function of percent TiO_2 in solution. The titanium dioxide used in the solutions was Nanophase NanoTek® TiO_2 (d=28 nm) because it did not adsorb onto the fiber surface and therefore made it easy to change between solutions.

Fiber responses were calibrated by the glycerol response curves in Figure 4.1 and were used to measure the refractive indices of other solutions. The refractive indices of various titanium dioxide solutions were estimated by matching the peak wavelength of a fiber in different TiO_2 solutions to the corresponding refractive index on each respective response curve. The estimated refractive indices for seven TiO_2 solutions on the three fibers from Figures 4.1 and 4.3 are shown in Table 4.3. A

titanium dioxide solution of 13% has a refractive index of 1.44 and at this point the fiber operates in the region of high sensitivity as shown in Figure 4.3. Also included in the table are the differences between the calculated refractive indices and the estimated values. It is evident from Table 4.3 that once a fiber's response curve has been calibrated against known solutions, the LPG fiber is an accurate tool for measuring the refractive indices of unknown solutions.

One thought was to put the titanium dioxide in solution with the ligand, bovine serum albumin (BSA), for deposition onto the LPG surface. Viscosity tests were performed on TiO_2/BSA solutions to find the maximum amount of BSA that can exist in solution with TiO_2. Figure 4.4 shows the viscosity results for increasing amounts of BSA in a 13% TiO_2 solution. Up to a concentration of approximately 7.5 mg BSA/mL in TiO_2 solution, the mixture had a low viscosity and retained a smooth consistency. Above that, the BSA aggregated the titanium dioxide and the complex fell out of solution. Although BSA can exist in solution with TiO_2 this method was not feasible because Nanophase TiO_2 did not stick to the fiber. A larger diameter TiO_2 from DuPont (d=300 nm) did stick to the LPG surface, so viscosity tests with titanium dioxide/BSA solutions were done with the larger TiO_2. These TiO_2 particles are coated with aluminum oxide (Al_2O_3) and this chemistry did permit adsorption onto the fiber surface. Viscosity tests revealed that at BSA concentrations up to 10 mg/mL, a maximum of 1 to 2% TiO_2 could exist before aggregation occurred. The resulting mixture had excessive viscosity and did not scatter light as efficiently as primary TiO_2 particles. It was not feasible to make a film to modify the local refractive index of the fiber by this manner, thus, a format of titanium dioxide deposition followed by a dextran hydrogel layer and then attachment of the ligand was explored.

By knowing the fiber's initial peak wavelength, the glycerol sensitivity curves were used to determine the peak shift needed to bring the refractive index of the fiber into the sensitive region of the curve. DuPont TiO_2 was then adsorbed onto the surface until the desired peak shift was obtained as described in section 3.2.1. A hydrogel layer of dextran was attached to the titanium dioxide film and the ligand anchored to this matrix as explained in sections 3.2.2 and 3.2.3, respectively.

4.1.3 Refractive Index of Dextran Solutions

Once the LPG surface had been modified by a titanium dioxide layer, a dextran hydrogel was attached to serve as an anchor matrix for the ligand. Refractive index measurements were also taken on an array of dextran solutions to see what effect, if any, the hydrogel would have on the refractive index of the fiber. The refractive index of a series of dextran solutions was measured on a refractometer. The results from these measurements are shown below in Table 4.4.

Table 4.4 Refractive indices of dextran (T-500)—water solutions measured with a refractometer.

% Dextran T500	Measured RI
5	1.337
10	1.343
15	1.350
20	1.357

The response of fibers to dextran solutions was also determined. In a manner similar to the previously described sensitivity curves, the peak shifts of the same three fibers were monitored through the four dextran solutions listed in Table

4.4. The resulting curves are shown in Figure 4.5. All three fibers showed a similar response to an increase in dextran concentration. When compared to the shifts in glycerol and titanium dioxide solutions, peak shifts in dextran solutions were small. Thus, the dextran layer did not have a big influence on the refractive index properties of the fibers.

4.1.4 Refractive Index Measurements of Bovine Serum Albumin

The final component of the fiber coating was the ligand, bovine serum albumin. Assuming that by the time the BSA ligand was attached to the fiber's coating the refractive index was essentially 1.44, any peak shifts stemming from ligand attachment were addressed. To do this, solutions of BSA in 75% glycerol were measured with a refractometer. Readings were taken in 75% glycerol because it increases the baseline refractive index to 1.44, which was theoretically the refractive index of the fiber coating when the ligand was attached. Table 4.5 shows the measured refractive indices of various BSA concentrations in 75% glycerol.

Table 4.5 Refractive indices of solutions containing bovine serum albumin in 75% glycerol, measured with a refractometer.

Concentration of BSA (mg/mL)	Measured RI
0	1.440
0.625	1.440
1.25	1.441
2.5	1.441
5	1.441
10	1.442

From Table 4.5, it can be seen that BSA in solution, even at a high concentration, has very little effect on the refractive index of the resulting solution. It was expected that any shift in peak wavelength due to the addition of BSA would also be small.

The response of the three fibers is graphed in Figure 4.6. The results show that all fibers respond similarly to the presence of ligand in 75% glycerol, and the peak shift due to the addition of BSA was minimal when compared to that in glycerol and titanium dioxide. It can be concluded from the previous fiber response studies that the only contributor to the fibers' refractive index came from the titanium dioxide film adsorbed onto the LPG surface.

4.2 Refractometry Function of Fiber after Coating

Modifying the refractive index of the LPG sensing area by coating it with TiO_2 did not give easily reproducible results. In the laboratory, it was not possible to systematically increase the refractive index of the fiber to a predefined level. Titanium dioxide in solution behaved differently than titanium dioxide adsorbed onto the fiber surface. Once the titanium dioxide was dried on the fiber surface, the effect on the optical signal was often quite different from fiber to fiber, and even between fibers whose initial peak wavelengths were similar. Sometimes the dried titanium dioxide weakened a fiber's signal to a point that response to a target binding event was undetectable. In other instances, the drying of the titanium dioxide actually lead to a further increase in peak shift and hence pushed the fiber further into the high sensitivity region of the response curve. Yet, with other fibers the wavelength of the peak decreased (losing sensitivity) without a loss of signal strength. The effects of

titanium dioxide adsorption on several fibers of similar initial points are described in Table 4.6.

Table 4.6 Peak wavelengths measured with an OSA of four LPG sensor elements in DDW H_2O before TiO_2 (d=300 nm) coating, after surface adsorption of TiO_2 (but prior to drying), and after drying of adsorbed TiO_2.

Fiber	Initial Peak Wavelength (nm)	Peak wavelength before drying of TiO_2 film (nm)	Peak wavelength after drying of TiO_2 film (nm)
Fiber 525-11	1509.8	1555.2	1565.9
Fiber 616-10	1507.4	1586.1	1542.2
Fiber 508-4	1505.5	1560.0	1558.0
Fiber 504-2	1515.6	1569.7	Signal too weak to detect

The results in Table 4.6 are representative of the variance encountered with the adsorption of titanium dioxide on the fibers' surface. As a result, the process of making a fiber started with coating a batch of fibers with titanium dioxide and evaluating them after drying. By examining many fibers with initial peak wavelengths varying over a 150 nm range, it was found that fibers starting in the low to mid 1400's would lose their peak upon titanium dioxide coating. The signal of these fibers had a low left shoulder that would disappear upon TiO_2 coating (instead of the peak shifting into the region of high sensitivity) due to some aspect of the optics that resulted in quenching of the signal. Therefore, only those fibers whose initial peak wavelength were between 1500 and 1520 nm were chosen, and titanium dioxide was adsorbed until a peak shift of 40 to 60 nm was reached. It was found through many trials that coating the fibers with titanium dioxide to a peak shift over 70 nm often led to the

inability to detect a signal after drying. Therefore, only the fibers that maintained a peak shift of 40 to 60 nm after drying and retained a strong signal were used for further development.

Since it was not feasible to modify the refractive index of the fiber solely with titanium dioxide, detection in glycerol was still needed. Once again, glycerol profiles were done on the titanium dioxide-coated fibers to determine what percent glycerol was needed push the fiber into the high sensitivity region of the response curve. Each titanium dioxide-coated fiber was monitored in low percentage glycerol solutions. Based on the peak shift and signal strength, the optimum glycerol solution was chosen for target detection. Figure 4.7 tracks the response of three titanium dioxide coated fibers to glycerol solutions of 5, 10, 12, 14, and 18% glycerol. The three fibers have different peak shifts resulting from titanium dioxide coating (731-4 equals Δ27 nm, 731-7 equals Δ37 nm, and 716-15 equals Δ46 nm), but the peak wavelength after coating with titanium dioxide is within the same range (1553.7 nm, 1554.3 nm, and 1560.2 nm, respectively). It was noticed that fibers having the same peak wavelength after titanium dioxide adsorption, regardless of the magnitude of the peak shift, responded to increasing glycerol solutions with very similar increases in wavelength. Titanium dioxide can be adsorbed onto the surface of the LPG to raise the mass averaged refractive index to approximately 1.42, and then low amounts of glycerol can be used to further increase the refractive index to 1.44. The low percent of glycerol that is now needed is much more practical than the amount needed (approximately 75%) when no titanium dioxide is used.

4.3 Optical Spectrum Analyzer Noise

In order to determine the magnitude of wavelength shift that constituted a true response to target, the noise level of the OSA was assessed. An array of experiments was designed so that the noise associated with thermal effects and change in flow conditions could be analyzed. A fiber coated with titanium dioxide, a dextran hydrogel, and ligand immobilization (recombinant human Protein C, in this case) was tested in phosphate buffer (0.1 M KPO_4, pH 7.2) flowing at 5 mL/min and at 0 mL/min. The fiber was tested under two sets of experimental conditions. First, it was tested uninsulated at ambient laboratory temperature (varied between 21 and 23°C). It was also tested submerged in an insulated water bath with the phosphate buffer at the same temperature as the water bath (T=22°C). The insulated water bath was allowed to equilibrate for 24 hours prior to any experiments. The fiber used in this experiment (729-4) had an initial peak at 1512 nm in DDW and a peak reading of 1575 nm after all coatings, giving a shift of 63 nm. Fiber 729-4 was representative of a typical fiber used in this research, complete with all coatings. Table 4.7 shows the noise levels from the uninsulated versus insulated fiber for static and 5 mL/min trials. The noise levels are consistent at 0.1 nm except for the insulated/static trial, which was elevated slightly to 0.15 nm.

Table 4.7 LPG noise levels recorded using an OSA. LPG sensor element coated with TiO_2 (d=300 nm), dextran (T-500), and rhPC. Measurements taken in static 0.1 M KPO_4, pH 7.2 at ambient (approximately 22°C) conditions, and while sensor was immersed in an insulated water bath.

	Static	5 mL/min
Uninsulated	0.1 nm	0.1 nm
Insulated	0.15 nm	0.1 nm

In comparison, the same experiments were conducted on two bare fibers (both with the same peak wavelength in DDW), one in 60% glycerol and the other in 10% TiO_2. The glycerol and titanium dioxide solutions were chosen because the wavelength associated with their refractive index put the bare fibers into the same wavelength range as the coated fiber previously described. Both fibers had a peak in DDW at 1524 nm, while Fiber 924-5A had a peak wavelength of 1574 nm in 60% glycerol and Fiber 924-11 had a peak wavelength at 1571 nm in 10% TiO_2. Each fiber was run under the conditions described above and the noise levels recorded. Results are shown in Table 4.8.

Table 4.8 LPG noise levels recorded using an OSA. Two blank LPG sensor elements in ambient (approximately 22°C) conditions are compared to sensors immersed in an insulated water bath. Fiber 924-5A was exposed to 60% glycerol and Fiber 924-11 exposed to 10% TiO_2 (d=28 nm), both solutions flowed through the holder at 0 mL/min (static) and 5 mL/min.

	60% Glycerol (924-5A)		10% TiO_2 (924-11)	
	Static	**5 mL/min**	**Static**	**5 mL/min**
Uninsulated	0.1 nm	0.1 nm	0.1 nm	0.1 nm
Insulated	0.1 nm	0.1 nm	0.15 nm	0.15 nm

The results in Table 4.8 coincide with the results of Table 4.7 in that the noise level of the OSA varies between 0.1 nm and 0.15 nm. With noise existing at these levels, a signal to noise ratio of three would mean that the peak wavelength shift would have to be approximately 0.5 nm to constitute a true response. For a signal to noise ration of ten, the shift would have to be 1.5 nm to be considered real. Since the fibers are not operating at the optimum point of sensitivity on the response curve, a 1.0 nm peak shift necessitates a large change in refractive index, and hence small refractive index changes due to a low number of binding events would go undetected. The fibers were not operating at maximum sensitivity due to the inability to modify the fibers' refractive index to the optimum level. To increase the performance of these fibers, another spectrum analyzer or an improvement in the demodulation software used to evaluate the optical signal was needed.

4.4 Film Stability

Once the titanium dioxide layer, dextran hydrogel and ligand were attached to the fiber, the stability of this film against harsh regeneration agents needed to be assessed. The end goal was to develop a biosensor with high sensitivity that

could be regenerated for multiple screenings. The film had to able to withstand the extreme conditions used to dissociate the target from the ligand, without disruption to the signal or lowering of the refractive index properties of the film. Prior to any target exposure, film stability was tested to assure constant baseline readings. Stability was tested by cycling each fiber with the solutions used to dissociate the target/ligand complex. The solutions used for dissociation are 2 M NaSCN and 0.1 M glycine in 2% acetic acid (pH 2.5). Multiple cycles of regeneration on numerous fibers found that the titanium dioxide/dextran/ligand film remained stable. The fiber described below is one with responses typical of all fibers tested.

Following titanium dioxide deposition, dextran attachment, and BSA immobilization, Fiber 603-8 was cycled ten times with the sodium thiocyanate and glycine solutions with rinses of phosphate buffer after each solution. The peak wavelength before cycling was 1574.5 nm in phosphate buffer and after ten cycles was 1574.2 in phosphate buffer. The sensorgram for the initial cycling is shown in Figure 4.8. The sensorgram shows the change in peak wavelength as the cycles progress through the two regenerates. Note that the baseline readings in phosphate buffer were stable.

Sensorgrams may be read by following the changing peak wavelength over time as the fiber progresses through the various solutions used in that particular experiment. The regeneration cycles shown in Figure 4.8 start in phosphate buffer (marked "A" on the sensorgram) and proceed to the first regeneration solution, sodium thiocyanate. The spike resulting from the sodium thiocyanate solution (marked "B") occurs because the thiocyanate solution flattens the peak signal and the OSA marks this loss of signal as a spike. Looking at Figure 4.8 one notices that there is a break in

the sensorgram around the thiocyanate spike. This break represents the point in time when the data acquisition was turned off so that the spike would not throw the entire sensorgram off-scale, making it difficult to follow in real-time. After thiocyanate, the fiber was rinsed in phosphate buffer (marked "C") and subjected to glycine in acetic acid (marked "D"). Following this second regeneration solution, the fiber was again rinsed in phosphate buffer (marked "E") and then the second cycle started. The remaining regeneration cycles follow this one just described.

Stability can also be introduced to the film by crosslinking cellulose to the dextran forming a "net" around the fiber. One percent cellulose was crosslinked to the dextran layer and the fiber again tested through eleven cycles of thiocyanate and glycine in acetic acid. Figure 4.9 shows the sensorgram for the regeneration cycles after cellulose crosslinking. The baseline wavelength after these eleven cycles again remains constant with an initial wavelength of 1559.8 nm and a final wavelength of 1560.0 nm. The slight increase in peak wavelength is not significant when the noise of the OSA is taken into account. The drop in baseline reading from 1574.2 nm after the first set of ten cycles to 1559.8 nm at the initiation of the second set of regeneration cycles occurred during the cellulose crosslinking. Figure 4.9 can be read just like the first set of regeneration cycles, with sections A, B, C, D, and E being the same as in Figure 4.8.

After a series of target binding experiments and negative control tests, the fiber was once again cycled through the regeneration solutions ten times. The initial baseline in phosphate buffer was at 1559.2 nm and the final reading at 1559.7 nm. Even after challenge with target, the film remained stable through numerous regeneration steps. This fiber was extensively tested and it was found that after a total

of 50 regeneration cycles (after cellulose crosslinking), which includes 25 target test runs, the baseline reading in phosphate buffer only dropped from 1559.8 nm to 1558.5 nm. This decrease in peak wavelength is due to some small change in the film that has slightly altered the refractive index properties of the fiber.

4.5 Target Detection

To accurately investigate the ability of the BSA biosensor to bind anti-BSA IgG several aspects were evaluated. First, the biosensor needed to show a specific response to the target antibody without interference from competing antibodies. Also, this specificity had to exist in complex mixtures where the presence of proteins could bind non-specifically to the ligand or inhibitors could prevent the formation of a stable ligand/target complex. The biosensor also had to show reproducible binding of the target antibody. The actual amount of target bound was estimated by challenging the fiber with target, eluting the bound material, and quantifying it by enzyme-linked immunosorbent assay (ELISA). The fiber was then rechallenged with the "affinity purified" material to see if the response correlated with the initial binding response. Finally, the mass transfer effects were investigated to find the most efficient system for target exposure.

4.5.1 Specificity

The BSA fiber, 603-8, previously described in section 4.4 was used as a model for the target detection experiments. After cycling with the regeneration solutions following crosslinking of the dextran with 1% cellulose, the fiber's peak was at a wavelength of 1560 nm. To increase the sensitivity, and thus increase the response, target detection was determined by a baseline shift in 0.1 M KPO_4, pH 7.2

with 10% glycerol. In this glycerol-phosphate buffer, the peak was at a wavelength of 1576 nm. More concentrated glycerol solutions were not used because the peak signal started to weaken and move out of the OSA's operating wavelength range. Target detection was tested by diluting rabbit anti-BSA IgG (whole serum) 1:100 in 0.1 M KPO_4, pH 7.2 and recycling through the fiber holder for 5 minutes, as outlined in section 3.3.2. Three trials were completed and Figure 4.10 shows the resulting sensorgram.

By following the target detection method described in section 3.3.2, one can understand the sensorgram in Figure 4.10. Initially the fiber was put in phosphate buffer and then transferred to 10% glycerol in phosphate buffer. This process is marked by "A" and "B" on the sensorgram, respectively. After the baseline in 10% glycerol-phosphate buffer was recorded, the fiber was incubated in the anti-BSA IgG sample (marked "C") and then rinsed with phosphate buffer to remove any unbound target (marked "D"). The final baseline reading in 10% glycerol-phosphate buffer recorded (marked "E"). Following another wash with plain phosphate buffer to remove any residual glycerol (marked "F"), the fiber was regenerated as outlined in section 3.3.4 with "G" being the thiocyanate spike, and "H" representing a phosphate buffer rinse. A second exposure to 2 M NaSCN (marked "I") was done to remove any anti-BSA IgG that was not eluted by the first wash. These two thiocyanate elutions were saved for ELISA quantification. The fiber was rinsed with phosphate buffer (marked "J") after the second NaSCN elution, then regenerated with 0.1 M glycine/2% acetic acid, pH 2.5 (marked "K"). After this cycle, two more binding experiments were done following these steps. Again, the data acquisition was turned off when the thiocyanate solution was used to avoid throwing the sensorgram off-scale.

Peak shifts in 10% glycerol-phosphate buffer were 3.0 nm, 2.5 nm, and 2.2 nm for the three exposures, respectively. With OSA noise at 0.1 nm, even a 2.2 nm shift has a signal to noise ratio of 22, and hence represents a true binding event. Comparing the baseline readings in plain phosphate buffer before and after sample incubation gives peak shifts of 2.1 nm, 1.3 nm, and 1.1 nm, respectively. While the peak shifts in plain phosphate buffer still represent true binding events, the fiber responds with greater sensitivity when it is operating at a higher refractive index (i.e., when in phosphate buffer with glycerol).

Another three target exposures were run having peak shifts of 2.6 nm, 2.0 nm, and 2.1 nm, respectively in phosphate buffer with 10% glycerol. Peak shifts in plain phosphate buffer were 2.0 nm, 1.3 nm, and 1.4 nm, respectively. Again, notice the increased sensitivity of the fiber when it operates at a higher refractive index. Figure 4.11 is the sensorgram for this series of target challenges. The sensorgram can be read like that in Figure 4.10, with one exception. The ligand regeneration in cycle one consisted of two washes with 2 M NaSCN (marked "G" and "I") followed by one wash with 0.1 M glycine/2% acetic acid, pH 2.5 (marked "K"), as in Figure 4.10. Ligand regeneration in cycles two and three consisted of only one 2 M NaSCN wash, one wash with 0.1 M glycine/2% acetic acid, pH 2.5 and one wash with 4 M NaCl (marked "L"). As the experiment proceeded, the baseline slightly shifted up about 2 nm, and the salt solution was used in an attempt to bring the baseline back down. The salt solution had no noticeable effect on the baseline. Again, the bound target was eluted and saved for an ELISA. Following the last target exposure (cycle 3) a final regeneration cycle of 2 M NaSCN (marked "M") and 0.1 M glycine/2% acetic acid,

pH 2.5 (marked "N") was added. This was done to insure that all possible anti-BSA IgG or other bound material was removed from the ligand.

The fiber showed reproducible binding of rabbit anti-BSA IgG in whole serum with peak shifts ranging from 2.0 nm to 3.0 nm, in 10% glycerol-phosphate buffer. The next step was to test the fiber with negative controls as a check for non-specific binding. Goat serum and rabbit anti-cholera toxin (whole serum) were both diluted 1:100 in phosphate buffer and tested on the fiber as described in section 3.3.3 under recycle conditions of 5 mL/min for 5 minutes. The goat serum was chosen to show that there was no cross reactivity with antibodies and proteins of another species. The rabbit anti-cholera toxin IgG was tested to show that the fiber did not bind other antibodies produced in the same species as the ligand. As shown in Figure 4.12, the goat serum gave a baseline shift of 0.4 nm and the anti-cholera toxin IgG gave no noticeable peak shift. The small peak shift from the goat serum is not significant since it represents a signal to noise ratio of 4. For our purposes any signal to noise ratio less than 5 was not considered to be a real binding event. The sensorgram in Figure 4.12 follows the same labeling scheme as in the previous figures, the exception being that instead of incubating in anti-BSA antisera, the fiber was incubated in goat serum (marked "C") and rabbit anti-cholera toxin (marked "J").

Figures 4.13 and 4.14 are the sensorgrams for ten repetitions of challenge with 1:100 rabbit anti-BSA IgG (whole serum). The peak shifts range from 1.6 nm to 2.1 nm and it should be noted that no glycerol was present in the phosphate buffer used for the baseline readings. Again, it was noticed that the baseline reading after the thiocyanate and glycine in acetic acid regeneration was slightly higher than at the start of the experiment. A third regeneration solution was tried in these ten

challenges to lower the baseline back to the original wavelength. A solution of 0.1 M TEA, pH 11.5 was tried. The solution did help to return the baseline to the initial point, but because of the harshness of this basic solution its use was kept to a minimum. The sensorgrams in Figures 4.13 and 4.14 can be interpreted as previously described, noting that section "H" represents the TEA solution.

The recovery of bound antibody was done as described in section 3.3.5. The bound anti-BSA eluted from the ten trials was combined with the eluted antibody from the first six experiments and assayed by ELISA as outlined in section 3.3.6. From the ELISA it was estimated that approximately 25 ng of anti-BSA IgG was bound by the fiber during each run. The amount of anti-BSA bound by Fiber 603-8 corresponds with the amount bound by another BSA fiber (525-11). Fiber 525-11 was made in the same manner as Fiber 603-8 and was also exposed to anti-BSA IgG, which was eluted from the fiber and assayed. The ELISA determined that approximately 26 ng of anti-BSA was bound by Fiber 525-11 per run. From the observed wavelength shifts, a theoretical estimate of the amount of anti-BSA bound by the fibers for each run was determined. The change in refractive index of the film (ΔRI) was calculated from the wavelength shift (Δnm) multiplied by the fiber sensitivity (ΔRI/Δnm). The target film concentration (g/mL) was determined by scaling the change in refractive index by the constitutive value for proteins, $(dn/dc)_{protein} \approx 0.18$ mL/g. Finally, the amount of target bound during each trial was calculated by multiplying the target film concentration by the gel volume. The gel volume was calculated using a fiber diameter of 120 μm, an LPG length of 1 cm, and a gel thickness of 500 nm. For Fiber 603-8, a total of 251 ng of anti-BSA IgG was estimated to have bound during the 16 trials, giving an average of 16 ng bound per run.

Table 4.9 summarizes the calculated amounts of anti-BSA IgG bound during each of the sixteen runs. Using the same calculations, approximately 60 ng of anti-BSA was bound by Fiber 525-11 over 10 trials, an average of 6 ng per run. Comparing the theoretical versus experimental value shows a large difference between the two in terms of target amount bound. Several assumptions were used which can explain these differences. First, the theoretical calculations are based on a gel thickness of 500 nm. From ESEM photographs (discussed in section 4.7), the gel thickness is shown to be at least 300 nm thick, but actual size cannot be determined. Therefore, while 500 nm is a reasonable estimate, the gel may actually be thicker. A thicker gel would bind more target, but if the gel thickness extended beyond the evanescent field, target binding on the outer edge of the affinity matrix would go undetected. Target binding in this area would be reflected in the ELISA data but not the theoretical calculations, hence, the difference between the ELISA-determined amount and the predicted amount. Secondly, the theoretical calculations are based solely on the amount of target bound within the defined area of the LPG. In reality, the film is larger than just the LPG area and hence target was bound on regions of the hydrogel that were not necessarily within the LPG sensing area. Consequently, when the target was eluted all of the anti-BSA IgG, whether or not it was bound within the LPG sensing area, was stripped from the fiber and assayed by ELISA. This would undoubtedly give a greater amount of anti-BSA IgG detected than that just within the LPG area.

Table 4.9 Theoretical estimates of adsorbed anti-BSA IgG by a LPG sensor element coated with TiO_2 (d=300 nm), dextran (T-500), and BSA. Based on peak wavelength shifts measured using an OSA. Sensor element exposed to 16 cycles of anti-BSA IgG with the bound target eluted and the LPG sensor element regenerated between each exposure.

Shift Observed (nm)	RI/nm	Δ RI	dn/dc Target (mL/g)	Target Film Conc. (g/mL)	Gel Volume (mL)	Target Bound (ng)
2.1	8.5E-04	1.8E-03	0.18	9.9E-03	1.88E-06	18.7
1.3	8.5E-04	1.1E-03	0.18	6.1E-03	1.88E-06	11.6
1.1	8.5E-04	9.4E-04	0.18	5.2E-03	1.88E-06	9.8
2.0	8.5E-04	1.7E-03	0.18	9.4E-03	1.88E-06	17.8
1.3	8.5E-04	1.1E-03	0.18	6.1E-03	1.88E-06	11.6
1.4	8.5E-04	1.2E-03	0.18	6.6E-03	1.88E-06	12.5
1.9	8.5E-04	1.6E-03	0.18	9.0E-03	1.88E-06	16.9
1.8	8.5E-04	1.5E-03	0.18	8.5E-03	1.88E-06	16.0
1.6	8.5E-04	1.4E-03	0.18	7.6E-03	1.88E-06	14.2
1.8	8.5E-04	1.5E-03	0.18	8.5E-03	1.88E-06	16.0
2.0	8.5E-04	1.7E-03	0.18	9.4E-03	1.88E-06	17.8
2.1	8.5E-04	1.8E-03	0.18	9.9E-03	1.88E-06	18.7
2.0	8.5E-04	1.7E-03	0.18	9.4E-03	1.88E-06	17.8
2.0	8.5E-04	1.7E-03	0.18	9.4E-03	1.88E-06	17.8
2.0	8.5E-04	1.7E-03	0.18	9.4E-03	1.88E-06	17.8
1.8	8.5E-04	1.5E-03	0.18	8.5E-03	1.88E-06	16.0
Total Target Bound (ng)						251.0

In essence, the fiber functioned as an affinity column. Once the bound anti-BSA IgG was eluted, it had essentially been "affinity purified". The ability of the fiber to re-bind this purified sample was investigated. Prior to challenging the fiber

with the target collected and assayed by ELISA, the fiber was checked to assure that it would still respond to anti-BSA IgG in whole serum. A peak shift of 1.3 nm was observed by detection with phosphate buffer containing no glycerol after exposure to 1:100 anti-BSA (whole serum) under static conditions. The purified anti-BSA IgG assayed by ELISA was brought up to 4 mL with 0.1 M KPO_4, pH 7.2 buffer and recycled through the fiber holder for 30 minutes. Within the first five minutes, the peak wavelength had shifted from 1557.3 nm to 1558.7 nm but then remained steady throughout the remaining 25 minutes. When the fiber was washed with phosphate buffer containing no glycerol, the peak wavelength returned to the initial baseline level of 1557.2 nm, as depicted in Figure 4.15. In this sensorgram, "A" represents the initial baseline reading in phosphate buffer, "B" is the 30 minute exposure to the purified anti-BSA, and "C" is the final baseline reading in phosphate buffer after sample binding. The fiber detected some change in refractive index due to an increase in mass accumulation within the evanescent field, but after washing (marked "C") the peak wavelength returned to the initial baseline reading. This implied that the purified anti-BSA IgG was collecting in the film, but was either not bound, or else not enough was bound to be detected. When the fiber was exposed to anti-BSA (whole serum), the concentration was approximately 20 μg/mL, which was 200 times more concentrated than the purified sample (approximately 100 ng/mL), after being brought up to 4 mL in order to recycle it through the holder. Since the fiber was not operating at maximum sensitivity, it did not respond to small changes in refractive index within the film. It can detect the antibody concentrating in the film, but upon washing, the unbound target was removed and the small amount that did complex with the ligand was undetectable. Additionally, the anti-BSA IgG may not have bound at all due to the

possibility that the NaSCN may have altered the antibody, hence affecting its binding ability. The antibody may have become partially denatured, and therefore, exhibited a lower avidity for the ligand. Also, the other proteins present in the whole serum may have aided in the antibody binding, and without their presence, the binding of the anti-BSA IgG was not facilitated. A final check of fiber function was made following this experiment and a peak shift of 1.2 nm in phosphate buffer was detected for 20 μg/mL anti-BSA (whole serum) recycled over the fiber. This indicates that the fiber was still functioning properly and therefore the inability to detect target as just described was not due to a problem with the fiber or the affinity ligand film.

After the antibody trials, but prior to reapplication of the affinity purified target to the fiber, a third series of ten cycles with regeneration solutions was performed on the fiber to further test its stability. The sensorgram for this experiment is shown in Figure 4.16. It may be read just as the sensorgrams for Figures 4.8 and 4.9. The baseline in 0.1 M KPO_4, pH 7.2 buffer was initially at 1559.2 nm and remained fairly constant throughout the ten cycles, giving a final reading of 1559.7 nm. At this point, the fiber had been through a total of 39 regeneration cycles after cellulose crosslinking. The titanium dioxide/dextran/BSA film on the LPG has been shown to remain stable, with the first baseline reading of 1559.8 nm and the final reading after this third regeneration experiment of 1558.5 nm.

4.5.2 Mass Transfer Effects

Resistance to mass transfer between the target in solution and the ligand was also investigated. Three scenarios for sample delivery were tested: sample solution injected into the fiber holder and allowed to incubate (linear velocity of 0 cm/min) for five minutes; sample solution pumped through the fiber holder at 5

mL/min (linear velocity of 125 cm/min) for five minutes; and sample solution pumped through the fiber holder at 50 mL/min (linear velocity of 1250 cm/min) for five minutes. As described in section 3.3.2, 20 μg/mL anti-BSA (whole serum) in phosphate buffer was either injected by pipette into the fiber holder or recycled through the holder by a peristaltic pump at the specified flow rate. The observed peak shifts in phosphate buffer for static, 5 mL/min, and 50 mL/min flows were 1.5 nm, 1.9 nm, and 1.7 nm, respectively. The sensorgrams representing the phosphate buffer baseline to sample introduction to buffer wash for the three scenarios have been overlaid in Figure 4.17. The three sensorgrams in Figure 4.17 show the initial baseline reading in phosphate buffer (marked "A"), the sample incubation (marked "B"), and the final baseline reading in phosphate buffer (marked "C") for each mass transfer experiment. Comparing the fiber's response in each situation, the slopes of the response curves for the static trial and at 5 mL/min were essentially the same. When sample is flowed at 50 mL/min the slope is slightly less than for the other cases, indicating that the initial response to target may be slower. Within the first 120 seconds of sample exposure, the peak shift under static conditions and at 5 mL/min is the same at 0.8 nm. The overall difference in final peak shift between the three trials is not significant when compared to the variance in peak shifts of multiple runs under the same conditions. This is clearly demonstrated in Figures 4.12 and 4.13 where in ten trials of target flowing at 5 mL/min, the peak shifts varied between 1.6 nm and 2.1 nm. There seems to be little, if any, resistance to mass transfer in this system. Hence, the ability of the target to diffuse into the hydrogel layer and complex with the ligand does not appear to be greatly influenced by sample flow rate at the analyte concentration used in this experiment.

4.6 Queensgate Noise

To investigate other signal detection and demodulation methods, Fiber & Sensor Technologies provided a Queensgate tunable Fabry-Perot spectrometer. The same noise experiments done on the OSA were done on the Queensgate. Fiber 729-4, coated with titanium dioxide, dextran and ligand was tested in phosphate buffer at the previous conditions (i.e., insulated and uninsulated with buffer flowing at 5 mL/min and 0 mL/min). The noise results are shown in Table 4.10.

Table 4.10 LPG noise levels recorded using a Queensgate spectrometer. LPG sensor element coated with TiO_2 (d=300 nm), dextran (T-500), and rhPC. Measurements taken in static 0.1 M KPO_4, pH 7.2 at ambient (approximately 22°C) conditions, and while sensor was immersed in an insulated water bath.

	Static	5 mL/min
Uninsulated	0.015 nm	0.01 nm
Insulated	0.01 nm	0.01 nm

The noise results on the Queensgate were an order of magnitude lower than those previously given by the OSA.

Again, Fibers 924-5A and 924-11 were tested in 60% glycerol and 10% TiO_2, respectively, under insulated/uninsulated and static/flowing conditions. Table 4.11 shows the results from these experiments.

Table 4.11 LPG noise levels recorded using a Queensgate spectrometer. Two blank LPG sensor elements in ambient (approximately 22°C) conditions are compared to sensors immersed in an insulated water bath. Fiber 924-5A was exposed to 60% glycerol and Fiber 924-11 exposed to 10% TiO_2 (d=28 nm), both solutions flowed through the holder at 0 mL/min (static) and 5 mL/min.

	60% Glycerol (924-5A)		10% TiO_2 (924-11)	
	Static	**5 mL/min**	**Static**	**5 mL/min**
Uninsulated	0.01 nm	0.01 nm	0.01 nm	0.015 nm
Insulated	0.01 nm	0.01 nm	0.01 nm	0.015 nm

The noise levels are again an order of magnitude lower than those previously given on the OSA. With the decrease in noise levels, the Queensgate lends itself to be the more sensitive of the two analyzers. A peak shift of just 0.1 nm on the Queensgate equals a signal to noise ratio of ten. This decrease in observed noise is desirable to help compensate for the decreased sensitivity of the fibers because they were not acting in the most sensitive region of the response curve. With the Queensgate, it is possible to get a reliable peak shift from a much smaller refractive index change than with the OSA.

4.7 ESEM Photographs

To visualize the LPG fibers and the titanium dioxide/dextran film, multiple fibers were photographed on an environmental scanning electron microscope (ESEM). This provided verification of the coating procedure and allowed for generalizations regarding the thickness of the hydrogel film. A photograph of a fiber with no coating is shown in Figure 4.18. This picture shows that the fiber is measured to be approximately 120 μm and the surface has a smooth even appearance. Once the fiber had been coated with titanium dioxide, the surface became rough and the

titanium dioxide particle distribution can be visualized. Figure 4.19 shows a fiber heavily coated with titanium dioxide. The titanium dioxide film appears to be grainy, but consistently dense all over. A fiber with a lighter titanium dioxide film is shown in Figure 4.20. While the titanium dioxide layer can still be seen, the film is less consistent and the underlying fiber is visible.

To estimate the thickness of the dextran hydrogel layer, a section of the fiber was excavated by burning away the dextran hydrogel layer under intense magnification and photographing it as the dextran was rehydrated. In Figure 4.21 a fiber coated with titanium dioxide/dextran has been excavated. The underlying titanium dioxide layer is visible through the dextran matrix, which is dehydrated at low water pressure in the ESEM chamber. As the water pressure is increased, the dextran layer hydrates and expands. Figure 4.22 shows the fiber once the dextran layer has been fully rehydrated and now the underlying titanium dioxide is not visible. The titanium dioxide layer under the removed dextran remains and clearly outlines the excavated area. The diameter of the titanium dioxide used to coat the fiber was 300 nm and hence the dextran layer is at least this thick, and probably more, since when fully hydrated the titanium dioxide particles are completely invisible. Figure 4.23 shows a similar excavation site, although this fiber does not have a titanium dioxide layer and was coated four times with dextran. Upon hydration, the dextran shows to be thick and even in appearance. This photograph supports our ability to successfully attach a thick layer of dextran evenly over the fiber surface.

These pictures confirm that titanium dioxide and dextran layers are being deposited on the fiber. While we can not completely measure the thickness of the dextran layer in these photographs, we can conclude that it is definitely 300 nm thick

and suggest it probably is even thicker. The ESEM also provides a good way to visualize the titanium dioxide layer and determine the extent of coverage.

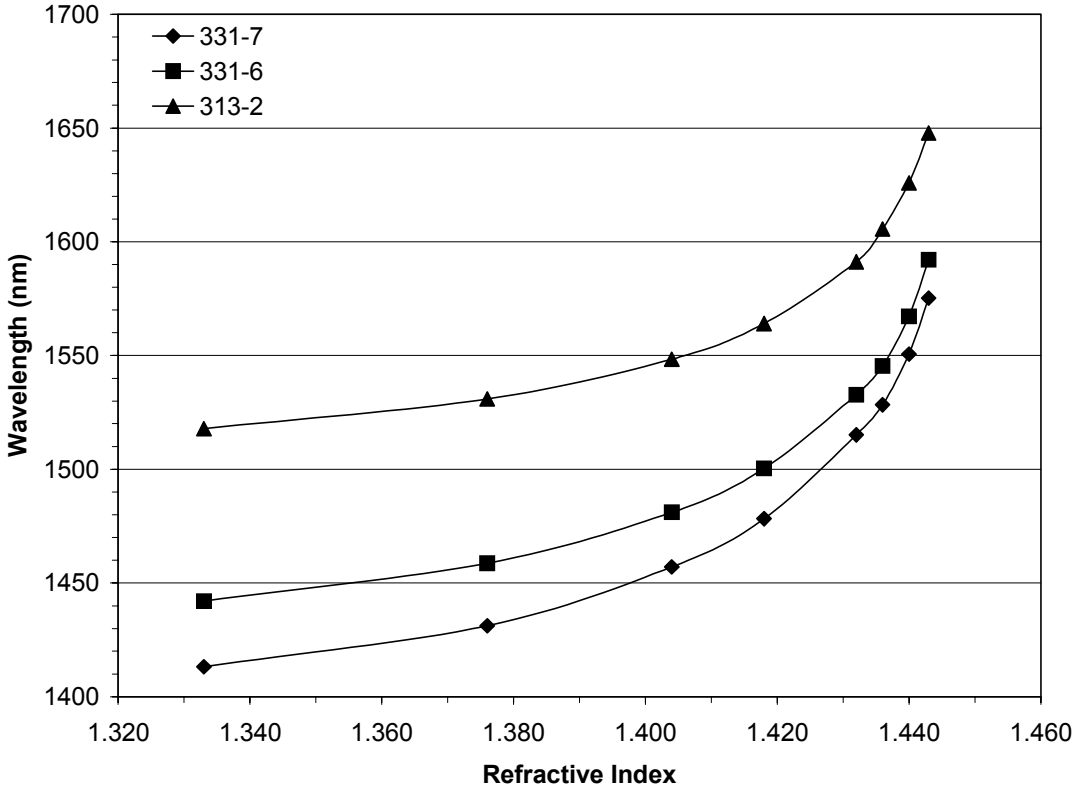

Figure 4.1 **Signal curves from three blank LPG sensor elements versus RI of glycerol-water solutions. Peak wavelengths were measured with an OSA on each fiber exposed to 0%, 30%, 50%, 60%, 70%, 72.5%, 75%, and 77.5% glycerol under static conditions. Refractive indices were calculated from Equation 4.1.**

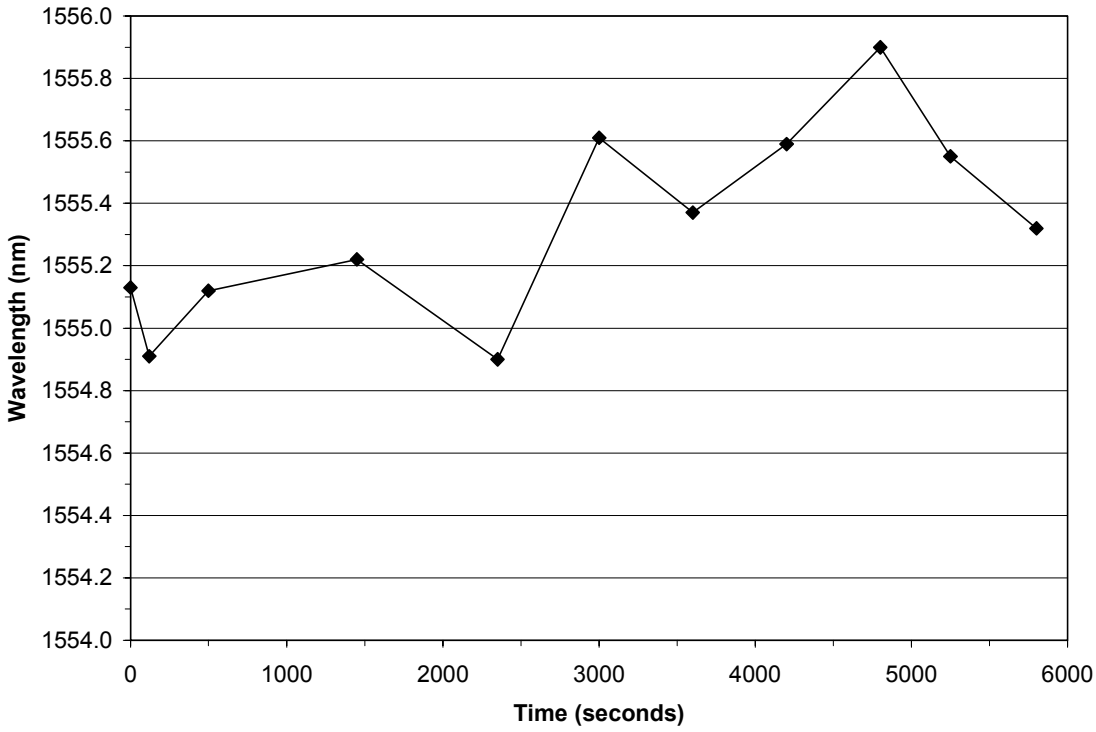

Figure 4.2 OSA signal from a blank LPG sensor element exposed to 75% glycerol-water under static conditions. Peak wavelength reading (baseline) is unstable over a ten minute exposure time.

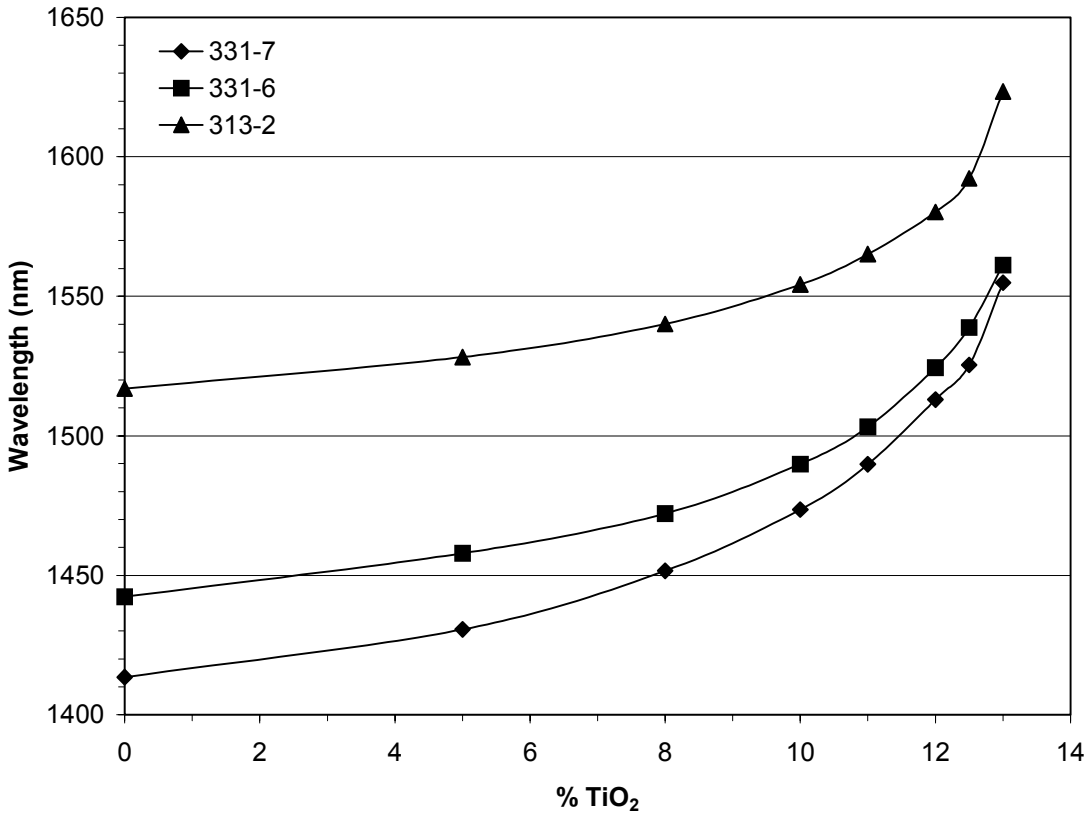

Figure 4.3 **Signal curves from three blank LPG sensor elements versus percent TiO_2 (d=28 nm) in water. Peak wavelength readings were measured with an OSA on each fiber exposed to 0%, 5%, 8%, 10%, 11%, 12%, 12.5%, and 13% TiO_2 under static conditions. Refractive indices of the TiO_2 solutions were 1.333, 1.373, 1.397, 1.414, 1.422, 1.431, 1.435, and 1.439, respectively (Table 4.3).**

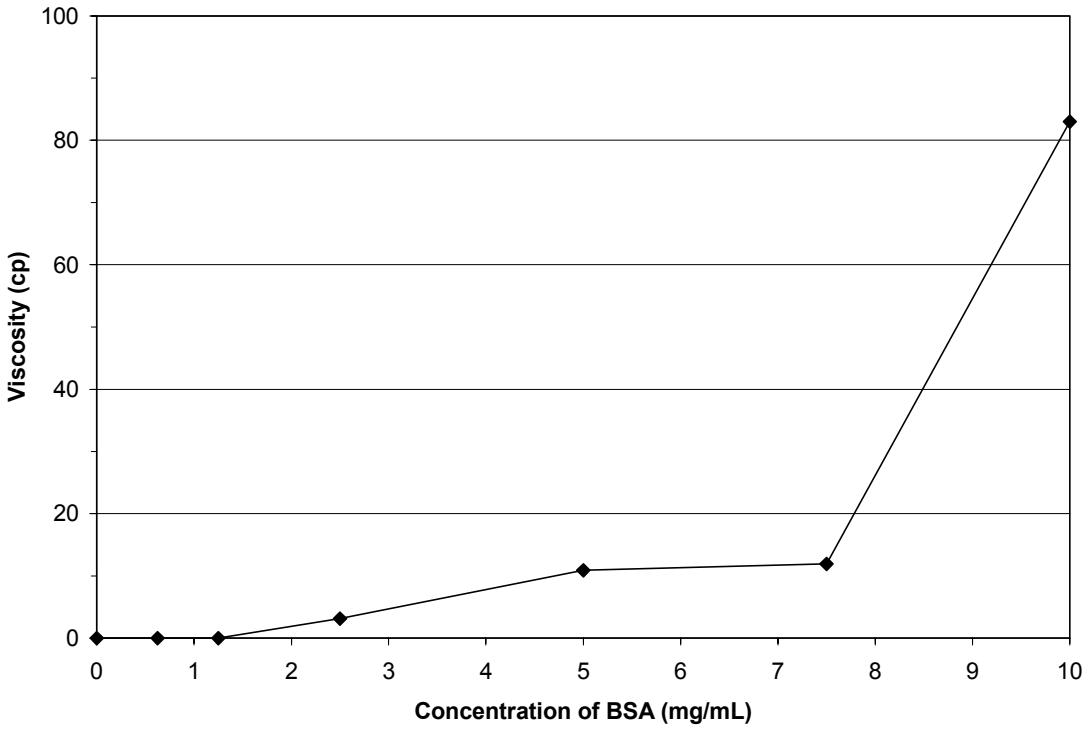

Figure 4.4 Viscosity measurements of BSA in TiO_2 (d=28 nm)-water. Solutions of 0, 0.625, 1.25, 2.5, 5, and 10 mg/mL BSA in 13% TiO_2 were measured with a viscometer.

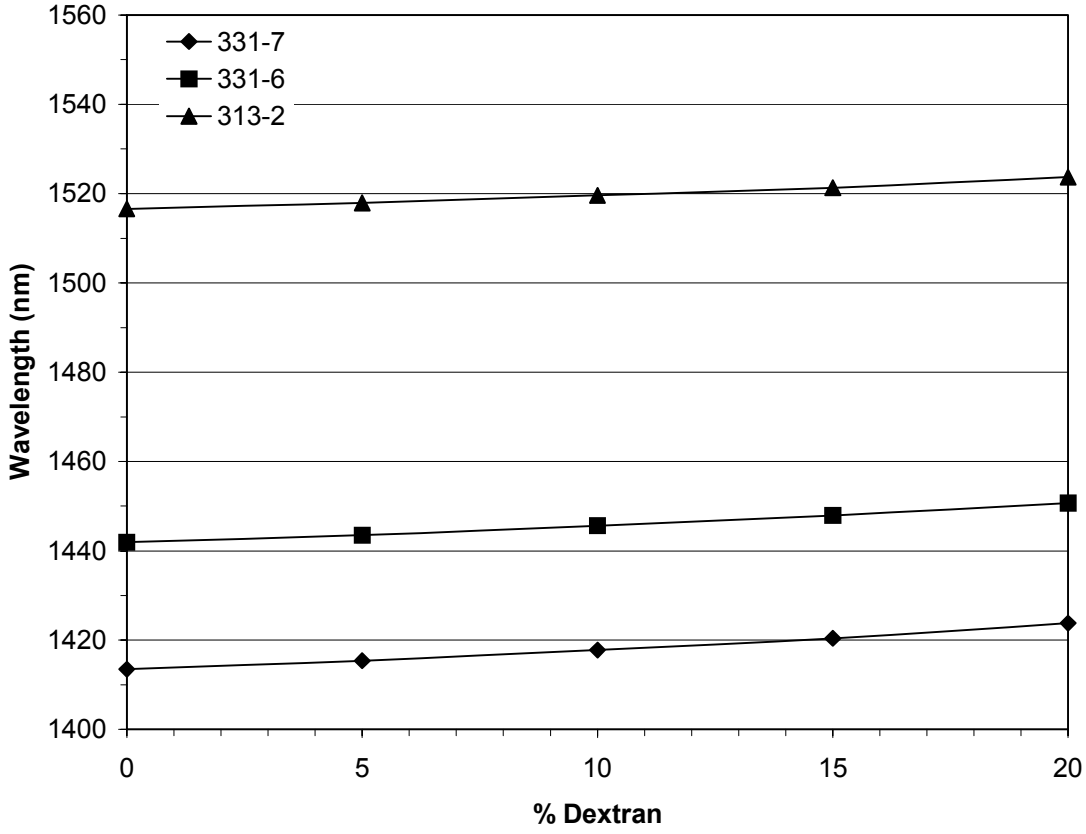

Figure 4.5 **Signal from three blank LPG sensor elements versus percent dextran (T-500) in water. Peak wavelengths were measured with an OSA on each fiber exposed to 0%, 5%, 10%, 15%, and 20% dextran under static conditions. Refractive indices of the dextran solutions were 1.333, 1.337, 1.343, 1.350, and 1.357, respectively (Table 4.4).**

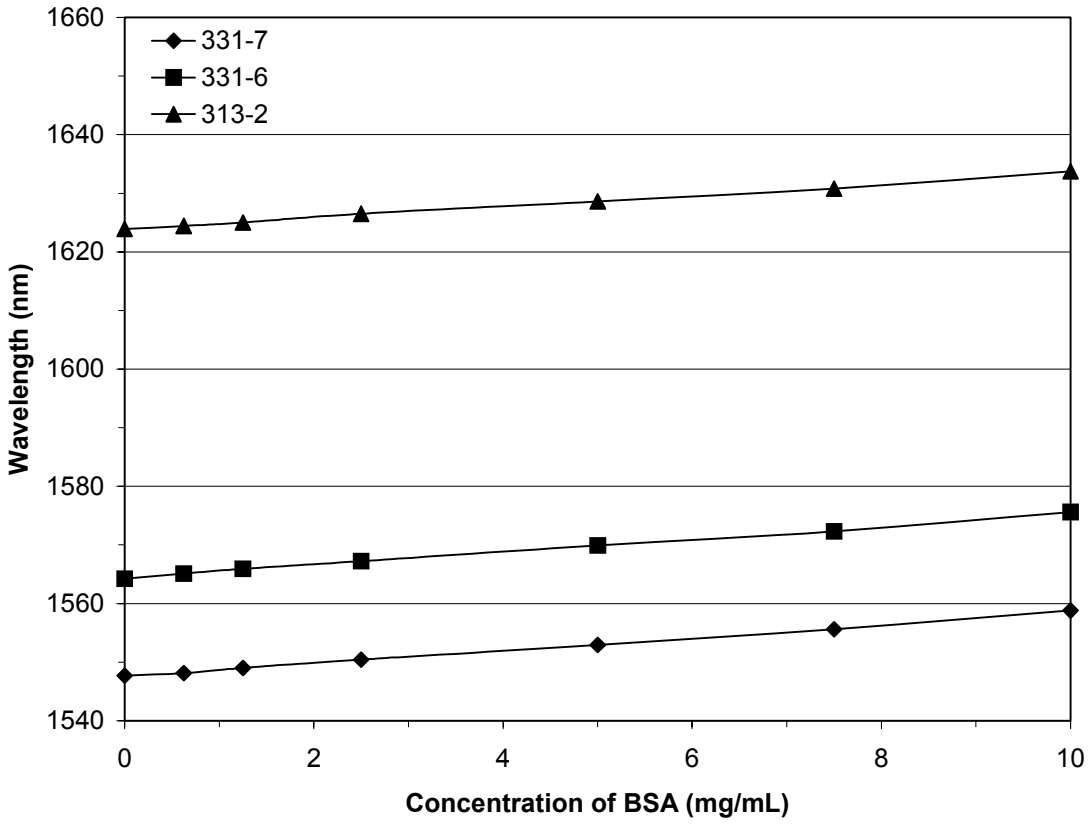

Figure 4.6 **Signal from three blank LPG sensor elements versus increasing concentration of BSA in 75% glycerol-water. Peak wavelengths were measured with on OSA on each fiber exposed to 0, 0.625, 1.25, 2.5, 5, and 10 mg/mL of BSA in 75% glycerol-water under static conditions. Refractive indices of the BSA/glycerol/water solutions were 1.440, 1.440, 1.441, 1.441, 1.441, and 1.442, respectively (Table 4.5).**

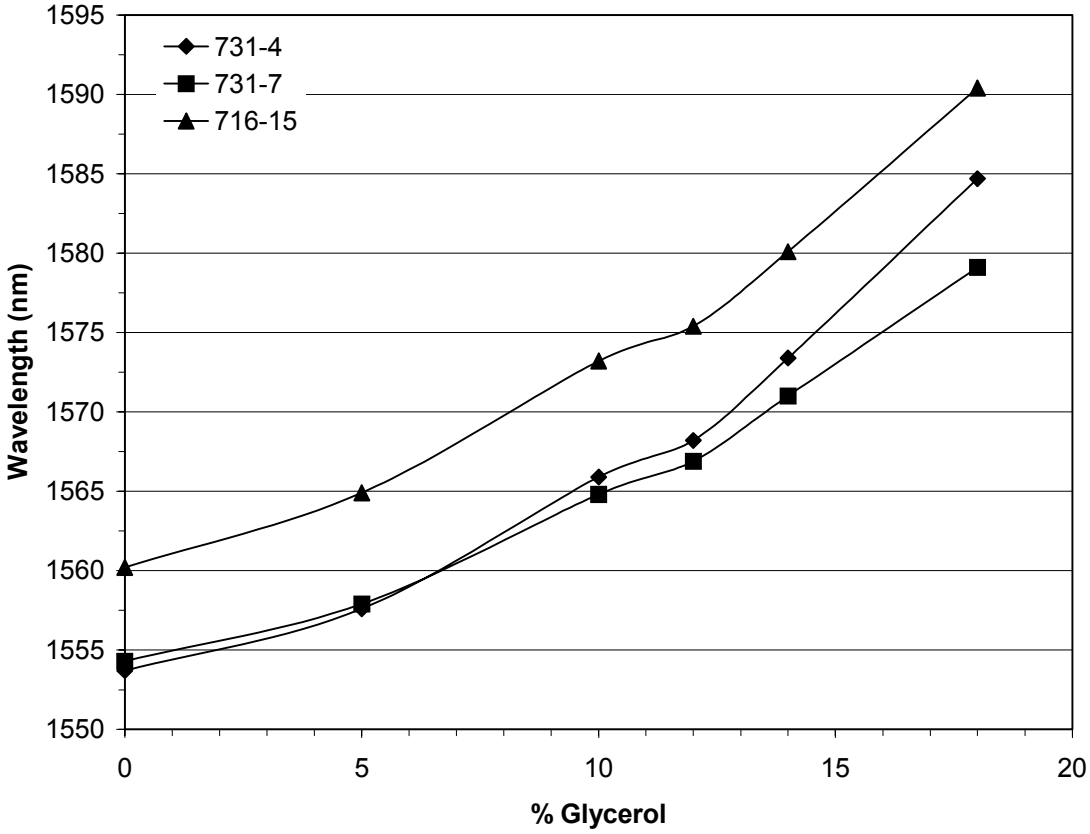

Figure 4.7 **Signal from three TiO_2 (d=300 nm) coated LPG sensor elements versus percent glycerol in water. Peak wavelengths were measured with an OSA on each fiber exposed to 0%, 5%, 10%, 12%, 14%, and 18% glycerol under static conditions. Refractive indices of the glycerol solutions were 1.333, 1.340, 1.347, 1.350, 1.353, 1.359, and 1.361, respectively (calculated from Equation 4.1).**

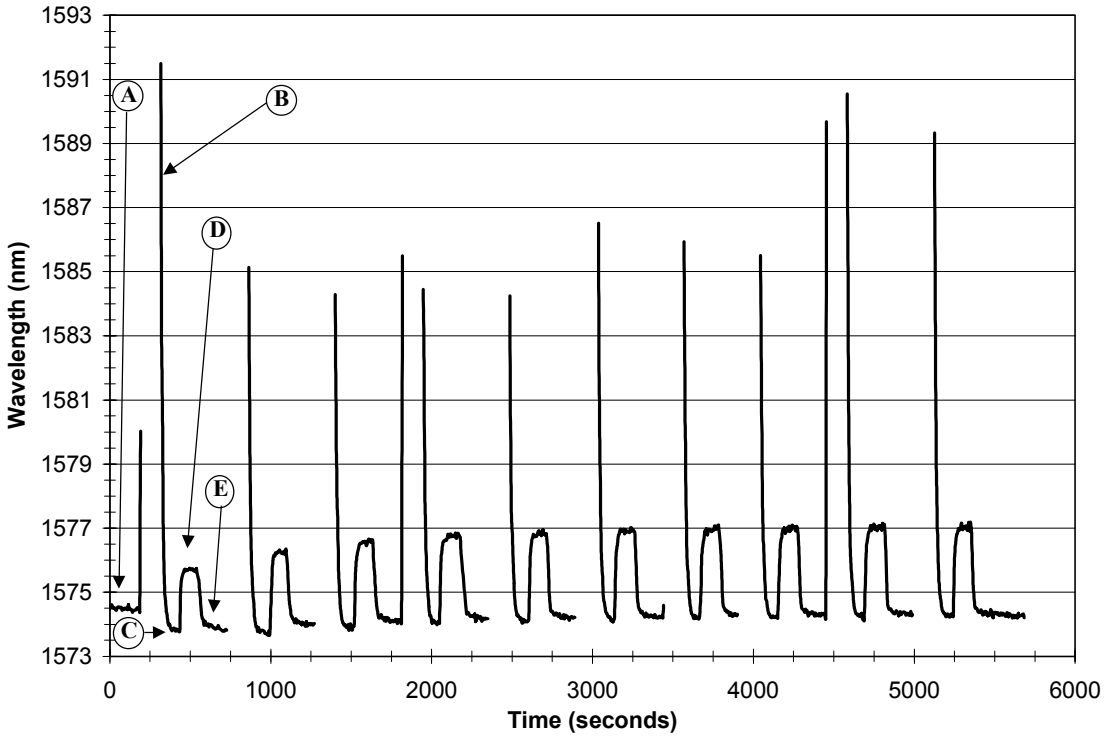

Figure 4.8 **Sensorgram from an OSA for a LPG sensor element coated with TiO_2 (d=300 nm), dextran (T-500), and BSA cycled ten times through two regeneration solutions to test film stability. One cycle consists of: A—2 minute baseline exposure to 0.1 M KPO_4, pH 7.2; B—2 minute exposure to 2 M NaSCN (to remove bound anti-BSA target, but this fiber was not exposed to anti-BSA); C—2 minute rinse with 0.1 M KPO_4, pH 7.2; D—2 minute exposure to 0.1 M glycine/2% acetic acid, pH 2.5 (to remove any bound target); and E—final 2 minute wash with 0.1 M KPO_4, pH 7.2. In each step, the solution was flowing through the sensor holder at 5 mL/min.**

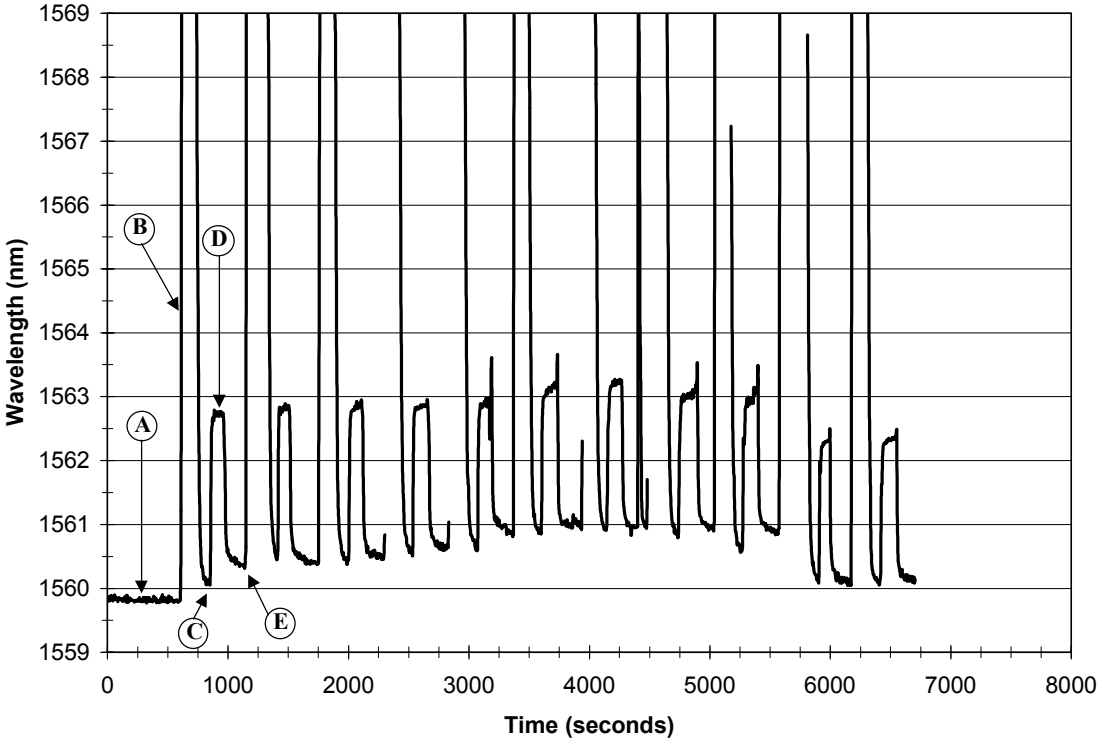

Figure 4.9 **Sensorgram from an OSA for a LPG sensor element coated with TiO_2 (d=300 nm), dextran (T-500), and BSA cycled eleven times through two regeneration solutions after cellulose cross-linking of the dextran hydrogel to test film stability. One cycle consists of: A—2 minute baseline exposure to 0.1 M KPO_4, pH 7.2; B—2 minute exposure to 2 M NaSCN (to remove bound anti-BSA target, but this fiber was not exposed to anti-BSA); C—2 minute rinse with 0.1 M KPO_4, pH 7.2; D—2 minute exposure to 0.1 M glycine/2% acetic acid, pH 2.5 (to remove any bound target); and E—final 2 minute wash with 0.1 M KPO_4, pH 7.2. In each step, the solution was flowing through the sensor holder at 5 mL/min.**

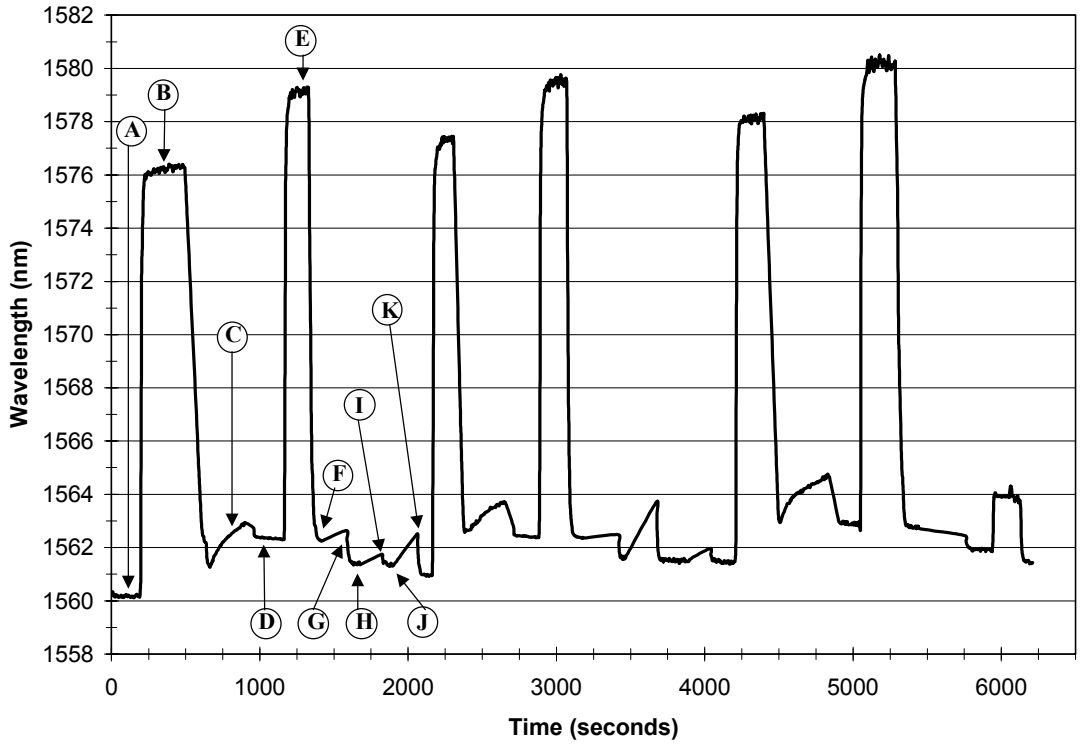

Figure 4.10 **Sensorgram from an OSA for a LPG sensor element coated with TiO_2 (d=300 nm), dextran (T-500), and BSA cycled three times through the affinity capture of anti-BSA antisera with the peak wavelength shift amplified by glycerol. One cycle consists of: A—3 minute baseline exposure to 0.1 M KPO_4, pH 7.2; B—7 minute baseline exposure to 10% glycerol in 0.1 M KPO_4, pH 7.2; C—5 minute recycle of 20 μg/mL anti-BSA antisera in 0.1 M KPO_4, pH 7.2; D—3 minute wash with 0.1 M KPO_4, pH 7.2 to remove any unbound anti-BSA; E—3 minute exposure to 10% glycerol in 0.1 M KPO_4, pH 7.2 to record peak wavelength shift; F—2 minute wash with 0.1 M KPO_4, pH 7.2 to remove any residual glycerol; G—2 minute exposure to 2 M NaSCN to remove bound anti-BSA target (injected into holder and saved for ELISA quantification); H—2 minute wash with 0.1 M KPO_4, pH 7.2; I—a second 2 minute exposure to 2 M NaSCN (injected into the holder and saved for ELISA quantification); J—2 minute wash with 0.1 M KPO_4, pH 7.2; K—2 minute exposure to 0.1 M glycine/2% acetic acid, pH 2.5 to remove bound anti-BSA target. In each of the above steps, the solutions were flowing through the sensor holder at 5 mL/min, unless otherwise noted.**

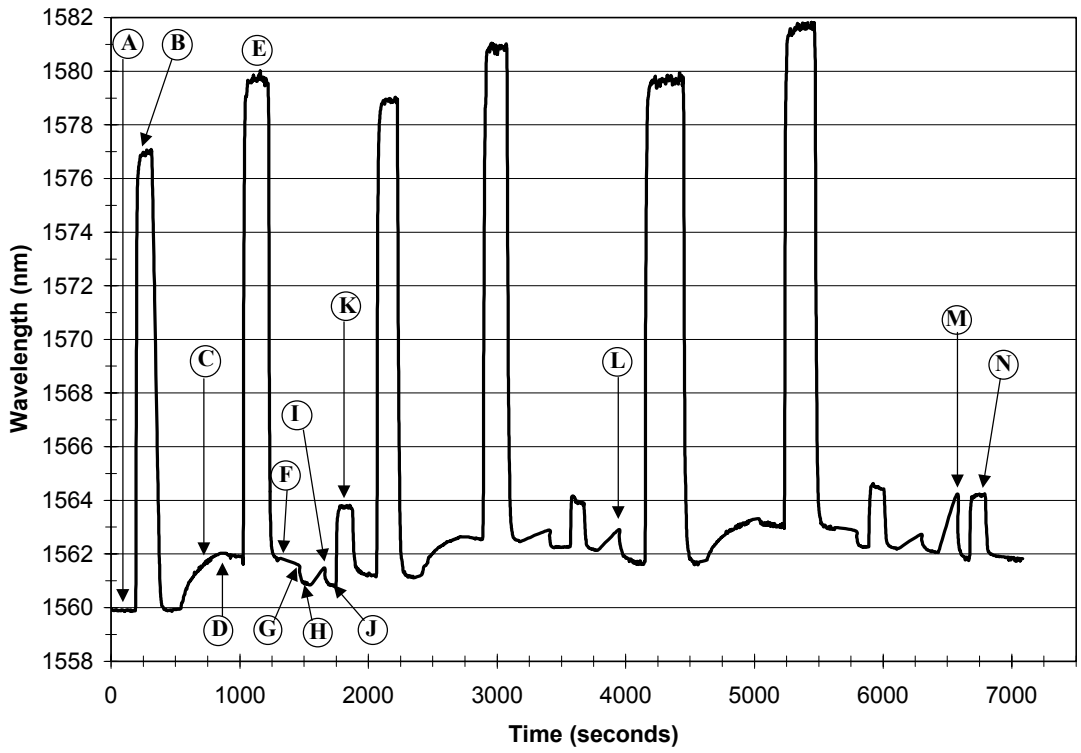

Figure 4.11 **Sensorgram from an OSA for a LPG sensor element coated with TiO_2 (d=300 nm), dextran (T-500), and BSA cycled three times through the affinity capture of anti-BSA antisera with the peak wavelength shift amplified by glycerol. One cycle consists of: A—3 minute baseline exposure to 0.1 M KPO_4, pH 7.2; B—3 minute baseline exposure to 10% glycerol in 0.1 M KPO_4, pH 7.2; C—5 minute recycle of 20 μg/mL anti-BSA antisera in 0.1 M KPO_4, pH 7.2; D—2 minute wash with 0.1 M KPO_4, pH 7.2 to remove any unbound anti-BSA; E—3 minute exposure to 10% glycerol in 0.1 M KPO_4, pH 7.2 to record peak wavelength shift; F—2 minute wash with 0.1 M KPO_4, pH 7.2 to remove any residual glycerol; G—2 minute exposure to 2 M NaSCN to remove bound anti-BSA target (injected into holder and saved for ELISA quantification); H—2 minute wash with 0.1 M KPO_4, pH 7.2; I—a second 2 minute exposure to 2 M NaSCN (injected into the holder and saved for ELISA quantification); J—2 minute wash with 0.1 M KPO_4, pH 7.2; K—2 minute exposure to 0.1 M glycine/2% acetic acid, pH 2.5 to remove bound anti-BSA target; L—2 minute exposure to 4 M NaCl to remove anti-BSA target; M—final 2 minute exposure to 2 M NaSCN to remove any bound material; N—final 2 minute exposure to 0.1 M glycine/2% acetic acid, pH 2.5 to remove any bound material. In each of the above steps, the solutions were flowing through the sensor holder at 5 mL/min, unless otherwise noted.**

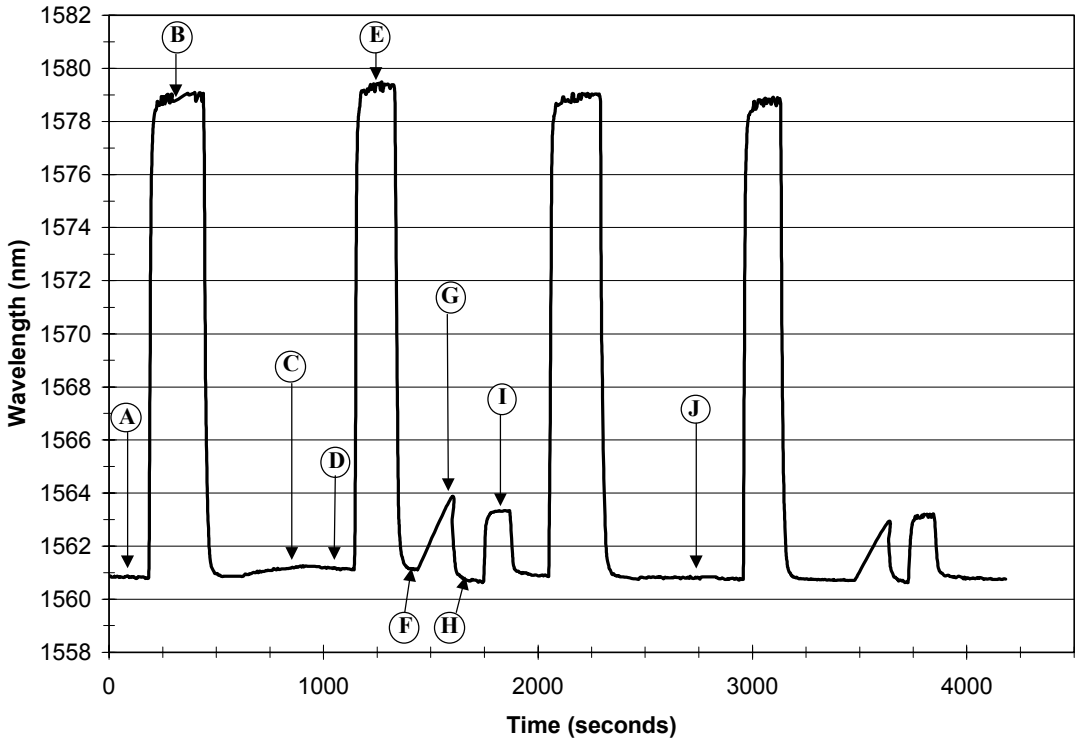

Figure 4.12 **Negative control sensorgram from an OSA for a LPG sensor element coated with TiO_2 (d=300 nm), dextran (T-500), and BSA exposed goat serum and rabbit anti-cholera toxin IgG with peak wavelength shifts amplified by glycerol. A—3 minute baseline exposure to 0.1 M KPO_4, pH 7.2. B—4 minute baseline exposure to 10% glycerol in 0.1 M KPO_4, pH 7.2. C—5 minute recycle of 1:100 dilution of goat antisera in 0.1 M KPO_4, pH 7.2. D—2 minute wash with 0.1 M KPO_4, pH 7.2 to remove any unbound antibodies/proteins. E—3 minute exposure to 10% glycerol in 0.1 M KPO_4, pH 7.2 to record peak wavelength shift. F—2 minute wash with 0.1 M KPO_4, pH 7.2 to remove any residual glycerol. G—2 minute exposure to 2 M NaSCN to remove bound antibodies. H—2 minute wash with 0.1 M KPO_4, pH 7.2. I—2 minute exposure to 0.1 M glycine/2% acetic acid, pH 2.5 to remove bound antibodies/proteins. The second cycle consisted of the same above steps, except that specificity was tested against rabbit anti-cholera toxin in step J. In each of the above steps, the solutions were flowing through the sensor holder at 5 mL/min.**

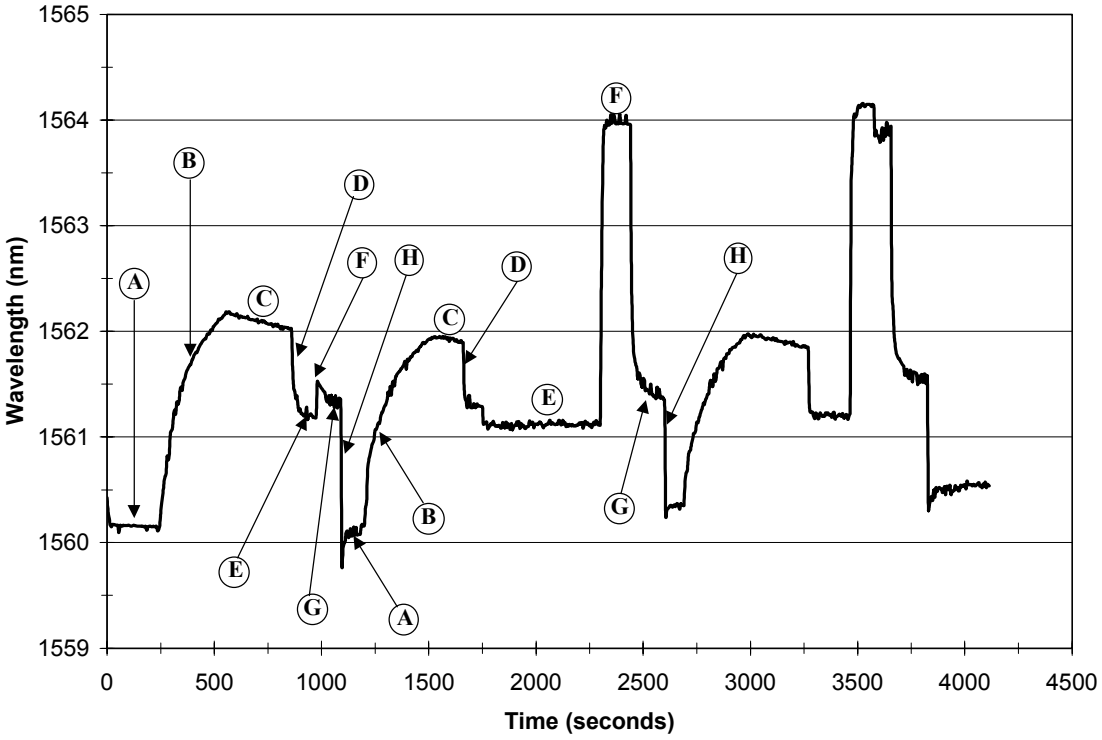

Figure 4.13 Sensorgram from an OSA for a LPG sensor element coated with TiO_2 (d=300 nm), dextran (T-500), and BSA cycled three times through the affinity capture of anti-BSA antisera with the peak wavelength shift NOT amplified by glycerol. One cycle consists of: A—5 minute baseline exposure to 0.1 M KPO_4, pH 7.2; B—5 minute recycle of 20 μg/mL anti-BSA antisera in 0.1 M KPO_4, pH 7.2; C—5 minute wash with 0.1 M KPO_4, pH 7.2 to remove any unbound anti-BSA, and record peak wavelength shift; D—2 minute exposure to 2 M NaSCN to remove bound anti-BSA target (injected into holder and saved for ELISA quantification); E—2 minute wash with 0.1 M KPO_4, pH 7.2; F—2 minute exposure to 0.1 M glycine/2% acetic acid, pH 2.5 to remove bound anti-BSA target; G—2 minute wash with 0.1 M KPO_4, pH 7.2; H—2 minute exposure to 0.1 M TEA, pH 11.5 to remove bound anti-BSA target. In each of the above steps, the solutions were flowing through the sensor holder at 5 mL/min, unless otherwise noted.

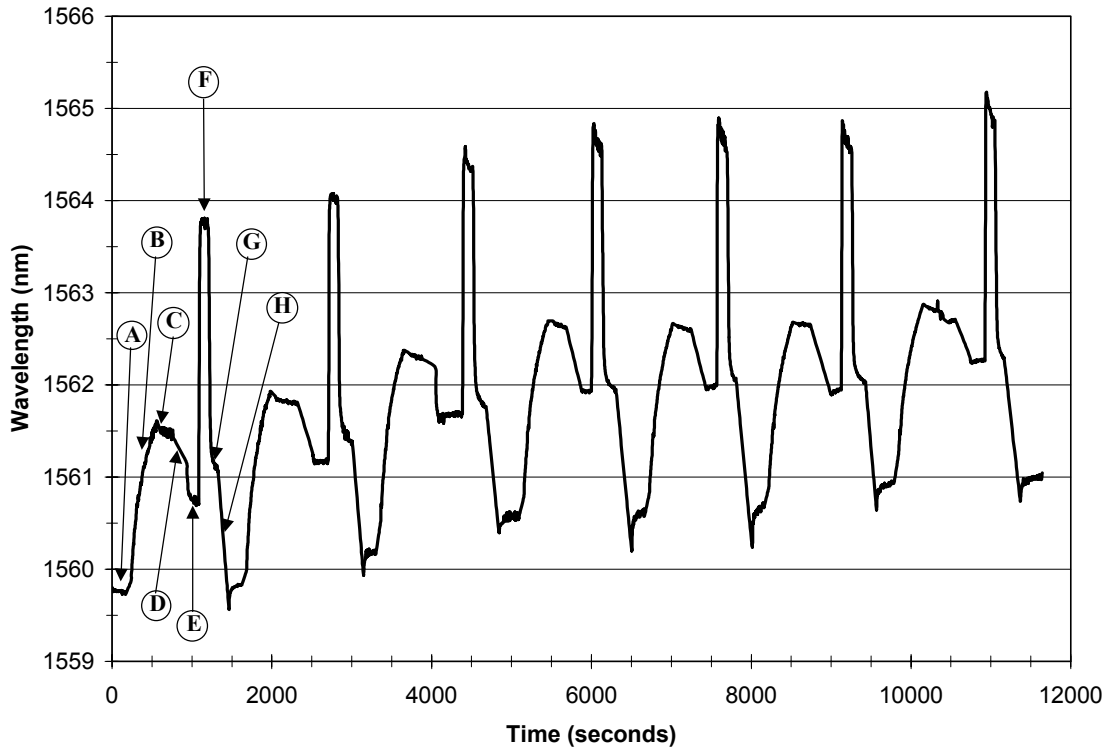

Figure 4.14 Sensorgram from an OSA for a LPG sensor element coated with TiO_2 (d=300 nm), dextran (T-500), and BSA cycled ten times through the affinity capture of anti-BSA antisera with the peak wavelength shift NOT amplified by glycerol. One cycle consists of: A—5 minute baseline exposure to 0.1 M KPO_4, pH 7.2; B—5 minute recycle of 20 μg/mL anti-BSA antisera in 0.1 M KPO_4, pH 7.2; C—5 minute wash with 0.1 M KPO_4, pH 7.2 to remove any unbound anti-BSA, and record peak wavelength shift; D—2 minute exposure to 2 M NaSCN to remove bound anti-BSA target (injected into holder and saved for ELISA quantification); E—2 minute wash with 0.1 M KPO_4, pH 7.2; F—2 minute exposure to 0.1 M glycine/2% acetic acid, pH 2.5 to remove bound anti-BSA target; G—2 minute wash with 0.1 M KPO_4, pH 7.2; H—2 minute exposure to 0.1 M TEA, pH 11.5 to remove bound anti-BSA target. In each of the above steps, the solutions were flowing through the sensor holder at 5 mL/min, unless otherwise noted.

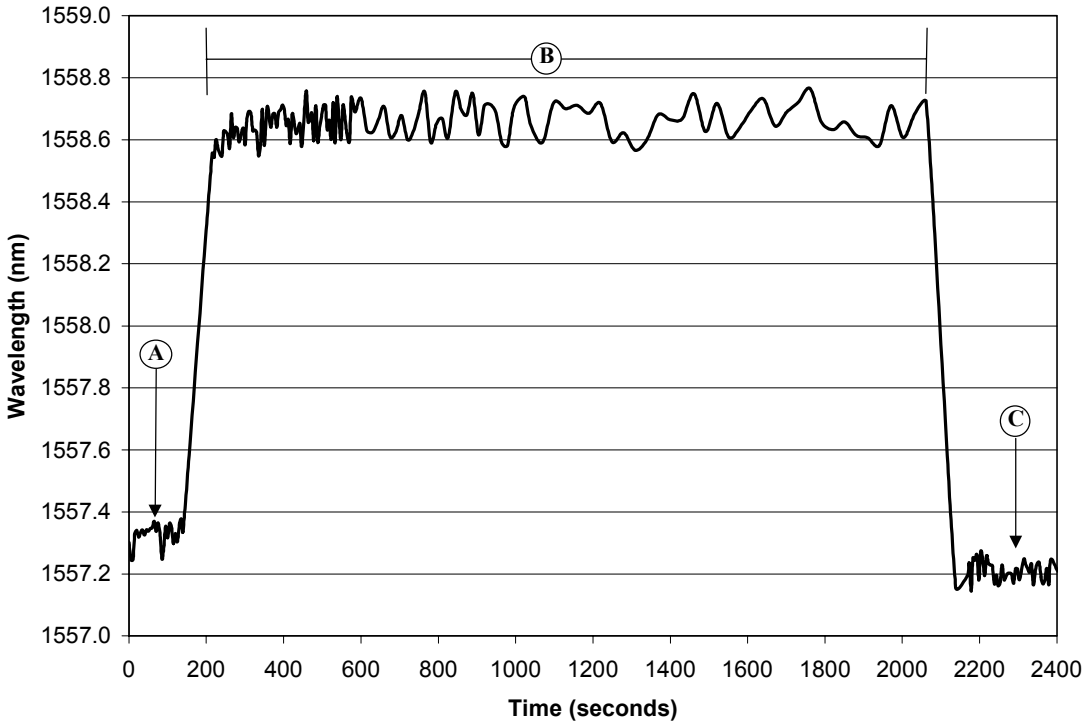

Figure 4.15 Sensorgram from an OSA for a LPG sensor element coated with TiO_2 (d=300 nm), dextran (T-500), and BSA showing the rebinding of "affinity purified" anti-BSA IgG. A—3 minute baseline exposure to 0.1 M KPO_4, pH 7.2. B—30 minute recycle of "affinity purified" anti-BSA IgG in 0.1 M KPO_4, pH 7.2. C—5 minute wash with 0.1 M KPO_4, pH 7.2 to remove any unbound anti-BSA, and record peak wavelength shift. In each of the above steps, the solutions were flowing through the sensor holder at 5 mL/min.

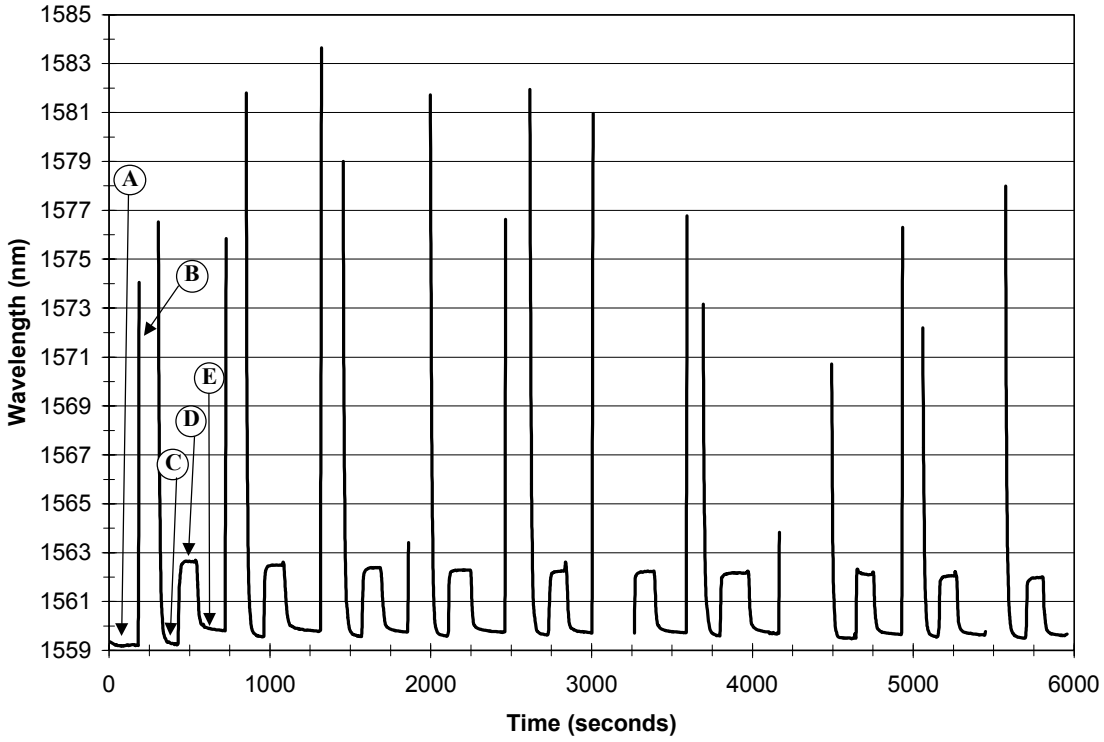

Figure 4.16 Sensorgram from an OSA for a LPG sensor element coated with TiO_2 (d=300 nm), dextran (T-500), and BSA cycled ten times through two regeneration solutions after target binding experiments to test film stabilty. One cycle consists of: A—2 minute baseline exposure to 0.1 M KPO_4, pH 7.2; B—2 minute exposure to 2 M NaSCN (to remove bound anti-BSA target, but this fiber was not exposed to anti-BSA); C—2 minute rinse with 0.1 M KPO_4, pH 7.2; D—2 minute exposure to 0.1 M glycine/2% acetic acid, pH 2.5 to remove any bound target; and E—final 2 minute wash with 0.1 M KPO_4, pH 7.2. In each step, the solution was flowing through the sensor holder at 5 mL/min.

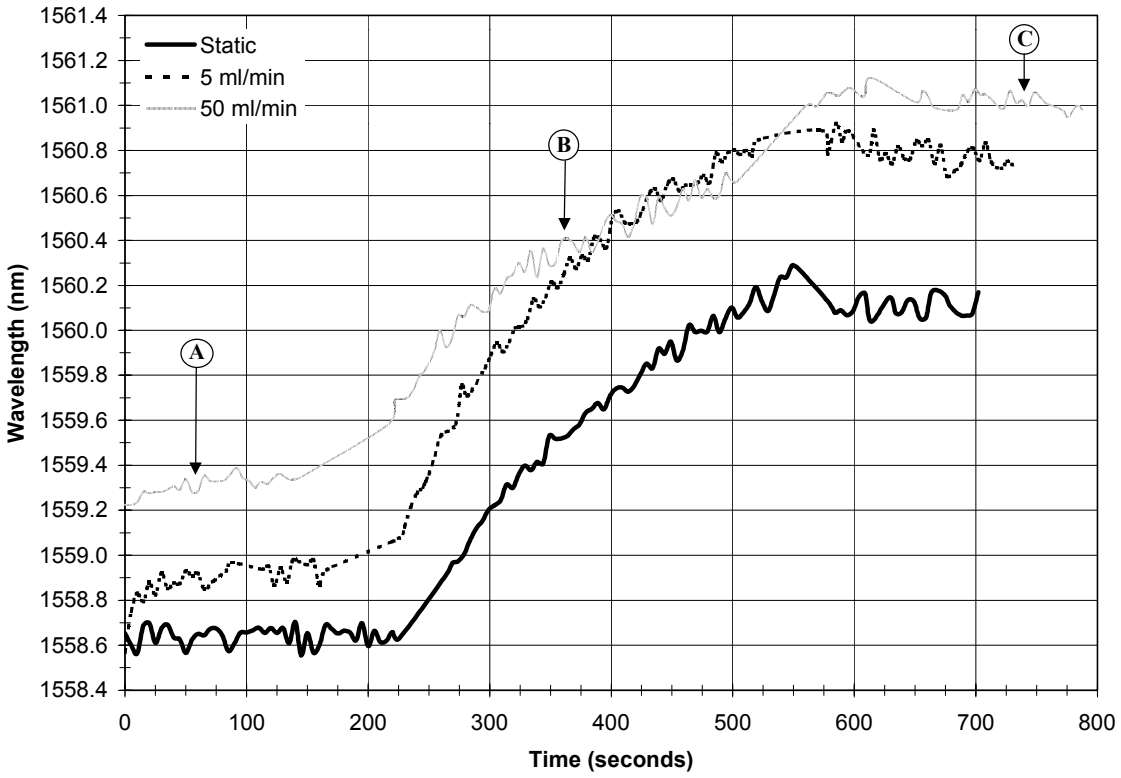

Figure 4.17 Sensorgram from an OSA for a LPG sensor element coated with TiO_2 (d=300 nm), dextran (T-500), and BSA showing the effect of flowrate through the sensor holder on overall target binding. A—4 minute baseline exposure to 0.1 M KPO_4, pH 7.2. B—5 minute exposure to 20 μg/mL anti-BSA antisera in 0.1 M KPO_4, pH 7.2 under conditions of 0 mL/min (static), 5 mL/min, and 50 mL/min. C—3 minute wash with 0.1 M KPO_4, pH 7.2 to remove any unbound anti-BSA, and record peak wavelength shift. Steps A and C were conducted with phosphate buffer flowing through the sensor holder at 5 mL/min.

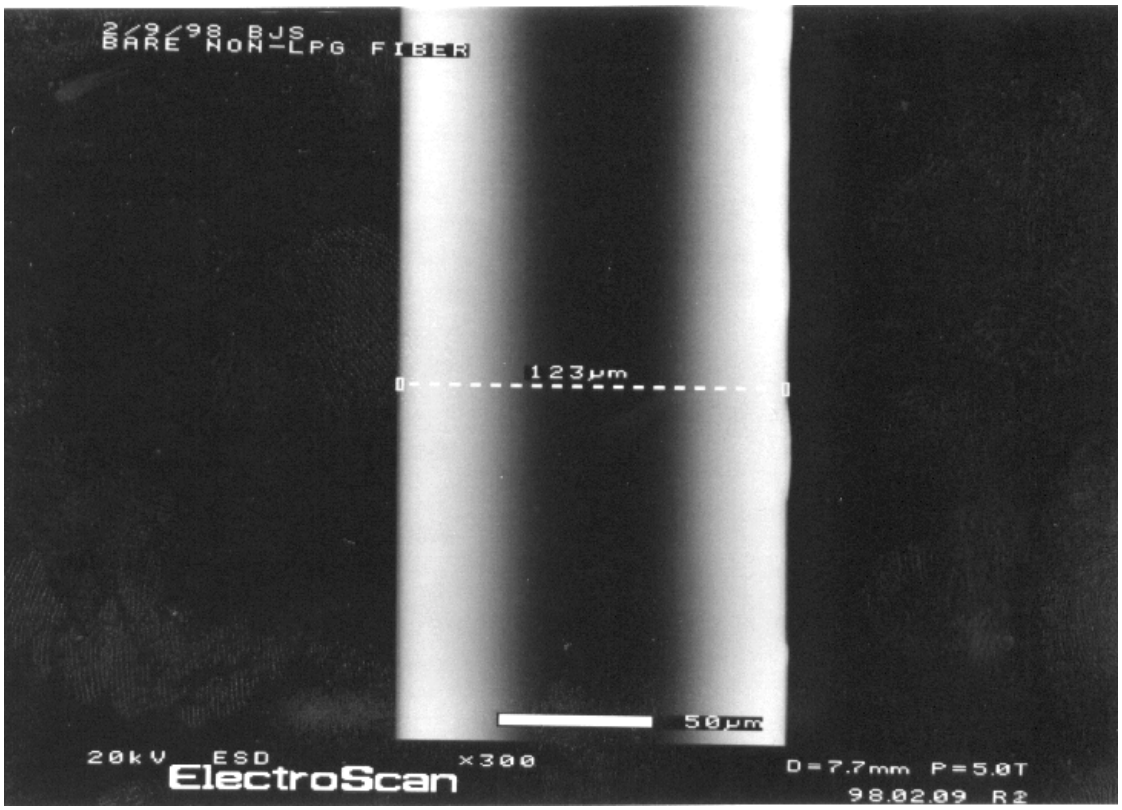

Figure 4.18 Environmental scanning electron microscope (ESEM) image of a blank, non-LPG optical fiber.

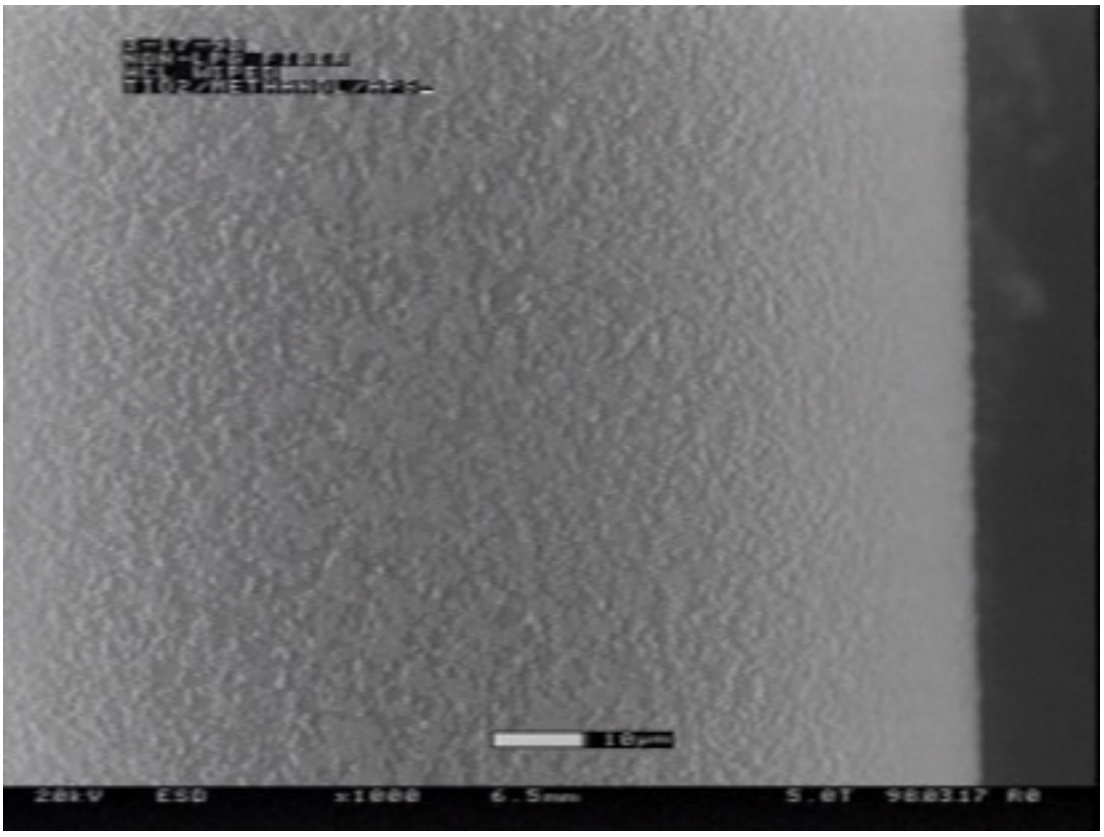

Figure 4.19 Environmental scanning electron microscope (ESEM) image of a blank, non-LPG optical fiber densely coated with TiO_2 (d=300 nm) particles.

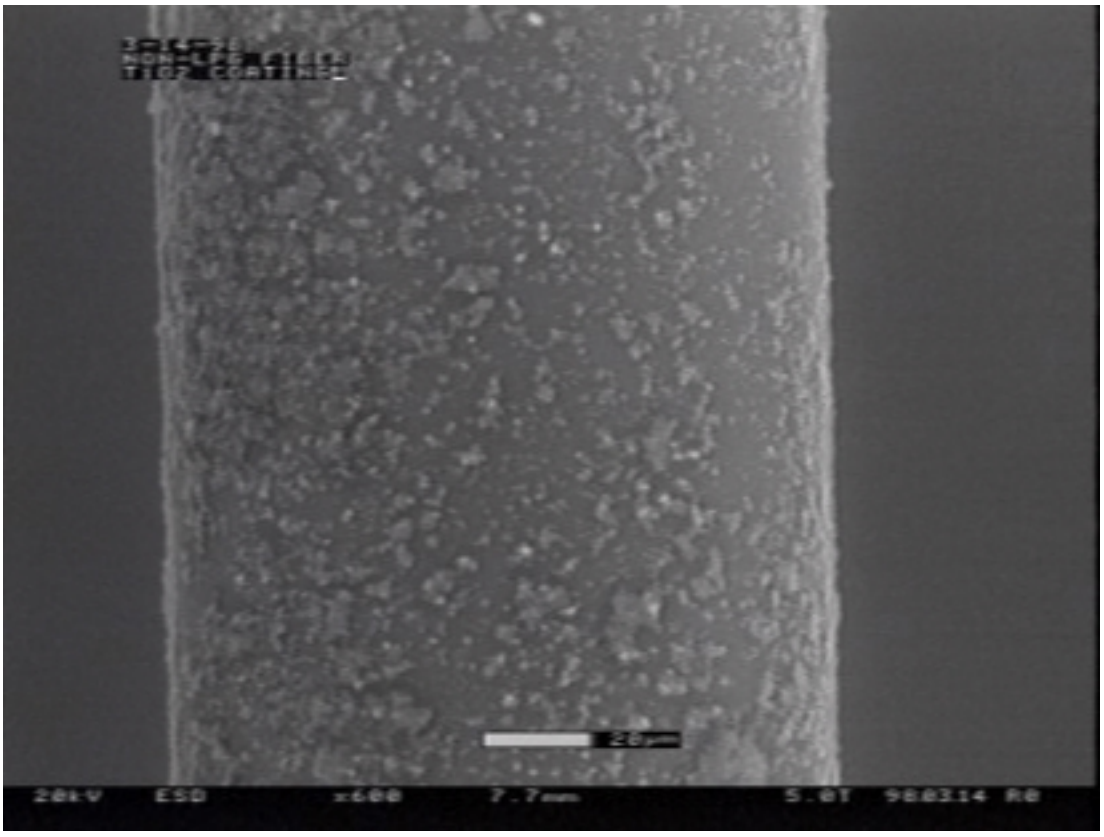

Figure 4.20 Environmental scanning electron microscope (ESEM) image of a blank, non-LPG optical fiber sparsely coated with TiO_2 (d=300 nm) particles.

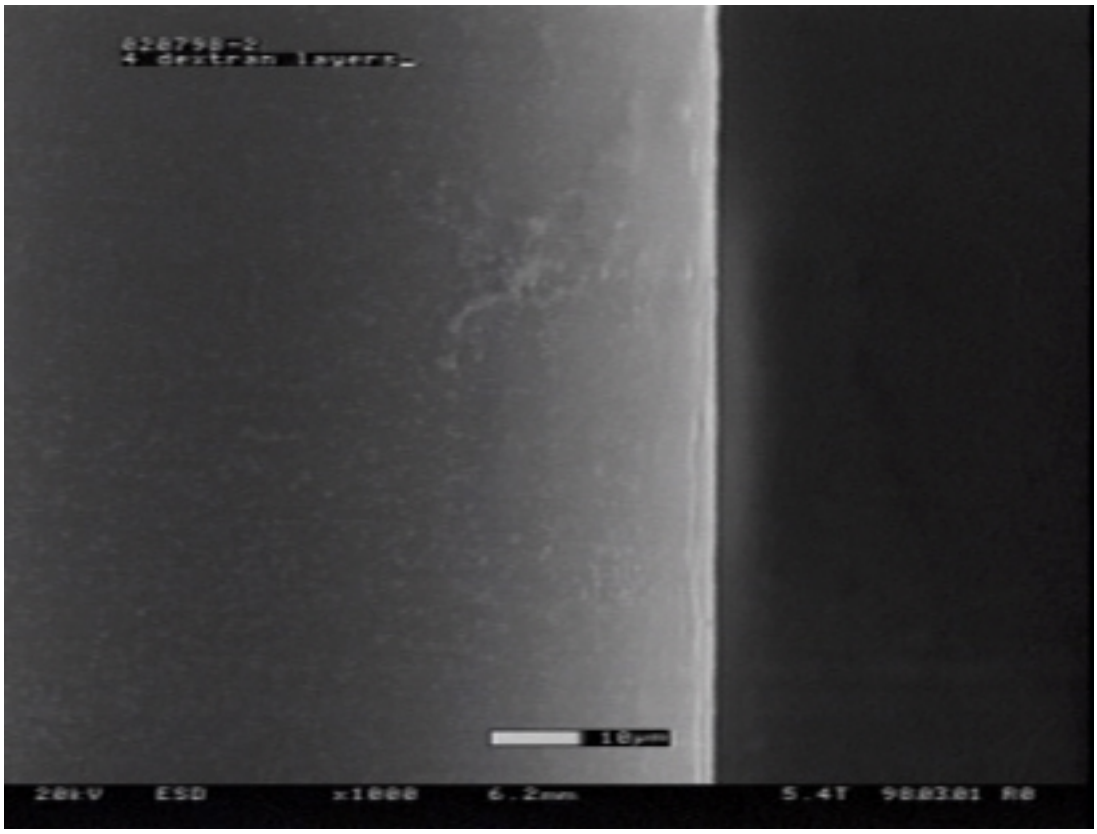

Figure 4.21 Environmental scanning electron microscope (ESEM) image of a LPG sensor element coated with TiO_2 (d=300 nm) and a dextran (T-500) hydrogel in a dehydrated state, after a section of hydrogel has been excavated. The TiO_2 particles of the underlayer are visible through the dextran film and in the excavated area.

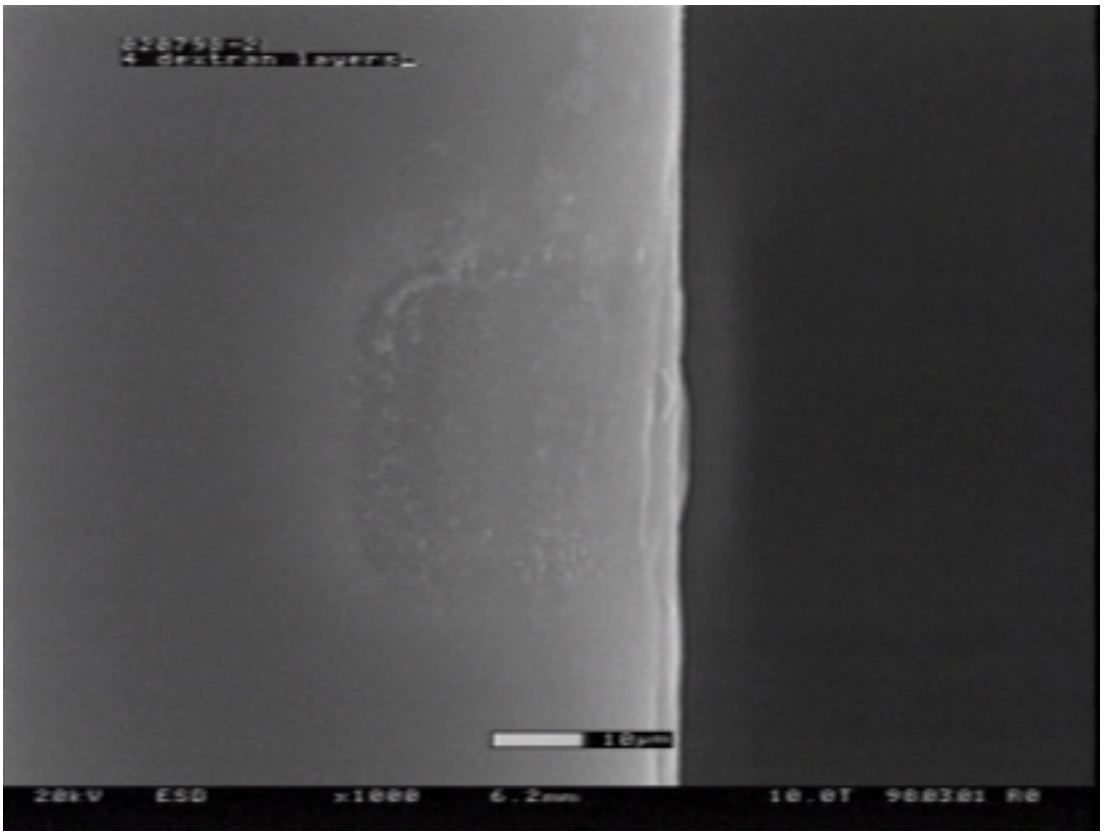

Figure 4.22 Environmental scanning electron microscope (ESEM) image of a LPG sensor element coated with TiO_2 (d=300 nm) and a dextran (T-500) hydrogel in a fully hydrated state. The hydrated film masks the TiO_2 underlayer except for the excavated area where the TiO_2 particles are still visible.

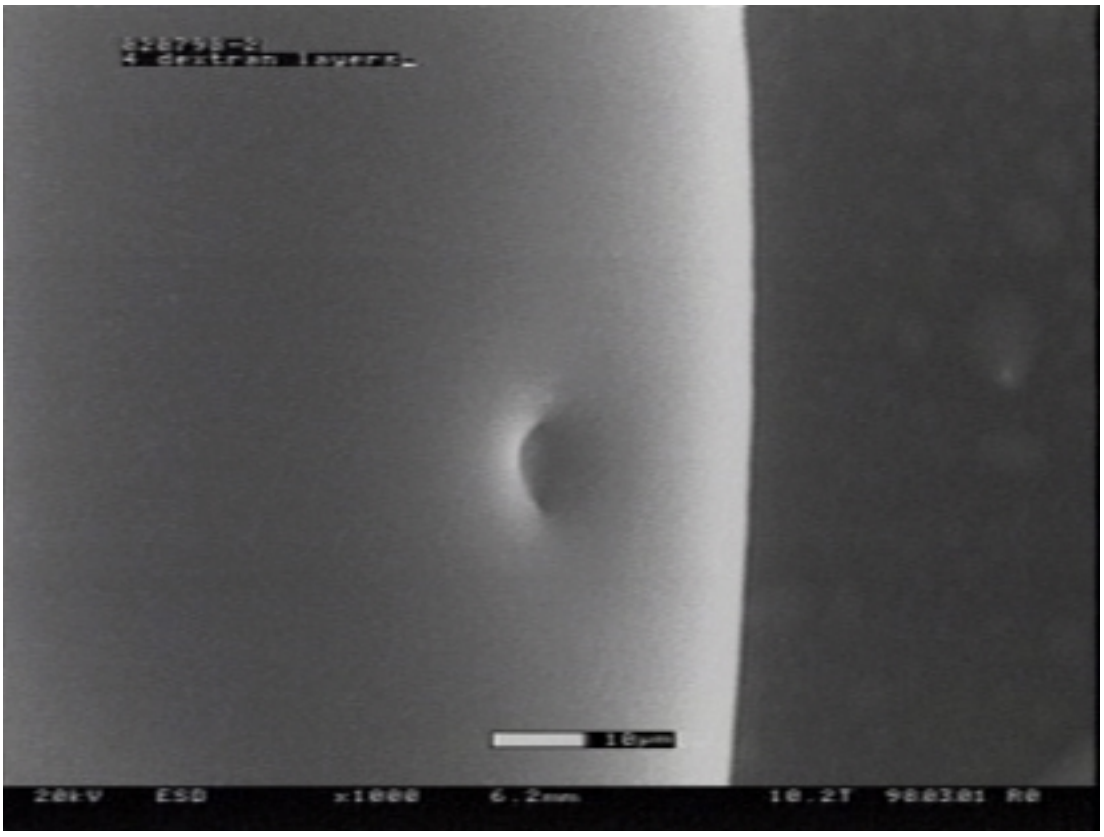

Figure 4.23 Environmental scanning electron microscope (ESEM) image of a LPG sensor element coated with a fully hydrated layer of dextran (T-500) after a small region has been excavated. The thick hydrogel layer is present everywhere except for the excavated area.

Chapter 5

CONCLUSIONS AND RECOMMENDATIONS

5.1 Conclusions

This research further demonstrates the feasibility of developing a fiber optical biosensor based on long-period gratings. Affinity capture of anti-BSA IgG was demonstrated by monitoring the refractive index change within the evanescent field created by the LPG. However, the sensitivity of the LPG fiber is only on the order of 10^{-3} when in a local environment having a refractive index of 1.33.

The use of reagents like glycerol which raise the local refractive index within the biosensor film to 1.44 greatly increase the sensitivity of the LPG. The sensitivity of the sensor was tested against solutions of varying refractive indices such as 75% glycerol and was approximately 10^{-4}. The LPG surface was then modified by titanium dioxide deposition to raise the average local refractive index. The titanium dioxide film was visualized by ESEM and it was found that uniform coverage of the LPG element was difficult to reproduce from fiber to fiber. For some fibers the signal could be raised to that corresponding to an RI of approximately 1.42. The dextran hydrogel was also visualized by ESEM. It was found to consistently coat the titanium dioxide layer, and upon excavation was estimated to be approximately 500 nm thick. It was demonstrated that a composite film could be made to increase the mass averaged refractive index of the LPG. It can be concluded that this discontinuous

medium had the same effect on fiber sensitivity as did operation in a continuous medium of increased refractive index (75% glycerol).

Dextran T-500 was activated with aldehyde groups and attached to the silylated titanium dioxide layer. Since the dextran was not cross-linked into macromonomers prior to attachment, cellulose was cross-linked around the gel to form a "stocking" around the dextran. This method showed stability over 50 regeneration cycles with an overall baseline shift of only –1.3 nm.

The BSA ligand could be regenerated and used for multiple exposures. A regeneration system of 2 M NaSCN and 0.1 M glycine in 2% acetic acid was successful at removing bound anti-BSA IgG. Occasionally, a high concentration salt solution and a 0.1 M TEA solution were tried as regeneration systems. The salt solution showed negligible affects on regeneration. The TEA solution did aid in regeneration, however, it was used sparingly due to its harsh nature.

Reproducible binding was shown over multiple exposures, with no cross reactivity for non-specific antibodies and other proteins. A sample of 20 μg/mL of anti-BSA IgG in whole serum was recycled through the fiber holder; the accompanying peak wavelength shift averaged 2 nm on a desktop OSA with a noise level of 0.1 nm. A Queensgate scanning Fabry-Perot spectral filter was also evaluated. The noise of the Queensgate was an order of magnitude lower than the OSA. Additionally, reproducible construction of affinity fibers was demonstrated. Multiple anti-BSA IgG fibers showed approximately the same level of target binding, as quantified by ELISA.

Finally, mass transfer effects were found to be negligible in this system. The overall peak shifts between static (0 cm/min) incubation of sample, flow at 5

mL/min (125 cm/min), and flow at 50 mL/min (1250 cm/min) were all within the variance of shifts detected when experiments were conducted at the same flow conditions.

5.2 Recommendations

To further the technical optimization of LPG biosensors, more research needs to be done:

1. Optimize target capture by designing affinity ligand films that utilize the entire evanescent field. The films should not extend beyond the evanescent wave penetration depth since binding in that area is not detected.

2. An in depth evaluation of the binding kinetics between the affinity ligand and the target should be done. A true understanding of the rate limitations will aid in optimizing the density of the gel and the density of the immobilized ligands so that efficient target binding can occur. Creating an environment with the appropriate ligand density will help to maximize target detection by providing the optimal number of target binding sites, without introducing steric hindrance due to ligand overcrowding. Understanding the effect of immobilization on the dissociation rate constant will also be beneficial to deriving a system with increased binding affinity.

3. Reproducible titanium dioxide films need to be created. In depth research into the physical properties affecting titanium dioxide adsorption and film drying is needed to optimize the coating process.

4. Sensitivity can be increased by improving the LPG sensor. Modifying the physical properties of the optical fiber and grating so that operation is around 1.44 will preclude the use of titanium dioxide films, which were not always reproducible. Improvements in spectrometer and signal demodulation technology will also help to make detection of a shift in refractive index on the order of 10^{-6} possible.

REFERENCES

Aizawa, M., Morioka, A., Matsuoka, H., Suzuki, S., Nagamura, Y., Shinohara, R. and Ishiguro, I.: An Enzyme Immunosensor for IgG. *Journal of Solid-Phase Biochemistry*. **1**(4):319-328 (1976).

Aizawa, M., Kato, S. and Suzuki, S.: Immunoresponsive Membrane I. Membrane Potential Change Associated with an Immunochemical Reaction Between Membrane-Bound Antigen and Free Antibody. *Journal of Membrane Science*. **2**:125-132 (1977a).

Aizawa, M. and Suzuki, S.: An Immuno Sensor for Specific Protein. *Chemistry Letters*. 779-782 (1977b).

Aizawa, M., Morioka, A., Suzuki, S. and Nagamura, Y.: Enzyme Immunosensor III. Amperometric Determination of Human Chorionic Gonadotropin by Membrane-Bound Antibody. *Analytical Biochemistry*. **94**:22-28 (1979).

Aizawa, M., Kato, S. and Suzuki, S.: Electrochemical Typing of Blood Using Affinity Membranes. *Journal of Membrane Science*. **7**:1-10 (1980a).

Aizawa, M., Morioka, A. and Suzuki, S.: An Enzyme Immunosensor for the Electrochemical Determination of the Tumor Antigen α-Fetoprotein. *Analytica Chimica Acta*. **115**:61-67 (1980b).

Aizawa, M.: Immunosensors for Chemical Analysis. *Advances in Clinical Chemistry*. **31**:247-275 (1994).

Anderson, G.P., Breslin, K.A. and Ligler, F.S.: Assay Development for a Portable Fiberoptic Biosensor. *ASAIC Journal*. **42**:942-946 (1996).

Andle, J.C., Weaver, J.T., McAllister, D.J., Josse, F. and Vetelino, J.F.: Improved Acoustic-Plate-Mode Biosensor. *Sensors and Actuators*. **B13-14**:437-442 (1993).

Bhatia, V.: Properties and Sensing Applications of Long-Period Gratings. Ph.D. Dissertation, Department of Electrical Engineering, Virginia Polytechnic Institute and State University (1996).

Buckingham, A.D.: Intermolecular Forces. In *Principles of Molecular Recognition*. Blackie Academic and Professional, New York, 1993, pp. 1-17.

Byfield, M.P. and Abuknesha, R.A.: Biochemical Aspects of Biosensors. *Biosensors & Bioelectronics*. **9**:373-400 (1994).

Cullen, D.C. and Lowe, C.R.: A Direct Surface Plasmon-Polariton Immunosensor: Preliminary Investigation of the Non-Specific Adsorption of Serum Components to the Sensor Interface. *Sensors and Actuators*. **B1**:576-579 (1990).

Danielsson, B. and Larsson, P.O.: Specific Monitoring of Chromatographic Procedures. *Trends in Analytical Chemistry*. **9**:223-227 (1990).

Danielsson, B.: Calorimetric Biosensors. *Biochemical Society Transactions*. **19**(1):26-28 (1991).

De Feijter, J.A., Benjamins, J. and Veer, F.A.: Ellipsometry as a Tool to Study the Adsorption Behaviour of Synthetic and Biopolymers at the Air-Water Interface. *Biopolymers*. **17**:1759-1772 (1978).

De Gennes, P.G.: Scaling Concepts in Polymer Physics. Cornell University Press, Ithaca, NY, 1979.

Ebersole, R.C. and Ward, M.D.: Amplified Mass Immunosorbent Assay with a Quartz Crystal Microbalance. *Journal of the American Chemical Society*. **110**:8623-8628 (1988).

Gizeli, E., Goddard, N.J., Lowe, C.R. and Stevenson, A.C.: A Love Plate Biosensor Utilising a Polymer Layer. *Sensors and Actuators*. **B6**:131-137 (1992).

Glaser, R.W.: Antigen-Antibody Binding and Mass Transport by Convection and Diffusion to a Surface: A Two-Dimensional Computer Model of Binding and Dissociation Kinetics. *Analytical Biochemistry*. **213**:152-161 (1993).

Gleria, K.D., Hill, H.A.O. and McNeil, C.J.: Homogenous Ferrocene-Mediated Amperometric Immunoassay. *Analytical Chemistry*. **58**:1203-1205 (1986).

Guibault, G.G. and Luong, J.H.: Gas Phase Biosensors. *Journal of Biotechnology*. **9**:1-10 (1988).

Hartman, N.F.: Integrated Optic Interferometric Sensor. *United States Patent Number 5,623,561* (1997).

Hermanson, G.T, Mallia, A.K. and Smith, P.K.: Immobilized Affinity Ligand Techniques. Academic Press, San Diego, CA, 1992.

Hill, K.O., Fujii, Y. Johnson, D.C. and Kawasaki, B.S.: Photosensitivity in Optical Fiber Waveguides: Applications to Reflection Filter Fabrication. *Applied Physics Letters*. **32**(10):647-649 (1978).

Hill, K.O., Malo, B., Vineberg, K. Bilodeau, F., Johnson, D. and Skinner, I.: Efficient Mode Conversion in Telecommunication Fibre Using Externally Written Graftings, *Electronics Letters*. **26**:1270-1272 (1990).

Hirshfeld, T.E. and Block, M.J.: Fluorescent Immunoassay Employing Optical Fiber in a Capillary Tube. *United States Patent Number 4,447,546* (1984).

Hundeck, H.G., Hübner, U., Lübbert, A., Scheper, T., Schmidt, J., Weiß, M. and Schubert, F.: Development and Application of a Four-Channel Enzyme Thermistor System for Bioprocess Control. In *Proceedings of the International Seminar on Biosensors-Fundamentals, Technologies and Applications*, (Scheller, F. and Schmid, R.D., ed.). GBF Monographs, VCH Verlagsgesellschaft, Wienheim, Germany, 1992, pp. 321-330.

Ikariyama, Y., Kunoh, H. and Aizawa, M.: Electrochemical Luminescence-Based Homogeneous Immunoassay. *Biochemical and Biophysical Research Communications*. **128**(2):987-992 (1985).

Jönsson, U. and Malmqvist, M.: Real Time Biospecific Interaction Analysis, The Integration of Surface Plasmon Resonance Detection, General Biospecific Interface Chemistry and Microfluidics Into One Analytical System. *Advances in Biosensors*. **2**:291-336 (1992).

Karlsson, R. and Fält, A.: Experimental Design for Kinetic Analysis of Protein-Protein Interactions with Surface Plasmon Resonance Biosensors. *Journal of Immunological Methods*. **200**:121-133 (1997).

Kobatake, Y., Takeguchi, N., Toyoshima, Y. and Fujita, H.: Studies of Membrane Phenomena I. Membrane Potential. *Journal of Physical Chemistry*. **69**(11):3981-3988 (1965).

Lammers, F. and Scheper, T.: Thermal Biosensors in Biotechnology. *Advances in Biochemical Engineering/Biotechnology*. **64**:35-67 (1999).

Lave, W.F., Button, L.J. and Slovacek, R.E.: Optical Characteristics of Fiberoptic Evanescent Wave Sensors: Theory and Experiment. In *Biosensors With Fiberoptics*, (Wise, D.L. and Wingard, L.B., ed.). Humana Press, Clifton, NJ, 1991, pp. 139-180.

Lechuga, L.M., Lenferink, A.T.M., Kooyman, R.P.H. and Greve, J.: Feasibility of Evanescent Wave Interferometer Immunosensors for Pesticide Detection: Chemical Aspects. *Sensors and Actuators*. **B24-25**:762-765 (1995).

Ligler, F.S., Golden, J.P., Shriver-Lake, L.C., Ogert, R.A., Wijesuria, D. and Anderson, G.P.: Fiber-Optic Biosensor for the Detection of Hazardous Materials. *Immunomethods*. **3**:122-127 (1993).

Liu, Y. and Yu, T.: Polymers and Enzyme Biosensors. *Journal of Macromolecular Science, Reviews in Macromolecular Chemistry and Physics*. **C37**(3):459-500 (1997).

Marco, M-P. and Barceló, D.: Environmental Applications of Analytical Biosensors. *Measurement Science & Technology*. **7**(11)1547-1562 (1996).

Mattiasson, B., Borrebaeck, C., Sanfridson, B. and Mosbach, K.: Thermometric Enzyme Linked Immunosorbent Assay: TELISA. *Biochimica Et Biophysica Acta*. **483**:221-227 (1977).

Morton, T.A. and Myszka, D.G.: Kinetic Analysis of Macromolecular Interactions Using Surface Plasmon Resonance Biosensors. *Methods in Enzymology*. **295**:268-294 (1998).

Nagpal, V.J. and Davis, R.M.: Novel Thin Films of Titanium Dioxide Particles Synthesized by a Sol-Gel Process. *Journal of Materials Research*. **10**(12): 3068-3078 (1995).

Narang, U., Anderson, G.P., Ligler, F.S. and Burans, J.: Fiber Optic-Based Biosensor for Ricin. *Biosensors & Bioelectronics*. **12**(9-10):937-945 (1997).

North, J.R.: Immunosensors: Antibody-Based Biosensors. *Trends in Biotechnology*. **3**(7):180-186 (1985).

Paddle, B.M.: Biosensors for Chemical and Biological Agents in Defence Interest. *Biosensors & Bioelectronics*. **11**(11):1079-1113 (1996).

Pearson, J.E., Gill, A. and Vadgama, P.: Analytical Aspects of Biosensors. *Annals of Clinical Biochemistry*. **37**:119-145 (2000).

Place, J.F., Sutherland, R.M. and Dahne, C.: Opto-Electronic Immunosensors: A Review of Optical Immunoassays at Continuous Surfaces. *Biosensors*. **1**:321-354 (1985).

Poli, M.A., Rivera, V.R., Hewetson, J.F. and Merrill, G.A.: Detection of Ricin by Colorimetric and Chemiluminescence ELISA. *Toxicology*. **32**(11):1371-1377 (1994).

Rabbany, S.Y., Donner, B.L. and Ligler, F.S.: Optical Immunosensors. *Critical Reviews in Biomedical Engineering*. **22**(5-6):307-346 (1994).

Robinson, G.A.: Optical Immunosensing Systems – Meeting the Market Needs. *Biosensors & Bioelectronics*. **6**:183-191 (1991).

Roitt, I.: Essential Immunology, 5th ed. Oxford: Blackwell Scientific, St. Louis, MO, 1984.

Sadana, A. and Madugula, A.: Binding Kinetics of Antigen by Immobilized Antibody or of Antibody by Immobilized Antigen: Influence of Lateral Interactions and Variable Rate Coefficients. *Biotechnology Progress*. **9**:259-266 (1993).

Sauerbrey, G.: The Use of Quartz Oscillators for Weighing Thin Layers and for Microweighing. *Journal of Physics*. **155**:206-222 (1959).

Schneider, B.H., Edwards, J.G. and Hartman, N.F.: Hartman Interferometer: Versatile Integrated Optic Sensor for Label-Free, Real-Time Quantification of Nucleic Acids, Proteins, and Pathogens. *Clinical Chemistry*. **43**(9):1757-1763 (1997).

Schuck, P.: Kinetics of Ligand Binding to Receptor Immobilized in a Polymer Matrix, as Detected with an Evanescent Wave Biosensor I. A Computer Simulation of the Influence of Mass Transport. *Biophysics Journal*. **70**:1230-1249 (1996).

Schuck, P.: Use of Surface Plasmon Resonance to Probe the Equilibrium and Dynamic Aspects of Interactions Between Biological Macromolecules. *Annual Review of Biophysics and Biomolecular Structure*. **26**:541-566 (1997).

Squillante III, E.: Applications of Fiber-Optic Evanescent Wave Spectroscopy. *Drug Development and Industrial Pharmacy*. **24**(12):1163-1175 (1998).

Stenberg, E., Persson, B., Roos, H. and Urbaniczky, C.: Quantitative Determination of Surface Concentration of Protein with Surface Plasmon Resonance Using Radiolabeled Proteins. *Journal of Colloid and Interface Science*. **143**(2):513-526 (1991).

Steward, M.W.: Affinity of the Antibody-Antigen Reaction and Its Biological Significance. In *Immunochemistry: An Advanced Textbook* (Glynn, L.E. and Steward, M.W., ed.). John Wiley and Sons, New York, 1977, pp. 233-262.

Subramanian, A., Van Cott, K.E., Milbrath, D.S. and Velander, W.H.: Role of Local Antibody Density Effects on Immunosorbent Efficiency. *Journal of Chromatography*. **A672**:11-24 (1994).

Thompson, M., Dhaliwal, G.K., Arthur, C.L. and Calabrese, G.S.: The Potential of the Bulk Acoustic Wave Device as a Liquid-Phase Immunosensor. *IEEE Transactions on Ultrasonics, Ferroelectrics, and Frequency Control*. **UFFC-34**(2):127-135 (1987).

Thompson, R. and Villaruel, C.: Waveguide-Binding Sensors for Use with Assays. *United States Patent Number 5,061,857* (1991).

Thompson, R.B. and Ligler, F.S.: Chemistry and Technology of Evanescent Wave Biosensors. In *Biosensors with Fiberoptics* (Wise, D.L. and Wingard, L.B., ed.). Humana Press, Clifton, NJ, 1991, pp. 111-138.

Tran, T.A., Bhatia, V., D'Alberto, T., Murphy, K.A. and Claus, R.O.: Real-Time Immunoassays Using Fiber-Optic Long-Period grating Sensors. *Proceedings of SPIE, The International Society for Optical Engineering Biomedical Sensing, Imaging and Tracking Technologies I*, San Jose, CA, USA. **2676**:165-170 (1996).

Witz, J.: Kinetic Analysis of Analyte Binding by Optical Biosensors: Hydrodynamic Penetration of the Analyte Flow into the Polymer Matrix Reduces the Influence of Mass Transport. *Analytical Biochemistry*. **270**:201-206 (1999).

Xie, B., Rumanathan, K. and Danielsson, B.: Principles of Enzyme Thermistor Systems: Applications to Biomedical and Other Measurements. *Advances in Biochemical Engineering/Biotechnology*. **64**:1-33 (1999).

APPENDIX

MICROSOFT EXCEL SPREADSHEET CALCULATIONS OF PREDICTED TARGET BINDING FOR VARIOUS LIGAND/TARGET PAIRS

Anti-Bovine Serum Albumin (BSA) IgG Binding To **Bovine Serum Albumin (BSA)**

Fiber Diameter = 0.012 cm
LPG Length = 1 cm
Gel Thickness = 0.00001 cm
Ligand Molecular Weight = 68,000 g/mol
Target Molecular Weight = 155,000 g/mol
Target:Ligand Stoichiometry = 1:1
Binding Efficiency = 20%
dn/dc Target = 0.18 ml/g
RI/nm (Sensitivity of Fiber) = 0.0001

LPG Surf Area [cm^2]	Gel Volume [ml]	**Ligand Conc [mg/ml]**	Ligand Present [g]	Ligand Present [moles]	Target Bound [moles]	Target Bound [g]	Target Film Conc [g/ml]	Δ RI	**Shift Observed [nm]**
3.77E-02	3.77E-07	**5**	1.88E-09	2.77E-14	5.54E-15	8.59E-10	0.0022794	4.10E-04	**4.1**
3.77E-02	3.77E-07	**10**	3.77E-09	5.54E-14	1.11E-14	1.72E-09	0.0045588	8.21E-04	**8.2**
3.77E-02	3.77E-07	**15**	5.65E-09	8.32E-14	1.66E-14	2.58E-09	0.0068382	1.23E-03	**12.3**
3.77E-02	3.77E-07	**25**	9.42E-09	1.39E-13	2.77E-14	4.30E-09	0.0113971	2.05E-03	**20.5**
3.77E-02	3.77E-07	**50**	1.88E-08	2.77E-13	5.54E-14	8.59E-09	0.0227941	4.10E-03	**41.0**

Anti-Bovine Serum Albumin (BSA) IgG Binding To **Bovine Serum Albumin (BSA)**

Fiber Diameter = 0.012 cm
LPG Length = 1 cm
Gel Thickness = 0.00001 cm
Ligand Molecular Weight = 68,000 g/mol
Target Molecular Weight = 155,000 g/mol
Target:Ligand Stoichiometry = 1:1
Binding Efficiency = 60%
dn/dc Target = 0.18 ml/g
RI/nm (Sensitivity of Fiber) = 0.0001

LPG Surf Area [cm^2]	Gel Volume [ml]	**Ligand Conc [mg/ml]**	Ligand Present [g]	Ligand Present [moles]	Target Bound [moles]	Target Bound [g]	Target Film Conc [g/ml]	Δ RI	**Shift Observed [nm]**
3.77E-02	3.77E-07	**5**	1.88E-09	2.77E-14	1.66E-14	2.58E-09	0.0068382	1.23E-03	**12.3**
3.77E-02	3.77E-07	**10**	3.77E-09	5.54E-14	3.33E-14	5.16E-09	0.0136765	2.46E-03	**24.6**
3.77E-02	3.77E-07	**15**	5.65E-09	8.32E-14	4.99E-14	7.73E-09	0.0205147	3.69E-03	**36.9**
3.77E-02	3.77E-07	**25**	9.42E-09	1.39E-13	8.32E-14	1.29E-08	0.0341912	6.15E-03	**61.5**
3.77E-02	3.77E-07	**50**	1.88E-08	2.77E-13	1.66E-13	2.58E-08	0.0683824	1.23E-02	**123.1**

Anti-Bovine Serum Albumin (BSA) IgG Binding To **Bovine Serum Albumin (BSA)**

Fiber Diameter = 0.012 cm
LPG Length = 1 cm
Gel Thickness = 0.00005 cm
Ligand Molecular Weight = 68,000 g/mol
Target Molecular Weight = 155,000 g/mol
Target:Ligand Stoichiometry = 1:1
Binding Efficiency = 20%
dn/dc Target = 0.18 ml/g
RI/nm (Sensitivity of Fiber) = 0.0001

LPG Surf Area [cm^2]	Gel Volume [ml]	**Ligand Conc [mg/ml]**	Ligand Present [g]	Ligand Present [moles]	Target Bound [moles]	Target Bound [g]	Target Film Conc [g/ml]	Δ RI	**Shift Observed [nm]**
3.77E-02	1.88E-06	**5**	9.42E-09	1.39E-13	2.77E-14	4.30E-09	0.0022794	4.10E-04	**4.1**
3.77E-02	1.88E-06	**10**	1.88E-08	2.77E-13	5.54E-14	8.59E-09	0.0045588	8.21E-04	**8.2**
3.77E-02	1.88E-06	**15**	2.83E-08	4.16E-13	8.32E-14	1.29E-08	0.0068382	1.23E-03	**12.3**
3.77E-02	1.88E-06	**25**	4.71E-08	6.93E-13	1.39E-13	2.15E-08	0.0113971	2.05E-03	**20.5**
3.77E-02	1.88E-06	**50**	9.42E-08	1.39E-12	2.77E-13	4.30E-08	0.0227941	4.10E-03	**41.0**

Anti-Bovine Serum Albumin (BSA) IgG Binding To **Bovine Serum Albumin (BSA)**

Fiber Diameter = 0.012 cm
LPG Length = 1 cm
Gel Thickness = 0.00005 cm
Ligand Molecular Weight = 68,000 g/mol
Target Molecular Weight = 155,000 g/mol
Target:Ligand Stoichiometry = 1:1
Binding Efficiency = 60%
dn/dc Target = 0.18 ml/g
RI/nm (Sensitivity of Fiber) = 0.0001

LPG Surf Area [cm^2]	Gel Volume [ml]	**Ligand Conc [mg/ml]**	Ligand Present [g]	Ligand Present [moles]	Target Bound [moles]	Target Bound [g]	Target Film Conc [g/ml]	Δ RI	**Shift Observed [nm]**
3.77E-02	1.88E-06	**5**	9.42E-09	1.39E-13	8.32E-14	1.29E-08	0.0068382	1.23E-03	**12.3**
3.77E-02	1.88E-06	**10**	1.88E-08	2.77E-13	1.66E-13	2.58E-08	0.0136765	2.46E-03	**24.6**
3.77E-02	1.88E-06	**15**	2.83E-08	4.16E-13	2.49E-13	3.87E-08	0.0205147	3.69E-03	**36.9**
3.77E-02	1.88E-06	**25**	4.71E-08	6.93E-13	4.16E-13	6.44E-08	0.0341912	6.15E-03	**61.5**
3.77E-02	1.88E-06	**50**	9.42E-08	1.39E-12	8.32E-13	1.29E-07	0.0683824	1.23E-02	**123.1**

Anti-Bovine Serum Albumin (BSA) IgG Binding To **Bovine Serum Albumin (BSA)**

Fiber Diameter = 0.012 cm
LPG Length = 1 cm
Gel Thickness = 0.00001 cm
Ligand Molecular Weight = 68,000 g/mol
Target Molecular Weight = 155,000 g/mol
Target:Ligand Stoichiometry = 2:1
Binding Efficiency = 20%
dn/dc Target = 0.18 ml/g
RI/nm (Sensitivity of Fiber) = 0.0001

LPG Surf Area [cm^2]	Gel Volume [ml]	**Ligand Conc [mg/ml]**	Ligand Present [g]	Ligand Present [moles]	Target Bound [moles]	Target Bound [g]	Target Film Conc [g/ml]	Δ RI	**Shift Observed [nm]**
3.77E-02	3.77E-07	**5**	1.88E-09	2.77E-14	1.11E-14	1.72E-09	0.0045588	8.21E-04	**8.2**
3.77E-02	3.77E-07	**10**	3.77E-09	5.54E-14	2.22E-14	3.44E-09	0.0091176	1.64E-03	**16.4**
3.77E-02	3.77E-07	**15**	5.65E-09	8.32E-14	3.33E-14	5.16E-09	0.0136765	2.46E-03	**24.6**
3.77E-02	3.77E-07	**25**	9.42E-09	1.39E-13	5.54E-14	8.59E-09	0.0227941	4.10E-03	**41.0**
3.77E-02	3.77E-07	**50**	1.88E-08	2.77E-13	1.11E-13	1.72E-08	0.0455882	8.21E-03	**82.1**

Anti-Bovine Serum Albumin (BSA) IgG Binding To **Bovine Serum Albumin (BSA)**

Fiber Diameter = 0.012 cm
LPG Length = 1 cm
Gel Thickness = 0.00001 cm
Ligand Molecular Weight = 68,000 g/mol
Target Molecular Weight = 155,000 g/mol
Target:Ligand Stoichiometry = 2:1
Binding Efficiency = 60%
dn/dc Target = 0.18 ml/g
RI/nm (Sensitivity of Fiber) = 0.0001

LPG Surf Area [cm^2]	Gel Volume [ml]	**Ligand Conc [mg/ml]**	Ligand Present [g]	Ligand Present [moles]	Target Bound [moles]	Target Bound [g]	Target Film Conc [g/ml]	Δ RI	**Shift Observed [nm]**
3.77E-02	3.77E-07	**5**	1.88E-09	2.77E-14	3.33E-14	5.16E-09	0.0136765	2.46E-03	**24.6**
3.77E-02	3.77E-07	**10**	3.77E-09	5.54E-14	6.65E-14	1.03E-08	0.0273529	4.92E-03	**49.2**
3.77E-02	3.77E-07	**15**	5.65E-09	8.32E-14	9.98E-14	1.55E-08	0.0410294	7.39E-03	**73.9**
3.77E-02	3.77E-07	**25**	9.42E-09	1.39E-13	1.66E-13	2.58E-08	0.0683824	1.23E-02	**123.1**
3.77E-02	3.77E-07	**50**	1.88E-08	2.77E-13	3.33E-13	5.16E-08	0.1367647	2.46E-02	**246.2**

Anti-Bovine Serum Albumin (BSA) IgG Binding To **Bovine Serum Albumin (BSA)**

Fiber Diameter = 0.012 cm
LPG Length = 1 cm
Gel Thickness = 0.00005 cm
Ligand Molecular Weight = 68,000 g/mol
Target Molecular Weight = 155,000 g/mol
Target:Ligand Stoichiometry = 2:1
Binding Efficiency = 20%
dn/dc Target = 0.18 ml/g
RI/nm (Sensitivity of Fiber) = 0.0001

LPG Surf Area [cm^2]	Gel Volume [ml]	**Ligand Conc [mg/ml]**	Ligand Present [g]	Ligand Present [moles]	Target Bound [moles]	Target Bound [g]	Target Film Conc [g/ml]	Δ RI	**Shift Observed [nm]**
3.77E-02	1.88E-06	**5**	9.42E-09	1.39E-13	5.54E-14	8.59E-09	0.0045588	8.21E-04	**8.2**
3.77E-02	1.88E-06	**10**	1.88E-08	2.77E-13	1.11E-13	1.72E-08	0.0091176	1.64E-03	**16.4**
3.77E-02	1.88E-06	**15**	2.83E-08	4.16E-13	1.66E-13	2.58E-08	0.0136765	2.46E-03	**24.6**
3.77E-02	1.88E-06	**25**	4.71E-08	6.93E-13	2.77E-13	4.30E-08	0.0227941	4.10E-03	**41.0**
3.77E-02	1.88E-06	**50**	9.42E-08	1.39E-12	5.54E-13	8.59E-08	0.0455882	8.21E-03	**82.1**

Anti-Bovine Serum Albumin (BSA) IgG Binding To **Bovine Serum Albumin (BSA)**

Fiber Diameter = 0.012 cm
LPG Length = 1 cm
Gel Thickness = 0.00005 cm
Ligand Molecular Weight = 68,000 g/mol
Target Molecular Weight = 155,000 g/mol
Target:Ligand Stoichiometry = 2:1
Binding Efficiency = 60%
dn/dc Target = 0.18 ml/g
RI/nm (Sensitivity of Fiber) = 0.0001

LPG Surf Area [cm^2]	Gel Volume [ml]	**Ligand Conc [mg/ml]**	Ligand Present [g]	Ligand Present [moles]	Target Bound [moles]	Target Bound [g]	Target Film Conc [g/ml]	Δ RI	**Shift Observed [nm]**
3.77E-02	1.88E-06	**5**	9.42E-09	1.39E-13	1.66E-13	2.58E-08	0.0136765	2.46E-03	**24.6**
3.77E-02	1.88E-06	**10**	1.88E-08	2.77E-13	3.33E-13	5.16E-08	0.0273529	4.92E-03	**49.2**
3.77E-02	1.88E-06	**15**	2.83E-08	4.16E-13	4.99E-13	7.73E-08	0.0410294	7.39E-03	**73.9**
3.77E-02	1.88E-06	**25**	4.71E-08	6.93E-13	8.32E-13	1.29E-07	0.0683824	1.23E-02	**123.1**
3.77E-02	1.88E-06	**50**	9.42E-08	1.39E-12	1.66E-12	2.58E-07	0.1367647	2.46E-02	**246.2**

Lipopolysaccharide (LPS) Binding To **Polymyxin B (PMB)**

Fiber Diameter = 0.012 cm
LPG Length = 1 cm
Gel Thickness = 0.00001 cm
Ligand Molecular Weight = 7,500 g/mol
Target Molecular Weight = 7,500 g/mol
Target:Ligand Stoichiometry = 1:1
Binding Efficiency = 20%
dn/dc Target = 0.18 ml/g
RI/nm (Sensitivity of Fiber) = 0.0001

LPG Surf Area [cm^2]	Gel Volume [ml]	**Ligand Conc [mg/ml]**	Ligand Present [g]	Ligand Present [moles]	Target Bound [moles]	Target Bound [g]	Target Film Conc [g/ml]	Δ RI	**Shift Observed [nm]**
3.77E-02	3.77E-07	**5**	1.88E-09	2.51E-13	5.03E-14	3.77E-10	0.001	1.80E-04	**1.8**
3.77E-02	3.77E-07	**10**	3.77E-09	5.03E-13	1.01E-13	7.54E-10	0.002	3.60E-04	**3.6**
3.77E-02	3.77E-07	**15**	5.65E-09	7.54E-13	1.51E-13	1.13E-09	0.003	5.40E-04	**5.4**
3.77E-02	3.77E-07	**25**	9.42E-09	1.26E-12	2.51E-13	1.88E-09	0.005	9.00E-04	**9.0**
3.77E-02	3.77E-07	**50**	1.88E-08	2.51E-12	5.03E-13	3.77E-09	0.01	1.80E-03	**18.0**

Lipopolysaccharide (LPS) Binding To **Polymyxin B (PMB)**

Fiber Diameter = 0.012 cm
LPG Length = 1 cm
Gel Thickness = 0.00001 cm
Ligand Molecular Weight = 7,500 g/mol
Target Molecular Weight = 7,500 g/mol
Target:Ligand Stoichiometry = 1:1
Binding Efficiency = 60%
dn/dc Target = 0.18 ml/g
RI/nm (Sensitivity of Fiber) = 0.0001

LPG Surf Area [cm^2]	Gel Volume [ml]	**Ligand Conc [mg/ml]**	Ligand Present [g]	Ligand Present [moles]	Target Bound [moles]	Target Bound [g]	Target Film Conc [g/ml]	Δ RI	**Shift Observed [nm]**
3.77E-02	3.77E-07	**5**	1.88E-09	2.51E-13	1.51E-13	1.13E-09	0.003	5.40E-04	**5.4**
3.77E-02	3.77E-07	**10**	3.77E-09	5.03E-13	3.02E-13	2.26E-09	0.006	1.08E-03	**10.8**
3.77E-02	3.77E-07	**15**	5.65E-09	7.54E-13	4.52E-13	3.39E-09	0.009	1.62E-03	**16.2**
3.77E-02	3.77E-07	**25**	9.42E-09	1.26E-12	7.54E-13	5.65E-09	0.015	2.70E-03	**27.0**
3.77E-02	3.77E-07	**50**	1.88E-08	2.51E-12	1.51E-12	1.13E-08	0.03	5.40E-03	**54.0**

Lipopolysaccharide (LPS) Binding To **Polymyxin B (PMB)**

Fiber Diameter = 0.012 cm
LPG Length = 1 cm
Gel Thickness = 0.00005 cm
Ligand Molecular Weight = 7,500 g/mol
Target Molecular Weight = 7,500 g/mol
Target:Ligand Stoichiometry = 1:1
Binding Efficiency = 20%
dn/dc Target = 0.18 ml/g
RI/nm (Sensitivity of Fiber) = 0.0001

LPG Surf Area [cm^2]	Gel Volume [ml]	**Ligand Conc [mg/ml]**	Ligand Present [g]	Ligand Present [moles]	Target Bound [moles]	Target Bound [g]	Target Film Conc [g/ml]	Δ RI	**Shift Observed [nm]**
3.77E-02	1.88E-06	**5**	9.42E-09	1.26E-12	2.51E-13	1.88E-09	0.001	1.80E-04	**1.8**
3.77E-02	1.88E-06	**10**	1.88E-08	2.51E-12	5.03E-13	3.77E-09	0.002	3.60E-04	**3.6**
3.77E-02	1.88E-06	**15**	2.83E-08	3.77E-12	7.54E-13	5.65E-09	0.003	5.40E-04	**5.4**
3.77E-02	1.88E-06	**25**	4.71E-08	6.28E-12	1.26E-12	9.42E-09	0.005	9.00E-04	**9.0**
3.77E-02	1.88E-06	**50**	9.42E-08	1.26E-11	2.51E-12	1.88E-08	0.01	1.80E-03	**18.0**

Lipopolysaccharide (LPS) Binding To **Polymyxin B (PMB)**

Fiber Diameter = 0.012 cm
LPG Length = 1 cm
Gel Thickness = 0.00005 cm
Ligand Molecular Weight = 7,500 g/mol
Target Molecular Weight = 7,500 g/mol
Target:Ligand Stoichiometry = 1:1
Binding Efficiency = 60%
dn/dc Target = 0.18 ml/g
RI/nm (Sensitivity of Fiber) = 0.0001

LPG Surf Area [cm^2]	Gel Volume [ml]	**Ligand Conc [mg/ml]**	Ligand Present [g]	Ligand Present [moles]	Target Bound [moles]	Target Bound [g]	Target Film Conc [g/ml]	Δ RI	**Shift Observed [nm]**
3.77E-02	1.88E-06	**5**	9.42E-09	1.26E-12	7.54E-13	5.65E-09	0.003	5.40E-04	**5.4**
3.77E-02	1.88E-06	**10**	1.88E-08	2.51E-12	1.51E-12	1.13E-08	0.006	1.08E-03	**10.8**
3.77E-02	1.88E-06	**15**	2.83E-08	3.77E-12	2.26E-12	1.70E-08	0.009	1.62E-03	**16.2**
3.77E-02	1.88E-06	**25**	4.71E-08	6.28E-12	3.77E-12	2.83E-08	0.015	2.70E-03	**27.0**
3.77E-02	1.88E-06	**50**	9.42E-08	1.26E-11	7.54E-12	5.65E-08	0.03	5.40E-03	**54.0**

Anti-B-Galactosidase IgG Binding To **B-Galactosidase**

Fiber Diameter = 0.012 cm
LPG Length = 1 cm
Gel Thickness = 0.00001 cm
Ligand Molecular Weight = 155,000 g/mol
Target Molecular Weight = 86,000 g/mol
Target:Ligand Stoichiometry = 1:1
Binding Efficiency = 20%
dn/dc Target = 0.18 ml/g
RI/nm (Sensitivity of Fiber) = 0.0001

LPG Surf Area [cm^2]	Gel Volume [ml]	**Ligand Conc [mg/ml]**	Ligand Present [g]	Ligand Present [moles]	Target Bound [moles]	Target Bound [g]	Target Film Conc [g/ml]	Δ RI	**Shift Observed [nm]**
3.77E-02	3.77E-07	**5**	1.88E-09	1.22E-14	2.43E-15	2.09E-10	0.0005548	9.99E-05	**1.0**
3.77E-02	3.77E-07	**10**	3.77E-09	2.43E-14	4.86E-15	4.18E-10	0.0011097	2.00E-04	**2.0**
3.77E-02	3.77E-07	**15**	5.65E-09	3.65E-14	7.30E-15	6.28E-10	0.0016645	3.00E-04	**3.0**
3.77E-02	3.77E-07	**25**	9.42E-09	6.08E-14	1.22E-14	1.05E-09	0.0027742	4.99E-04	**5.0**
3.77E-02	3.77E-07	**50**	1.88E-08	1.22E-13	2.43E-14	2.09E-09	0.0055484	9.99E-04	**10.0**

Anti-B-Galactosidase IgG Binding To **B-Galactosidase**

Fiber Diameter = 0.012 cm
LPG Length = 1 cm
Gel Thickness = 0.00001 cm
Ligand Molecular Weight = 155,000 g/mol
Target Molecular Weight = 86,000 g/mol
Target:Ligand Stoichiometry = 1:1
Binding Efficiency = 60%
dn/dc Target = 0.18 ml/g
RI/nm (Sensitivity of Fiber) = 0.0001

LPG Surf Area [cm^2]	Gel Volume [ml]	**Ligand Conc [mg/ml]**	Ligand Present [g]	Ligand Present [moles]	Target Bound [moles]	Target Bound [g]	Target Film Conc [g/ml]	Δ RI	**Shift Observed [nm]**
3.77E-02	3.77E-07	**5**	1.88E-09	1.22E-14	7.30E-15	6.28E-10	0.0016645	3.00E-04	**3.0**
3.77E-02	3.77E-07	**10**	3.77E-09	2.43E-14	1.46E-14	1.26E-09	0.003329	5.99E-04	**6.0**
3.77E-02	3.77E-07	**15**	5.65E-09	3.65E-14	2.19E-14	1.88E-09	0.0049935	8.99E-04	**9.0**
3.77E-02	3.77E-07	**25**	9.42E-09	6.08E-14	3.65E-14	3.14E-09	0.0083226	1.50E-03	**15.0**
3.77E-02	3.77E-07	**50**	1.88E-08	1.22E-13	7.30E-14	6.28E-09	0.0166452	3.00E-03	**30.0**

Anti-B-Galactosidase IgG Binding To **B-Galactosidase**

Fiber Diameter = 0.012 cm
LPG Length = 1 cm
Gel Thickness = 0.00005 cm
Ligand Molecular Weight = 155,000 g/mol
Target Molecular Weight = 86,000 g/mol
Target:Ligand Stoichiometry = 1:1
Binding Efficiency = 20%
dn/dc Target = 0.18 ml/g
RI/nm (Sensitivity of Fiber) = 0.0001

LPG Surf Area [cm^2]	Gel Volume [ml]	**Ligand Conc [mg/ml]**	Ligand Present [g]	Ligand Present [moles]	Target Bound [moles]	Target Bound [g]	Target Film Conc [g/ml]	Δ RI	**Shift Observed [nm]**
3.77E-02	1.88E-06	**5**	9.42E-09	6.08E-14	1.22E-14	1.05E-09	0.0005548	9.99E-05	**1.0**
3.77E-02	1.88E-06	**10**	1.88E-08	1.22E-13	2.43E-14	2.09E-09	0.0011097	2.00E-04	**2.0**
3.77E-02	1.88E-06	**15**	2.83E-08	1.82E-13	3.65E-14	3.14E-09	0.0016645	3.00E-04	**3.0**
3.77E-02	1.88E-06	**25**	4.71E-08	3.04E-13	6.08E-14	5.23E-09	0.0027742	4.99E-04	**5.0**
3.77E-02	1.88E-06	**50**	9.42E-08	6.08E-13	1.22E-13	1.05E-08	0.0055484	9.99E-04	**10.0**

Anti-B-Galactosidase IgG Binding To **B-Galactosidase**

Fiber Diameter = 0.012 cm
LPG Length = 1 cm
Gel Thickness = 0.00005 cm
Ligand Molecular Weight = 155,000 g/mol
Target Molecular Weight = 86,000 g/mol
Target:Ligand Stoichiometry = 1:1
Binding Efficiency = 60%
dn/dc Target = 0.18 ml/g
RI/nm (Sensitivity of Fiber) = 0.0001

LPG Surf Area [cm^2]	Gel Volume [ml]	**Ligand Conc [mg/ml]**	Ligand Present [g]	Ligand Present [moles]	Target Bound [moles]	Target Bound [g]	Target Film Conc [g/ml]	Δ RI	**Shift Observed [nm]**
3.77E-02	1.88E-06	**5**	9.42E-09	6.08E-14	3.65E-14	3.14E-09	0.0016645	3.00E-04	**3.0**
3.77E-02	1.88E-06	**10**	1.88E-08	1.22E-13	7.30E-14	6.28E-09	0.003329	5.99E-04	**6.0**
3.77E-02	1.88E-06	**15**	2.83E-08	1.82E-13	1.09E-13	9.41E-09	0.0049935	8.99E-04	**9.0**
3.77E-02	1.88E-06	**25**	4.71E-08	3.04E-13	1.82E-13	1.57E-08	0.0083226	1.50E-03	**15.0**
3.77E-02	1.88E-06	**50**	9.42E-08	6.08E-13	3.65E-13	3.14E-08	0.0166452	3.00E-03	**30.0**

Anti-B-Galactosidase IgG Binding To **B-Galactosidase**

Fiber Diameter = 0.012 cm
LPG Length = 1 cm
Gel Thickness = 0.00001 cm
Ligand Molecular Weight = 155,000 g/mol
Target Molecular Weight = 86,000 g/mol
Target:Ligand Stoichiometry = 2:1
Binding Efficiency = 20%
dn/dc Target = 0.18 ml/g
RI/nm (Sensitivity of Fiber) = 0.0001

LPG Surf Area [cm^2]	Gel Volume [ml]	**Ligand Conc [mg/ml]**	Ligand Present [g]	Ligand Present [moles]	Target Bound [moles]	Target Bound [g]	Target Film Conc [g/ml]	Δ RI	**Shift Observed [nm]**
3.77E-02	3.77E-07	**5**	1.88E-09	1.22E-14	4.86E-15	4.18E-10	0.0011097	2.00E-04	**2.0**
3.77E-02	3.77E-07	**10**	3.77E-09	2.43E-14	9.73E-15	8.37E-10	0.0022194	3.99E-04	**4.0**
3.77E-02	3.77E-07	**15**	5.65E-09	3.65E-14	1.46E-14	1.26E-09	0.003329	5.99E-04	**6.0**
3.77E-02	3.77E-07	**25**	9.42E-09	6.08E-14	2.43E-14	2.09E-09	0.0055484	9.99E-04	**10.0**
3.77E-02	3.77E-07	**50**	1.88E-08	1.22E-13	4.86E-14	4.18E-09	0.0110968	2.00E-03	**20.0**

Anti-B-Galactosidase IgG Binding To **B-Galactosidase**

Fiber Diameter = 0.012 cm
LPG Length = 1 cm
Gel Thickness = 0.00001 cm
Ligand Molecular Weight = 155,000 g/mol
Target Molecular Weight = 86,000 g/mol
Target:Ligand Stoichiometry = 2:1
Binding Efficiency = 60%
dn/dc Target = 0.18 ml/g
RI/nm (Sensitivity of Fiber) = 0.0001

LPG Surf Area [cm^2]	Gel Volume [ml]	**Ligand Conc [mg/ml]**	Ligand Present [g]	Ligand Present [moles]	Target Bound [moles]	Target Bound [g]	Target Film Conc [g/ml]	Δ RI	**Shift Observed [nm]**
3.77E-02	3.77E-07	**5**	1.88E-09	1.22E-14	1.46E-14	1.26E-09	0.003329	5.99E-04	**6.0**
3.77E-02	3.77E-07	**10**	3.77E-09	2.43E-14	2.92E-14	2.51E-09	0.0066581	1.20E-03	**12.0**
3.77E-02	3.77E-07	**15**	5.65E-09	3.65E-14	4.38E-14	3.77E-09	0.0099871	1.80E-03	**18.0**
3.77E-02	3.77E-07	**25**	9.42E-09	6.08E-14	7.30E-14	6.28E-09	0.0166452	3.00E-03	**30.0**
3.77E-02	3.77E-07	**50**	1.88E-08	1.22E-13	1.46E-13	1.26E-08	0.0332903	5.99E-03	**59.9**

Anti-B-Galactosidase IgG Binding To **B-Galactosidase**

Fiber Diameter = 0.012 cm
LPG Length = 1 cm
Gel Thickness = 0.00005 cm
Ligand Molecular Weight = 155,000 g/mol
Target Molecular Weight = 86,000 g/mol
Target:Ligand Stoichiometry = 2:1
Binding Efficiency = 20%
dn/dc Target = 0.18 ml/g
RI/nm (Sensitivity of Fiber) = 0.0001

LPG Surf Area [cm^2]	Gel Volume [ml]	**Ligand Conc [mg/ml]**	Ligand Present [g]	Ligand Present [moles]	Target Bound [moles]	Target Bound [g]	Target Film Conc [g/ml]	Δ RI	**Shift Observed [nm]**
3.77E-02	1.88E-06	**5**	9.42E-09	6.08E-14	2.43E-14	2.09E-09	0.0011097	2.00E-04	**2.0**
3.77E-02	1.88E-06	**10**	1.88E-08	1.22E-13	4.86E-14	4.18E-09	0.0022194	3.99E-04	**4.0**
3.77E-02	1.88E-06	**15**	2.83E-08	1.82E-13	7.30E-14	6.28E-09	0.003329	5.99E-04	**6.0**
3.77E-02	1.88E-06	**25**	4.71E-08	3.04E-13	1.22E-13	1.05E-08	0.0055484	9.99E-04	**10.0**
3.77E-02	1.88E-06	**50**	9.42E-08	6.08E-13	2.43E-13	2.09E-08	0.0110968	2.00E-03	**20.0**

Anti-B-Galactosidase IgG Binding To **B-Galactosidase**

Fiber Diameter = 0.012 cm
LPG Length = 1 cm
Gel Thickness = 0.00005 cm
Ligand Molecular Weight = 155,000 g/mol
Target Molecular Weight = 86,000 g/mol
Target:Ligand Stoichiometry = 2:1
Binding Efficiency = 60%
dn/dc Target = 0.18 ml/g
RI/nm (Sensitivity of Fiber) = 0.0001

LPG Surf Area [cm^2]	Gel Volume [ml]	**Ligand Conc [mg/ml]**	Ligand Present [g]	Ligand Present [moles]	Target Bound [moles]	Target Bound [g]	Target Film Conc [g/ml]	Δ RI	**Shift Observed [nm]**
3.77E-02	1.88E-06	**5**	9.42E-09	6.08E-14	7.30E-14	6.28E-09	0.003329	5.99E-04	**6.0**
3.77E-02	1.88E-06	**10**	1.88E-08	1.22E-13	1.46E-13	1.26E-08	0.0066581	1.20E-03	**12.0**
3.77E-02	1.88E-06	**15**	2.83E-08	1.82E-13	2.19E-13	1.88E-08	0.0099871	1.80E-03	**18.0**
3.77E-02	1.88E-06	**25**	4.71E-08	3.04E-13	3.65E-13	3.14E-08	0.0166452	3.00E-03	**30.0**
3.77E-02	1.88E-06	**50**	9.42E-08	6.08E-13	7.30E-13	6.28E-08	0.0332903	5.99E-03	**59.9**

VITA

Jennifer Martin was born on May 29, 1972 in Frederick, MD. Upon graduation from high school, she attended West Virginia University and studied Chemical Engineering. Jen received her B.S.Ch.E. in 1994, then worked for two years at the National Cancer Institute-Frederick Cancer Research and Development Center at Ft. Detrick, MD prior to attending graduate school. At Virginia Polytechnic Institute & State University she studied Chemical Engineering with research emphasis on biochemical engineering. Under Dr. William H. Velander, Jen worked on the development of a composite film to increase the sensitivity of long-period grating biosensors. After leaving Virginia Tech, she was commissioned as an officer in the United States Public Health Service and works as a research engineer at the National Institute for Occupational Safety & Health in Morgantown, WV. She currently resides in Morgantown with her husband, Steve, and their yellow lab, Ellie.